A STUDY OF ELECTRICAL DOUBLE LAYER STRUCTURE OVER A CORRODING STEEL SURFACE IN SEA WATER

by

PRATIK KALE

Presented to the Faculty of the Graduate School of

The University of Texas at Arlington in Partial Fulfillment

of the Requirements

for the Degree of

MASTER OF SCIENCE IN MECHANICAL ENGINEERING

THE UNIVERSITY OF TEXAS AT ARLINGTON

MAY 2016

Acknowledgements

First and foremost I offer my sincerest gratitude to my advisor, Dr. Bo, Yang, who has supported me throughout my thesis with his patience and knowledge. I attribute the level of my Master's degree to his encouragement and effort and without him this thesis, too, would not have been completed or written. One simply could not wish for a better or friendlier advisor.

Besides my advisor, I would like to thank the members of the committee Dr. Ashfaq Adna, Dr. Donghyun Shin for their encouragement, comments and feedback. I also thank my family who encouraged and prayed for me throughout the time of my research.

April 22, 2016

Abstract

A STUDY OF ELECTRICAL DOUBLE LAYER STRUCTURE OVER A CORRODING STEEL SURFACE IN SEA WATER

Pratik Kale, MS

The University of Texas at Arlington, 2016

Advisor: Bo Yang

Corrosion is a natural deterioration phenomenon that throws profound adverse effects on the performance of structural steel in marine applications. Seawater consists of various corrosive components such as chlorine ions, sulphate ions and many more. These chemical components are mainly responsible for the corrosion phenomenon. Even though their bulk concentrations are known, their local concentrations and distribution in the vicinity of a steel surface where the corrosion occurs are yet unclear. Without the knowledge, would any approach to deal with the corrosion be empirical, at best. The main objective of the present thesis is to investigate the interfacial structure of an electrical double layer (EDL) and provide mechanistic understanding of the formation of an EDL at a steel surface in seawater environment.

An analytical model is developed on basis of mass transport, electrostatics and fluid mechanics to simulate the specific system at a seawater-steel interface. Parameters such as voltage, corrosion flux and bulk concentrations are varied to examine their effects on the structure of the EDL and hopefully shed light on the mechanism of corrosion at the

nanometer scale. The EDL at an anode is considered. The anions, such as SO_4^{2-}, Cl^-, OH^-, which would be attracted to the anode, are included in the model. Many cations of corrosion products as well as Na^+, SO_4^{2-}, and other metal ions are also included. It is observed that when voltage increases in the low range from 0 to 0.6 V, the SO_4^{2-} and Cl^- concentrations rise at the metal surface. However, when the voltage is further increased, the SO_4^{2-} and Cl^- concentrations at the metal surface decreases. In contrast, the OH^- concentration at voltage range from 0 to 0.6 is low near the metal surface, due to its low concentration in the bulk electrolyte at pH 7. At higher voltage, it however rises while OH^- replacing SO_4^{2-} and Cl^- next to the metal surface. Attempt is made to interpret this phenomenon. It may be inferred that SO_4^{2-} and Cl^- should be responsible for corrosion, especially, pitting, in steel, at relatively low voltage. At higher voltages, surface coverage of OH^- may retard the corrosion.

Table of Contents

Acknowledgements III

Abstract IV

List of Illustrations VIII

List of Tables XII

Chapter 1 INTRODUCTION 1

1.1 Composition of Sea water 1

1.2 Composition of the steel 316L 2

1.3 Crevise and pitting corrosion 3

Chapter 2 THEORY OF AN ELECTRIC DOUBLE LAYER 6

2.1. Electric double layer 6

2.2 Chemical potential 7

2.3 Dynamic Transport and Other Field Governing Equations 8

2.4. Finite Volume Method for One-dimensional Planar Problems 10

Chapter 3 OBJECTIVE AND PROBLEM FORMULATION 15

Chapter 4 NUMERICAL ISSUSES 17

Chapter 5 NUMERICAL RESULTS AND OBSERVATIONS 19

5.1 Numerical results and observation varying voltage 19

5.1.1 Numerical observation applying 0.2V to the system 19

5.1.2 Numerical observation applying 0.5V to the system 21

5.1.3 Numerical observation applying 0.7V to the system 23

5.1.4 Numerical observation applying 0.8V to the system 24

5.1.5 Numerical observation applying 1.2V to the system 25

5.1.6 Numerical observation applying 1.7V to the system 27

5.2 Numerical results and observation varying voltage with electric flux 29

5.2.1 Numerical observation applying 3.365d-10 e/nm^2 /ns to the system 30

5.2.2 Numerical observation applying 2.993d-9 e/nm^2 /ns to the system 33

5.2.3 Numerical observation applying 1.153d-8 e/nm^2 /ns to the system 34

5.3 Numerical observations increasing Cl^- concentration 36

5.3.1 Numerical observations increasing Cl^- concentration to 0.501 e/nm^3 at 0.2V 37

5.3.2 Numerical observations increasing Cl^- concentration to 0.501 e/nm^3 at 0.8V 39

5.3.3 Numerical observations increasing Cl^- concentration to 0.501 e/nm^3 at 1.2V 40

5.4 Numerical observations increasing SO_4^{2-} concentration 43

5.4.1 Numerical observations increasing the SO_4^{2-} concentration to 0.138 at 0.2V 43

5.4.2 Numerical observations increasing the SO_4^{2-} concentration to 0.138 at 0.8V 44

5.4.3 Numerical observations increasing the SO_4^{2-} concentration to 0.138 at 1.2V 46

Chapter 6 NUMERICAL RESULTS DISCUSSION 49

6.1 Significance of varying voltage 49

6.2 Effect of change in initial concentration 54

Chapter 7 CONCLUSION 59

Appendix 60

REFERENCE 65

Biographical Information 68

List of Illustrations

Figure 1.1 Composition of seawater 1

Figure 1.2 Pitting site [10] 4

Figure 1.3.Corrosion in the crevice between the tube and tube sheet (both made of type 316 stainless steel) 5

Figure 2.1 Double layer structure 6

Figure 3.1.Detailed illustration of interfacial DL 15

Figure 4.1.Concentration Vs Distance graph for 0.5nm simulation domain 17

Figure 4.2.Concentration Vs Distance graph for 1.5nm simulation domain 18

Figure 4.3.Concentration Vs Distance graph for 1nm simulation domain 18

Figure 5.1.Concentration Vs Distance graph for 0.2V 19

Figure 5.2.Packing factor and Velocity Vs Distance graph for 0.2V 20

Figure 5.3.Concentration Vs Distance graph for 0.5V 21

Figure 5.4.Packing factor and Velocity Vs Distance graph for 0.5V 22

Figure 5.5. Concentration Vs Distance graph for 0.7V 23

Figure 5.6. Concentration Vs Distance graph for 0.8V 24

Figure 5.7.Packing factor and Velocity Vs Distance graph for 0.5V 25

Figure 5.8. Concentration Vs Distance graph for 1.2V 26

Figure 5.9. Packing factor and Velocity Vs Distance graph for 1.2V 26

Figure 5.10. Concentration Vs Distance graph for 1.7V 27

Figure 5.11. Packing factor and Velocity Vs Distance graph for 1.7V 28

Figure 5.12. Current density vs overpotential graph for steel 29

Figure 5.13. Concentration Vs Distance graph for 3.365d-10 e/nm2 /ns..... 31

Figure 5.14. Packing factor and Velocity Vs Distance graph 3.365d-10 e/nm2 /ns 32

Figure 5.15. Concentration Vs Distance graph for 2.993d-9 e/nm2 /ns 33

Figure 5.16. Packing factor and Velocity Vs Distance graph for 2.993d-9 e/nm2 /ns 34

Figure 5.17. Concentration Vs Distance graph for 1.153d-8 e/nm2 /ns 35

Figure 5.18. Packing factor and Velocity Vs Distance graph for 2.993d-9 e/nm2 /ns 36

Figure 5.19. Concentration Vs Distance graph for increase in Cl- concentration to 0.501 e/nm3 at 0.2V.....37

Figure 5.20. Packing factor and Velocity Vs Distance graph for increase in Cl- concentration to 0.501 e/nm3 at 0.2V 38

Figure 5.21. Concentration Vs Distance graph for increase in Cl- concentration to 0.501 e/nm3 at 0.8V 39

Figure 5.22. Packing factor and Velocity Vs Distance graph for increase in Cl- concentration to 0.501 e/nm3 at 0.8V 40

Figure 5.23. Concentration Vs Distance graph for increase in Cl- concentration to 0.501 e/nm3 at 1.2V 41

Figure 5.24. Packing factor and Velocity Vs Distance graph for increase in Cl- concentration to 0.501 e/nm3 at 0.8V 42

Figure 5.25. Concentration Vs Distance graph for increase in SO42- concentration to 0138 e/nm3 at 0.2V 43
Figure 5.26. Packing factor and Velocity Vs Distance graph for increase in SO42- concentration to 0138 e/nm3 at 0.2V 44
Figure 5.27. Concentration Vs Distance graph for increase in SO42- concentration to 0138 e/nm3 at 0.8V 45
Figure 5.28. Packing factor and Velocity Vs Distance graph for increase in SO42- concentration to 0138 e/nm3 at 0.8..... 46
Figure 5.29. Concentration Vs Distance graph for increase in SO42- concentration to 0138 e/nm3 at 1.2V 47
Figure 5.30. Packing factor and Velocity Vs Distance graph for increase in SO42- concentration to 0138 e/nm3 at1.2..... 48
Figure 6.1. Concentration Vs Distance logarithmic graph for 0.2V 49
Figure 6.2. Concentration Vs Distance graph for 0.8V 50
Figure 6.3. Concentration Vs Distance graph for 1.2V 51
Figure6.4.Concentration Vs Distance graph for 1.7V..... 51
Figure 6.5. Packing factor Vs ePressure graph for 0.2V 52
Figure 6.6 Packing factor and Vs ePressure graph for 0.8V..... 53
Figure 6.7. Comparison of concentration Vs distance graph for 0.301 and 0.501 e/nm3 at 0.2V..... 54
Figure 6.8.Concentration Vs Distance graph for increase in Cl- concentration to 0.301 e/nm3 at 0.8V 55

Figure 6.9.Concentration Vs Distance graph for increase in Cl- concentration to 0.501 e/nm3 at 0.8 55

Figure 6.10. Packing factor Vs ePressure graph for 0.2V for 0.301 e/nm3 56

Figure 6.11. Packing factor Vs ePressure graph for 0.2V for 0.501 e/nm3 57

Figure 6.12.Concentration Vs Distance graph for increase in SO42- concentration to 0.002 e/nm3 at 0.2V 58

Figure 6.13.Concentration Vs Distance graph for increase in SO42- concentration to 0138 e/nm3 at 0.2V 58

List of Tables

Table 1 Composition of steel 316L……11

Chapter 1

Introduction

Corrosion is a natural deterioration phenomenon and very destructive in nature. Corrosion is define as, electrochemical degradation of metal, as result of reaction with environment. [1] It results in many structural failures and great economic loss. In USA averagely $260 billion are spend on the corrosion that involves direct and indirect costs. [2]

Sea water is one of the most corroded and most abundant naturally occurring electrolytes. The corrosive behavior of seawater is reflected by the fact that most of the common structural metals and alloys are attacked by this liquid or its surrounding environments.[3] The destructive nature of seawater is because of its compositions. In order ,to understand the whole process of sea water corrosion, it is pre-requisite to understand the composition of sea water.

1.1 Composition of Sea water

Pictorial representation of Sea water Composition:

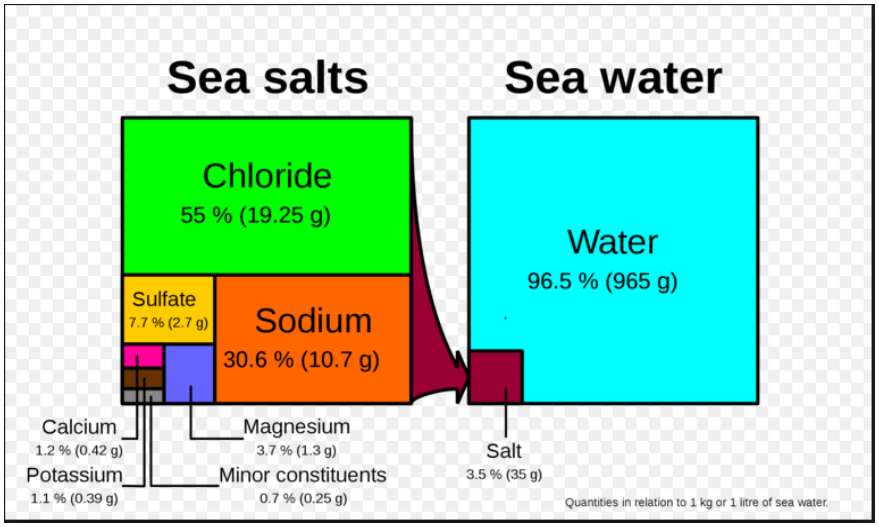

Figure 1.1. Composition of seawater [4]

Sea water consists of 96.5 % of water and 3.5 % of salt. Salt further constitutes of following elements:

- 55 % of Salt consists of Chlorides i.e (19.25 g in 35g of salt)
- 7.7 % of Salt consists of Sulphate i.e (2.7 g in 35g of salt)
- 1.2% of Salt consists of Calcium i.e (0.42 g in 35g of salt)
- 1.1% of Salt consists of Potassium i.e(0.39 g in 35g of salt)
- 3.7% of Salt consists of Magnesium i.e (1.3g in 35g of salt)
- 30.6% of Salt consists of Sodium i.e (10.7g in 35g of salt)
- 0.7% of Salt consists of other minute constitutes.

Sea water approximates 3.5 weight persent NaCl, and many naturally occuring elements in small percentages. The major chemical constituent of sea water is consistent throughout. Whereas as minor constituent such as gases and dissolve elemnts, changes according to the sea location. [5]

1.2 Composition of the steel 316L

Corrosion of material in marine engineering is depend on the various factor such as material composition, dissolve oxygen content, salinity, temperature , pH, galvanic interaction, fluid velocity characteristics, heat transfer rate, and many more. The material used for, offshore oilrig structure in marine engineering is steel 316L. The chemical composition of 316L is listed in the following table

Constituent	C	Mg	P	Si	Cr	Ni	Mo	N	Fe
%	0.08	2	0.045	0.75	16	10	2	0.10	69.025

Table 1 Composition of steel 316L [6]

The corrosion of offshore oil rig is generally considered through a series of electrochemical processes consisting of one or more anodic, oxidation reaction in which 316L alloy generates cations and electron and cathodic, reduction reactions where electrons consumed. The anodic and cathodic chemical reactions are

ANODIC: $Fe \longrightarrow Fe^{2+} + 2e^-$

CATHODIC: $O2+4H^+ + 4e^- \longrightarrow 4OH^-$

In marie environments, the oxygen reduction reaction is the eprimary cathodic reaction. The corrosion in offshore oil rigs structures can occur in many ways such as uniform corrosion, pitting, crevice corrosion, galvanic corrosion, intergranular corrosion, selective leaching or dealloying, erosion corrosion and many more. In general it is observed in many studies that, pitting and the crevice are the most common corrosion occur in marine engineering application. Therefore these two corrosion are called as main modes of corrosion in sea water.[7]

1.3 Crevise and pitting corrosion

Crevice and pitting corrosion are forms of localized corrosion, which means that the corrosion occurs in a limited area on the structure. The corrosion rate is often high and is generally higher than that for uniform corrosion, due to a large cathode/anode ratio. A severe attack is therefore usually observed, and the pit or crevice may cut through the structure wall thickness to form a hole.

Certain conditions, such as low concentrations of oxygen or high concentrations of species such as chloride which complete as anions, can interfere with a given alloy's ability to re-form a passivating film. In the worst case, almost all of the surface will remain protected, but tiny local fluctuations will degrade the oxide film in a few critical points. Corrosion at these points will be greatly amplified, and can cause corrosion pits of several types, depending upon

conditions. While the corrosion pits only nucleate under fairly extreme circumstances, they can continue to grow even when conditions return to normal, since the interior of a pit is naturally deprived of oxygen and locally the pH decreases to very low values and the corrosion rate increases due to an autocatalytic process. In extreme cases, the sharp tips of extremely long and narrow corrosion pits can cause stress concentration to the point that otherwise tough alloys can shatter; a thin film pierced by an invisibly small hole can hide a thumb sized pit from view. These problems are especially dangerous because they are difficult to detect before a part or structure fails. Pitting remains among the most common and damaging forms of corrosion in passivated alloy but it can be prevented by control of the alloy's environment.[8]

Pitting results when a small hole, or cavity, forms in the metal, usually as a result of de-passivation of a small area. This area becomes anodic, while part of the remaining metal becomes cathodic, producing a localized galvanic reaction. The deterioration of this small area penetrates the metal and can lead to failure. This form of corrosion is often difficult to detect due to the fact that it is usually relatively small and may be covered and hidden by corrosion-produced compounds.[9]

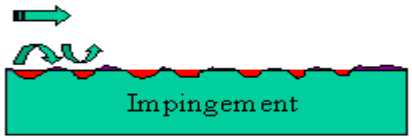

Figure 1.2 Pitting site [10]

Crevice corrosion is a localized form of corrosion occurring in confined spaces (crevices), to which the access of the working fluid from the environment is limited. Formation of a differential aeration cell leads to corrosion inside the crevices. Examples of crevices are gaps and contact areas between parts, under gaskets or seals, inside cracks and seams, spaces filled with deposits and under sludge piles. Crevice corrosion is influenced by the crevice type (metal-metal, metal-

nonmetal), crevice geometry (size, surface finish), and metallurgical and environmental factors. [11]

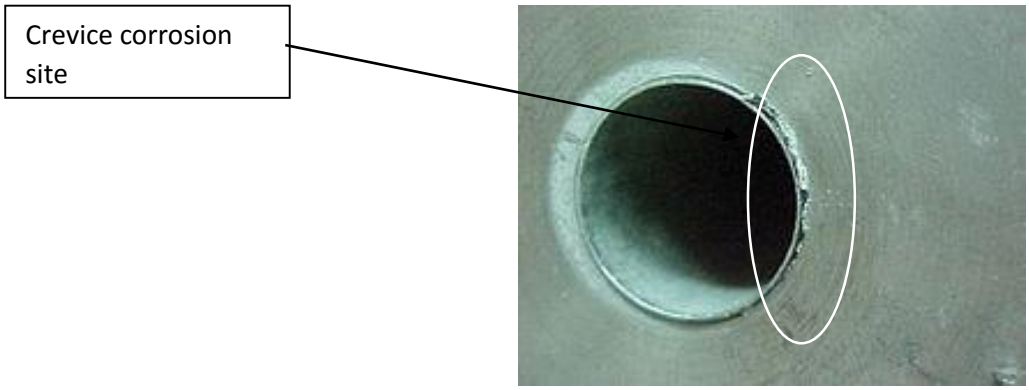

Figure 1.3.Corrosion in the crevice between the tube and tube sheet (both made of type 316 stainless steel) [12]

In the marine engineering corrosion the anion are the most domination factor[13]. The movement of the anions from the bulk to the metal surface to initiate the corrosion is important. In many general studies, it is studied that the Cl^- and SO_4^{2-} ions are the most dangerous anions which affects the corrosion rate.[14] Therefore it is important to study the effects of these anions in the marine engineering application. In this study, the area near the metal surface is studied. It is important to study the area near the metal surface because all the counter ions are getting attracted towards the metal surface. The specific characteristics such as movement, concentration, velocities, density and other characteristics can be studied. The approach to study the mechanism of corrosion in marine applications, is by Electric Double Layer structure.

Chapter 2

THEORY OF AN ELECTRIC DOUBLE LAYER

2.1. Electric double layer

An electrical double layer is the term given to any region between two different phases when charge is separated across the interface between them. It is the important phenomenon in the aqueous corrosion. In aqueous corrosion, this is the region between a corroding metal and the bulk of the aqueous environment ("free solution).[15][16]

In the sea water environment, the oil rigs structures are of steel. The Fe^{2+} ions deposited on the metal surface due to the oxidation reaction in the metal electrode. The counter ions such as Cl^-, SO_4^{2-}, OH^-, and other anions attracted towards the metal surface. There are two layers parallel to each other around the metal surface.[17] The first layer is of Fe^{2+} ions (positive charge) on the metal surface and the second layer is of the counter ions such as Cl^-, SO_4^{2-}, OH^-, and other anions. The Fe^{2+} ions adsorbed on to the metal surface due to chemical interaction and metal flux. The counter ions attracted towards the metal surface due to the Coulombs forces. This second layer is called diffuse layer, where the free ions is the bulk mover under the influence of electric attraction. [15][17]

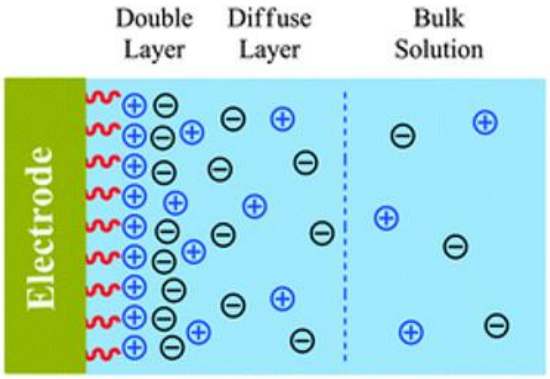

Figure 1.4 Double layer structure [18]

2.2 Chemical potential

In this system the steel surface is in the sea water. This is a distributive system. The seawater which is electrolyte, consists of mobile ions and polarizable solvent molecules. Therefore to calculate the chemical potential per particle the following expression is used to describe the electrolytic system:

$$\mu_i = k_B T \ln(n_i) + z_i e\phi - \int_0^{\boldsymbol{\tau}_i} \nabla\phi \cdot d\boldsymbol{\tau}_i + \gamma_i p, \quad (1)$$

The four terms represent the effects of configurational entropy, charge, dipole moment and mechanical pressure, respectively. Where k_B is the Boltzmann constant, *T* is the temperature, ϕ is the electrostatic potential, *p* is the (rate-independent) hydrostatic pressure, *e* is the unit charge, and n_i is the number concentration, z_i is the valance number, γ_i is the chemical expansion volume, and the $\boldsymbol{\tau}_i$ induced dipole moment of the i^{th} component, respectively. The index *i* includes all independent constituents including ions and solvent molecules.

The Langevin equation is adopted to describe the polarization of solvent molecules and ions, such as OH^-, Cl^-, H_2O and many more, carrying permanent dipole moment, in order to take into nonlinear polarization effect at high voltage. It is given by

$$\boldsymbol{\tau}_i = -\epsilon_0 \chi_i \nabla\phi, \text{ with } \chi_i \equiv \frac{3}{\bar{\tau}_{0i}E}\left(\coth(\bar{\tau}_{0i}E) - \frac{1}{\bar{\tau}_{0i}E}\right)\chi_{0i} \text{ and } \bar{\tau}_{0i} = \frac{\tau_{0i}}{k_B T}, \quad (2)$$

where ϵ_0 is the permittivity of vacuum, χ_{0i} and τ_{0i} are the linear polarization susceptibility per particle and the (permanent) dipole moment per particle of the i^{th} component, and $E = |\nabla\phi|$. It is worth noting that those Langevin mathematical statement is best appropriate will introduction polarization about permanent dipoles. In this study we extend it to describe all possible polarization mechanisms including electronic as well as orientation type so that a concise form as above can be presented relating the total polarization strength to measurable linear susceptibilityχ_{0i}. Substituting the value of $\boldsymbol{\tau}_i$ in Eq. (1) and integrating,

$$-\int_0^{\boldsymbol{\tau}_i} \nabla\phi \cdot d\boldsymbol{\tau}_i = k_B T \left(\ln\left(\frac{\sinh\bar{\tau}_{0i}E}{\bar{\tau}_{0i}E}\right) - \bar{\tau}_{0i}E\coth(\bar{\tau}_{0i}E) + 1 \right). \quad (3)$$

In Eq. (1), the first two terms of thermal and electrostatic change forces are considered in the classical formulation. In the chemical potential the polarization effect term is important to include. This term includes the transport of dipolar molecules such as H_2O and other neutral molecules towards the charged surface, and not only the ions in the electrolyte. The concentration transportation of neutral molecules with the other ions is required to be accurately known. This term is important for many applications including corrosion applications. Dipolar-Poisson-Boltzman, Quiroga, and others, attempted to include the term of electrostatic polarization effect. However, their expression seems only appropriate for constant (rather than induced) dipoles always in alignment with electrical field$-\nabla\phi$. Meanwhile, they applied the Langevin equation for the dipole moment in controversy.

2.3 Dynamic Transport and Other Field Governing Equations

As the particle is moving to attain the equilibrium. Taking derivative of the potential it gives the force. This force is driving force to the particle. There is resistance force to the motion of the particle in the system. Therefore these two forces are balance and we have the velocity to the particle. According to Fick's first law, the flux of the i^{th} species may be expressed as $\boldsymbol{j}_i = -M_i n_i \nabla\mu_i$, in which M_i is the mobility of the i^{th} species that can be a complex function of concentrations of all components. By substituting Eq. (1) in the flux equation and effecting Einstein's relation$D_i = M_i k_B T$, the flux of the i^{th} species is obtained as

$$\boldsymbol{j}_i = -D_i \nabla n_i + n_i \left[M_i \left(-z_i e \nabla\phi + \frac{\epsilon_0 \zeta_i}{2} \nabla(\nabla\phi \cdot \nabla\phi) - \gamma_i \nabla p \right) + \boldsymbol{u} \right], \quad (4)$$

where $\boldsymbol{u}$ is the velocity, and electric field-dependent constant ζ_i is given by

$$\zeta_i = 3\left(\frac{1}{(\bar{\tau}_{0i}E)^2} - \coth^2(\bar{\tau}_{0i}E) + 1 \right) \chi_{0i}. \quad (5)$$

The above constant $\zeta_i \cong \chi_{0i}$ if $\bar{\tau}_{0i}E \ll 1$. According to the law of mass conservation, the equation of dynamic transport is given by

$$\frac{\partial n_i}{\partial t} = -\nabla \cdot \boldsymbol{j}_i + R_i, \tag{6}$$

where t is the time, and R_i is the production rate of the i^{th} component from chemical reaction. All the above equation in this section completes the Mass transport theory for this study.

This process of mass transport involves electrostatic force and mechanical force. Therefore we have to supplement the mass transport theory with Gauss' law and mechanical equilibrium equations. For the electrostatic potential field, the Gauss' law/Poisson's equation is applied:

$$\nabla \cdot \epsilon_0(1 + \sum_i \chi_i n_i)\nabla\phi + \sum_i z_i e n_i = 0, \tag{7}$$

where the second term is the total charge density due to the separation of anions and cations, and the electric field-dependent susceptibility χ_i is given in Eq. (2). It is assumed that the polarization effect is additive from all constituents.

Assuming that the electrolyte used is a compressible Newtonian fluid, the equilibrium equation according to Newton's law is given by

$$-\nabla p + \nabla \cdot \eta\left(\nabla\boldsymbol{u} + \nabla^T\boldsymbol{u} - \frac{2}{3}\mathbf{I}\nabla\cdot\boldsymbol{u}\right) - \sum_i z_i e n_i \nabla\phi + \frac{1}{2}\epsilon_0 \sum_i \zeta_i n_i \nabla(\nabla\phi\cdot\nabla\phi) = 0, \tag{8}$$

where the hydrostatic pressure p is due to "elastic" deformation, given by an equation of state, the second term is due to viscous flow, the third term is the electrostatic charge force density, and the fourth term is the electrostatic polarization force density due to induced dipoles. It is well known that the electrostatic charge force density can be expressed as the divergence of Maxwell's stress. In contrast, the electrostatic polarization force thickness from claiming Langevin dipoles is determined starting with the Korteweg-Helmholz method. It may be steady of the thermodynamic force to mass transport in eq. (4), which is no astonishment since the Korteweg-Helmholz method

is concocted taking after the same principle on foundation of the chemical potential. It might a chance to be worth specifying that a few separate expressions about Korteweg-Helmholz force density can be found in Different papers. They are commonly effects for further inference under specific states. The present electrical force density is derived directly from Eq. (15) in Sec. 3.7 in reference [19]. It might also be worth noting that the above third term of polarization force density reduces to the Kelvin force density $\left(\equiv \frac{1}{2}\epsilon_0 \sum_i \chi_i n_i \nabla(\nabla\phi \cdot \nabla\phi)\right)$ when$\bar{\tau}_{0i}E \ll 1$. In other words, the Kelvin force density, can be express as product of the dipole moment with electric field gradient, which is not applicable in the nonlinear Langevin dipoles. The microscopic forces that singular induced dipoles (in average) encounter don't constantly include linearly likewise those perceptible electrical forces.

Lastly, rate-independent hydrostatic pressure *p* is expressed in an EOS as$p = p(N, V, T)$, where $N(\equiv \sum n_i)$ is the total number of particles per unit volume, and $V(\equiv \sum v_i = \sum n_i \gamma_i)$ is the packing density. The well-known Carnahan-Starling EOS for repulsion [20] plus van der Waals attraction term [21] is adopted, which is given by

$$\frac{p}{Nk_BT} = \frac{1+V+V^2-V^3}{(1-V)^3} - \frac{a}{k_BT}, \tag{9}$$

with $a = \sum n_i a_{ij} n_j$, where a_{ij} describes the attractive interaction effect between species *i* and *j*. Note that we generalize it for multicomponent mixtures, with $a_{ij} = \sqrt{a_{ii}a_{jj}}$, similar to how the literature has treated the Lennard-Jones potential for mixtures[4]. Constant a_{ii} for a single component can be found from the pressure and temperature at the critical liquid-vapor point.

2.4. Finite Volume Method for One-dimensional Planar Problems

A finite volume method is used to numerically solve the above set of governing equations (Eqs. (6)-(9)) along with required initial-boundary conditions for fields n_i, ϕ, ***u*** and *p* in one-dimensional planar problems of an EDL. By imputing a finite volume method, the first step is to

present the problem of a divergence equation governing a field over a domain with surface integrals of flux according to the divergence theorem. [23] This is applied to each one of the cells (i.e., finite volumes) used to discretize the overall domain. The flux at cell boundaries is then approximately evaluated from nodal values of a field defined within the cells. When the flux, though approximate, is applied identically to adjacent cells sharing the surface where it is defined, the law of conservation of the field quantity is always satisfied. Since the present multi-physics problem is highly nonlinear, an iterative scheme is indispensable.[22]

By discretize a one-dimensional finite domain into *M* cells, numbered in order from 1 to *M*. Each cell is assigned with a node at the middle point. Potential ϕ, concentration n_i and velocity $\boldsymbol{u}$ are the basic quantities, and are defined on the nodes. There are *M* nodal degrees of freedom for either one of ϕ, n_i or $\boldsymbol{u}$. Thus, one needs to gather *M* algebraic equations to solve for each one of them. This is attained by applying Eqs. (6)-(8) to each cell. Based on the nodal values, the fields of ϕ, n_i and $\boldsymbol{u}$ near a knot *m* are approximated as

$$\phi(x;x^m) = \sum_q N_q^m(x)\phi_q, \tag{10a}$$

$$n_i(x;x^m) = \sum_q N_q^m(x)n_{iq}, \tag{10b}$$

$$\boldsymbol{u}(x;x^m) = \sum_q N_q^m(x)\boldsymbol{u}_q, \tag{10c}$$

where superscript *m* indicates the m^{th} knot, subscript *q* indicates the q^{th} node selected to approximate the field around knot *m*, and $N_q^m(x)\left(=\prod_{p\neq q}\left(\frac{x-x_p}{x_q-x_p}\right)\right)$ is the Lagrange interpolation function in terms of selected nodal coordinates around knot *m*. In later numerical examples, two nodes from the left side and two nodes from the right side, if available, are chosen to approximate a field about a knot. For knots near the ends (i.e., domain boundary), lower-rank interpolation is used, since there may be less than two nodes available on the end side. Derivatives and integrals

of these fields around a knot can be conveniently obtained from Eq. (10). For the sake of brevity, their explicit expressions are not presented here.

Using the divergence theorem, the governing equation of electrostatics (Eq. (7)) over the m^{th} cell between knots m-1 and m is turned into

$$\epsilon^{m,l}\left(\phi_{,x}\right)^{m,l+1} - \epsilon^{m-1,l}\left(\phi_{,x}\right)^{m-1,l+1} + \sum_i z_i e n_{im}^{l} \left(\Delta x\right)_m = 0, \tag{11}$$

where $\epsilon^{m,l} \equiv \epsilon_0\left(1 + \sum_i \chi_i^{m,l} n_i^{m,l}\right)$, valid for $\epsilon^{m-1,l}$ as well, $(\Delta x)_m$ is the cell size, superscript l after comma indicates the l^{th} iterative step, and subscript comma indicates partial differentiation with respect to the indices that follow. Again, superscript m (or m-1) in the first two terms indicates that ϵ and $\phi_{,x}$ are evaluated at knot m (or m-1) based on nearby nodal values by Eq. (10) and its derivatives. For example, $\left(\phi_{,x}\right)^{m,l+1} = \sum_q N_{q,x}^{m}(x = x^m)\phi_q^{l+1}$. By assuming that all quantities at the l^{th} iterative step are known, Eq. (11) offers an algebraic equation of unknown nodal values of potential at the (l+1)$^{\text{th}}$ iterative step.

At the same time, the governing equations of mass transport (Eqs. (4) and (6)) within the m^{th} cell between knots m-1 and m are turned into

$$\frac{(\Delta x)_m}{\Delta t}\left(n_{im}^{l+1} - n_{im}^{0}\right) + \left(j_i^m - j_i^{m-1}\right) - (\Delta x)_m R_{im} = 0, \tag{12a}$$

$$j_i^* = -D_i^{*,l}\left(n_{i,x}\right)^{*,l+1} + \left(A^{*,l} + u^{*,l}\right)n_i^{*,l+1}, \text{ with } *= m, m-1, \tag{12b}$$

$$A \equiv M_i\left(-z_i e\phi_{,x} + \epsilon_0\zeta_i\phi_{,x}\phi_{,xx} - \gamma_i p_{,x}\right), \tag{12c}$$

where n_{im}^{0} is the nodal concentration at the previous time step, and Δt is the time step. Though more complicated, Eq. (12) works the same as Eq. (11) to offer an algebraic equation of unknown nodal values of n_i at the (l+1)$^{\text{th}}$ iterative step given all quantities at the previous iterative step. Above p is computed from Eq. (9). The time rate-of-change term in Eq. (6) is treated above as a source term with time-marching step Δt. Meanwhile, all other terms/quantities involved in Eq. (4)

of j_i are evaluated at the current time step; thus, an implicit finite difference scheme is used to treat the temporal dynamics of the problem.

Furthermore, the equilibrium equation of force balance (Eq. (8)) over the m^{th} cell between knots m-1 and m are turned into

$$-\left(p^{m,l}-p^{m-1,l}\right)+\frac{4}{3}\left(\eta^{m,l}\left(u_{,x}\right)^{m,l+1}-\eta^{m-1,l}\left(u_{,x}\right)^{m-1,l+1}\right)+(\Delta x)_m f_m=0, \tag{13a}$$

$$f=-\sum_i z_i e n_i \nabla\phi+\frac{1}{2}\epsilon_0\sum_i \zeta_i n_i \nabla(\nabla\phi\cdot\nabla\phi). \tag{13b}$$

This set of algebraic equations is solved for velocity field u at each iteration step.

Equations (11)-(13) are only applicable to interior cells. For boundary cells, the quantities evaluated at the knot at the boundary end should be replaced by a prescribed boundary condition. If a flux boundary condition is prescribed, the replacement is straightforward. If a potential/concentration boundary condition is prescribed, it is converted into a flux boundary condition with a penalty coefficient. For instance, for diffusion at the far end (i.e., knot M), it is written: $j_i^M=k^M\left(n_i^M-\bar{n}_i^M\right)$, where k^M is the penalty coefficient, a numerical parameter, $\bar{n}_i^M$ is the prescribed value of concentration, and n_i^M is the concentration at knot M and expressed in terms of two nodal values next to the end by Eq. (10). If k^M is set sufficiently large, $n_i^M=\bar{n}_i^M$ is approximately obtained, with controlled, negligible numerical error.

The solution procedure is briefly described as follows. Given appropriate initial and boundary conditions, the problem is solved incrementally in time and iteratively over each time step. Marching in time poses little issue in this case of a parabolic problem in nature. For each iterative step l+1, a system of algebraic equations with nodal potential $\phi_m^{,l+1}$ as variables and all coefficients and other quantities evaluated from previous iterative step l is assembled from Eq. (11). The stiffness matrix is inverted to solve for nodal potentials at the (l+1)th iterative step. Then, nodal concentrations of the first chemical component at the (l+1)th iterative step is solved by inverting

the stiffness matrix assembled from Eq. (12) with *i* =1. This is repeated until nodal concentrations of all chemical components are updated. Finally, Eq. (13) is solved to update velocity *u*. However, since the present problem is highly nonlinear, especially when concentrations reach their saturation values, this scheme with no relaxation may become unstable. Instead, the following over-relaxation scheme is used; for instance, for potential, $\phi_m^{,l+1} = \phi_m^{,l} + \alpha\Delta\phi_m$, where $\Delta\phi_m$ is the difference of above obtained new value of ϕ_m from $\phi_m^{,l}$, and α is the relaxation factor. Typically a larger α leads to faster convergence, but greater chance of numerical instability. Trials are needed to identify reasonable value of α.

CHAPTER 3

OBJE CTIVE AND PROBLEM FORMULATION

3.1 Objective

To study, the Electric Double Layer structure and its importance in the corrosion of steel in seawater, varying the important parameters such as voltage, metal flux, initial concentration and other.

3.2 Problem Formulation

- Offshore Oil Rigs installed in the sea water electrolyte.
- Finite Volume Method for One-dimensional Planar Problems
- Charges distribution is uniform at zero potential.

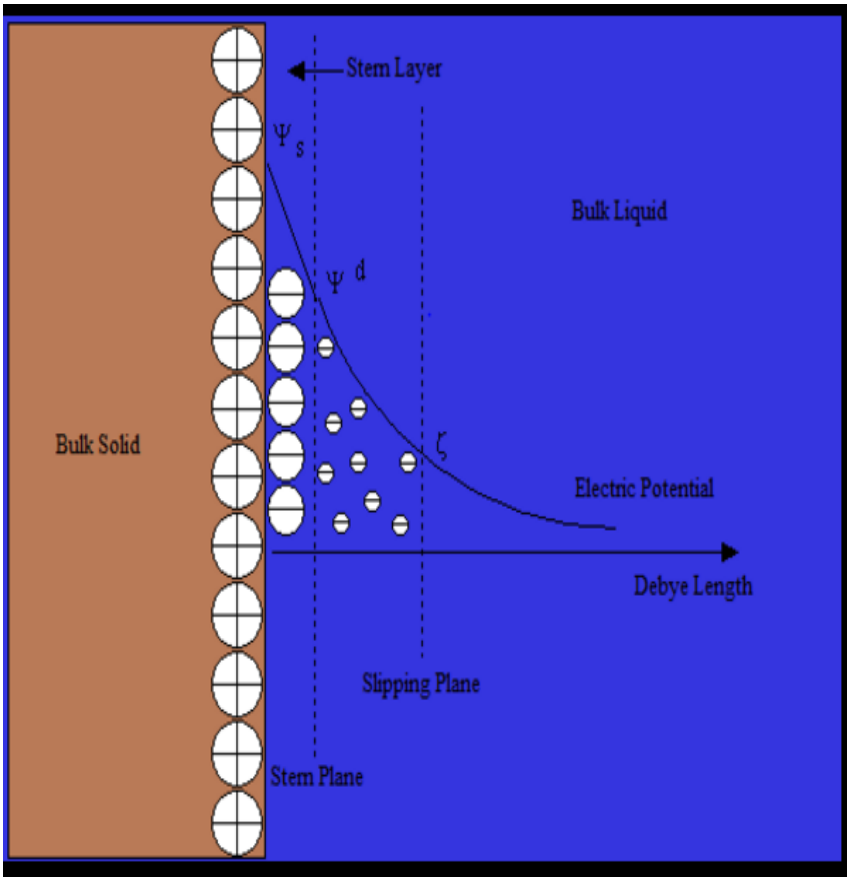

Figure3.1.Detailed illustration of interfacial DL [24]

3.3 Boundary conditions

- Potential is present at the metal surface end (electrode)
- Zero potential at infinite distance from electrode.
- Concentration are fixed at infinite distance.

CHAPTER 4

NUMERICAL ISSUSES

The electrolyte which is sea water in this system is spread at the infinite distance and diffusion of the ions continues over the infinite distance from the metal surface. Therefore it is important to truncate the simulation domain for the system. The Debye screening length gives the rough estimate to determine the simulation domain. However it is not accurate. Therefore trial and error method is used to truncate the simulation domain.

For0.5nm

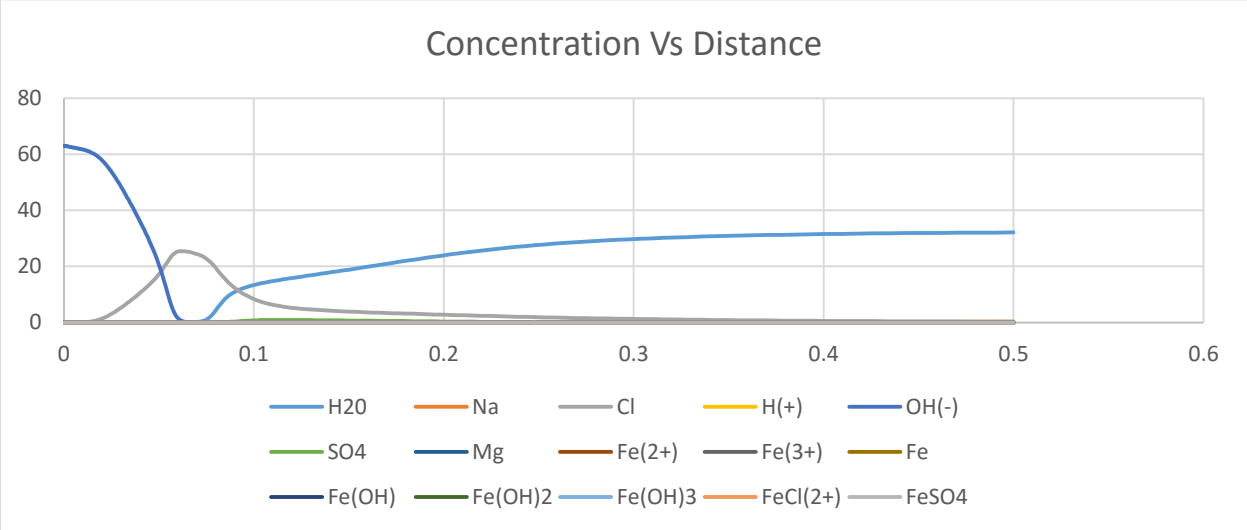

Figure4.1.Concentration Vs Distance graph for 0.5nm simulation domain

It is observed that all the ions and molecules have not yet attain the equilibrium over this domain. Therefore the large simulation domain is considered for this system.

For 1.5nm

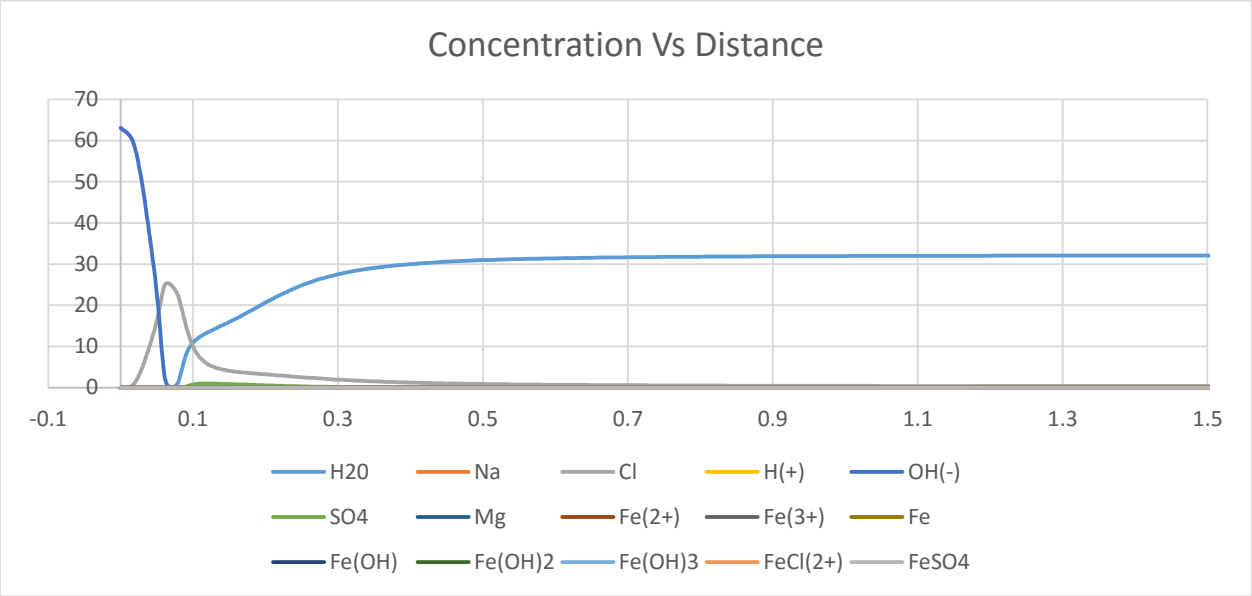

Figure 4.2.Concentration Vs Distance graph for 1.5nm simulation domain

For 1nm

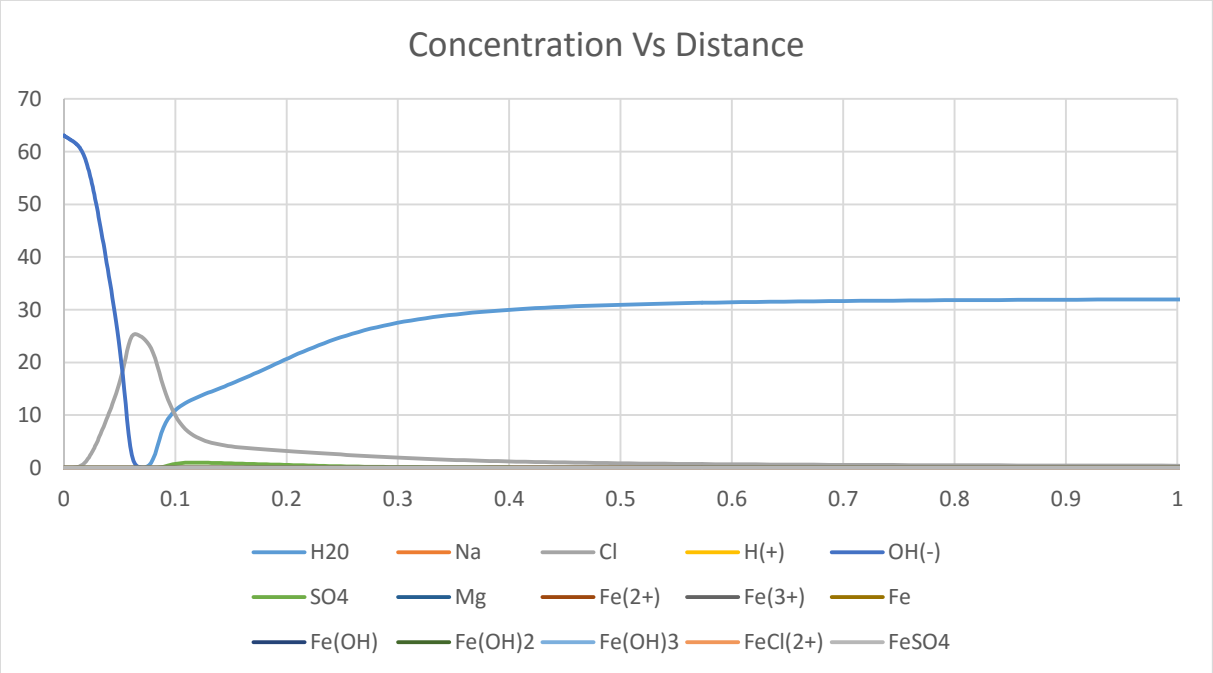

Figure 4.3.Concentration Vs Distance graph for 1nm simulation domain

It is observed that at 1 nm all the ions and molecules concentration is in equilibrium. Therefore 1nm is optimal and efficient solution for this system.

CHAPTER 5

NUMERICAL RESULTS AND OBSERVATIONS

The numerical result obtained by changing the integral parameter such as voltage, corrosion flux and bulk concentrations. To investigate the interfacial structure of an electrical double layer (EDL) and provide mechanistic understanding of the formation of an EDL at a metal surface in seawater environment, it is important to study the significance of all these parameter.

To stimulate the oil rig structure model in sea water, some important physical parameter are taken into consideration. In the model of electric double layer structure important parameter is the stoke radii of the ions in the sea water. The stoke radii is integral physical parameter in the double layer structure to study the concentration of the ions at the metal surface. Stokes radii of the ions present is calculated from the diffusion co-efficient at particular temperatures.

5.1 Numerical results and observation varying voltage

The voltage change in the model affects the structure of the double layer. Thus, it is important to study the voltage change in the system to predict and determine the corrosion mechanism.

5.1.1 Numerical observation applying 0.2V to the system

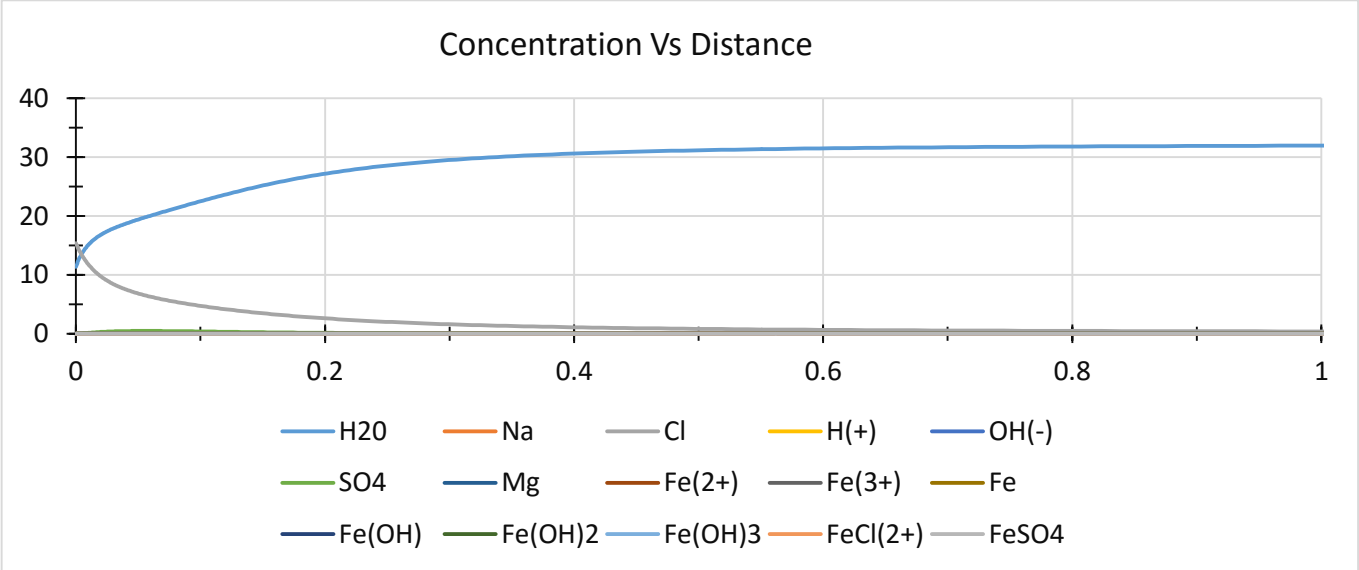

Figure 5.1.Concentration Vs Distance graph for 0.2V

It is observed that in electrical double layer structure, Cl^- concentration on the metal surface is high at this voltage, and it is decreasing away from the metal surface. The Cl^- ions are attracted toward the metal surface at higher concentration. The concentration of Cl^- ions at the metal surface is 15 e/nm^3. At the same time SO_4^{2-} concentration is very less at the metal surface and away from the metal surface. Meanwhile the water molecules are pushed away from the metal surface at this voltage. The water molecules concentration at this voltage is still on the higher side. This implies the Cl^- is the dominating corroding factor for the system at this voltage. Therefore it is observed, pitting is the mode of corrosion at this voltage.

Another important parameters are Packing factor and Velocity of the ions responsible for corrosion phenomenon. In the following figures the packing factor and velocities are plotted to illustrate their importance in the double layer structure.

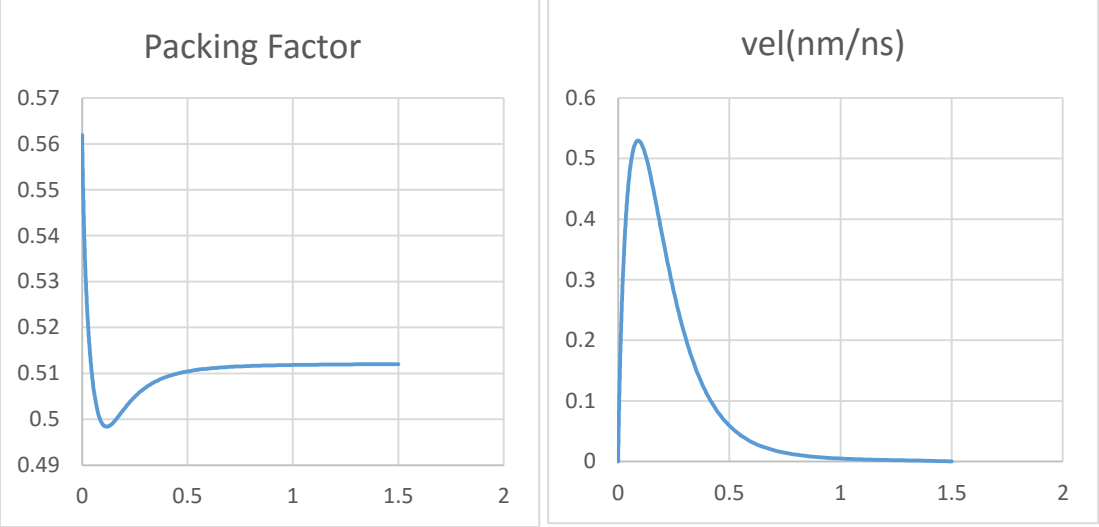

Figure 5.2.Packing factor and Velocity Vs Distance graph for 0.2V

It is observed that at the metal surface the packing factor is high (0.56) which implies the densiy near metal surace is maximum. The packing factor keep decreasing away from the metal surface till 0.2 nm. After 0.2 nm packing factor increase till 0.5nm and remians constant after this point.

Correspondingly the velocity of the ions present in the sea water at the metal surface is low. The velocity of the ions away from metal surface is observed to increas exponentially till 0.1 nm, afterward the velocity decreases exponentially till 0.5nm. From 0.5 to 1 nm the velocity of the ions decreases gradually and, thereafter it remains constant in the bulk.

5.1.2 Numerical observation applying 0.5V to the system

Increasing the voltage of the model to 0.5V, there is significant change in the electrical double layer.

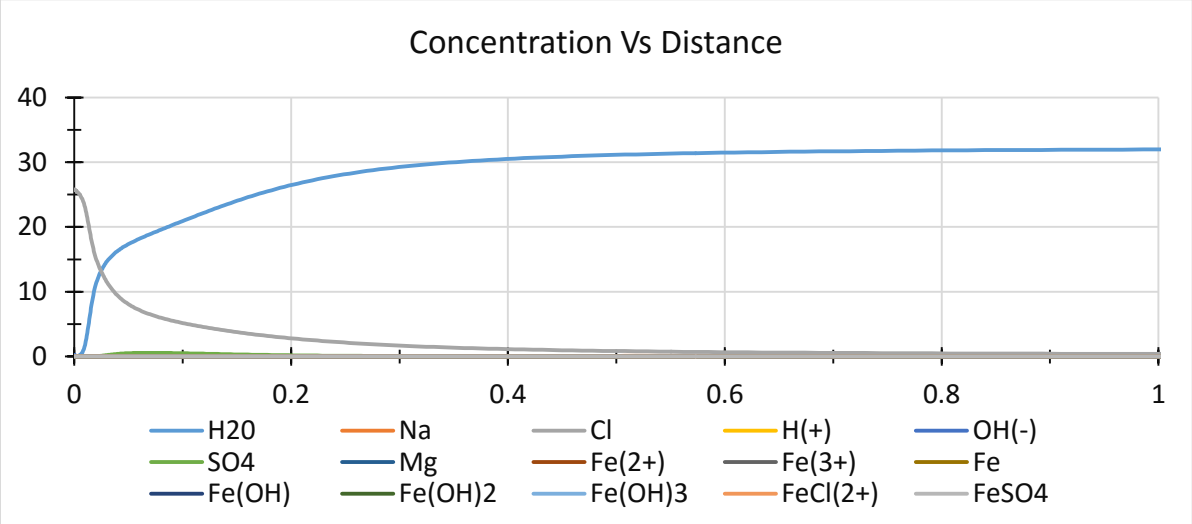

Figure 5.3.Concentration Vs Distance graph for 0.5V

It is observed that the Cl^- concentration is high towards the metal surface at this voltage. The Cl^- concentration has increased significantly compare to previous case at this higher voltage. The concentration is decreasing gradually away from the metal surface towards the bulk. Likewise the concentration of SO_4^{2-} ions also increase at the metal surface slightly, and then gradually decreases away from the metal surface. At this voltage it is observed that, the pitting corrosion is accelerated because of the higher concentration of Cl^- and SO_4^{2-} ions. In the meantime the water molecules are pushed away from the metal surface. The change in concentration of water

molecules at this voltage is an important observation. The water concentration on the metal surface at this higher voltage is low. As contrast with the lower voltage in previous case, the water molecules concentration exactly at the metal surface is immaterial in this case.

The packing factor profiles is similar to the earlier case at 0.2V. The significance change at 0.5V is, the ions density at the metal surface is higher 0.65. Compare to earlier case the density has been increased by 10% at the metal surface. The important observation in this case is that, the nature of the density curve where the packing increasing from 0.2nm and remains constant after 0.5 nm, is same for both the cases.

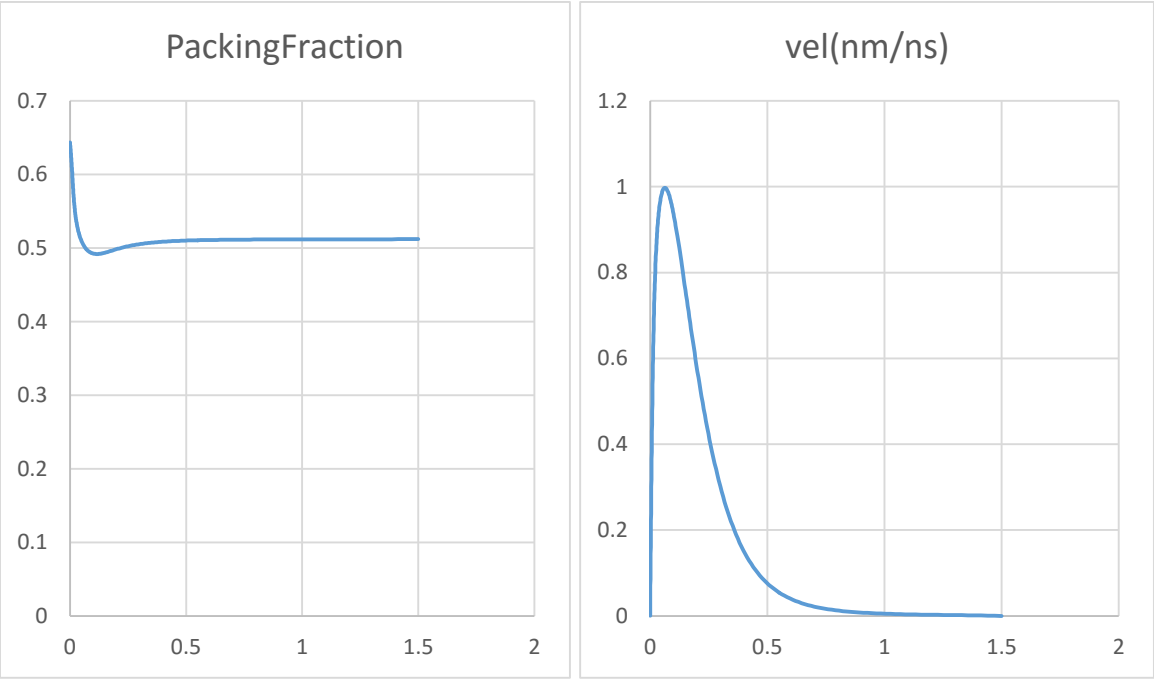

Figure 5.4.Packing factor and Velocity Vs Distance graph for 0.5V

In the same way the velocity profile at 0.5V is similar to the earlier case. At the metal surface the solution velocity is zero. It is observed the velocity of solution away from the metal surface exponentially increases till 0.1 nm. The important observation at this voltage is that, the maximum velocity is twice as compare to the earlier case.

5.1.3 Numerical observation applying 0.7V to the system

The change in the voltage reflects the significance importance in the system. Increasing the voltage to 0.7V changes the electrical double layer structure which can be notice in the following figures

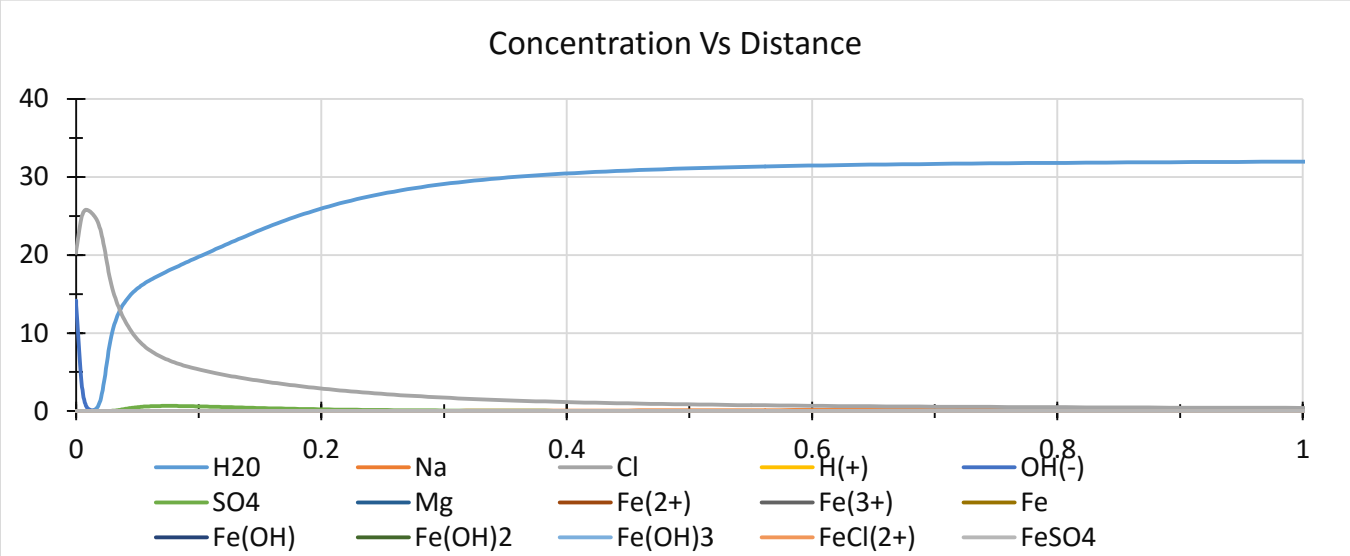

Figure 5.5. Concentration Vs Distance graph for 0.7V

At this voltage the vital observation is the concentration at the metal surface. The dominating concentration of ions near the metal surface is still the Cl^-, but OH^- ions concentration is also considerably increased. The increase in OH^- concentration is compare to earlier voltages (0.2 and 0.5) is high. The concentration of OH^- ions are higher than the SO_4^{2-} at this voltage, and the SO_4^{2-} ions are pushed away from the metal surface. The pitting corrosion effect at this voltage due to SO_4^{2-} ions decreases to significant level. Since the concentration of Cl^- ions are still soaring at this voltage, therefore Cl^- ions are responsible for pitting phenomenon.

5.1.4 Numerical observation applying 0.8V to the system

After varying the voltage from 0.5 to 0.7V the magnitude of concentrations near the metal surface changed considerably. It is vital to study the further increase in the voltage. Increasing the voltage to 0.8V there is an important observation compare to all the previous cases. At this voltage the dominating concentration at the metal surface is OH^- ions. The Cl^- ions concentration considerably decreases at the metal surface.

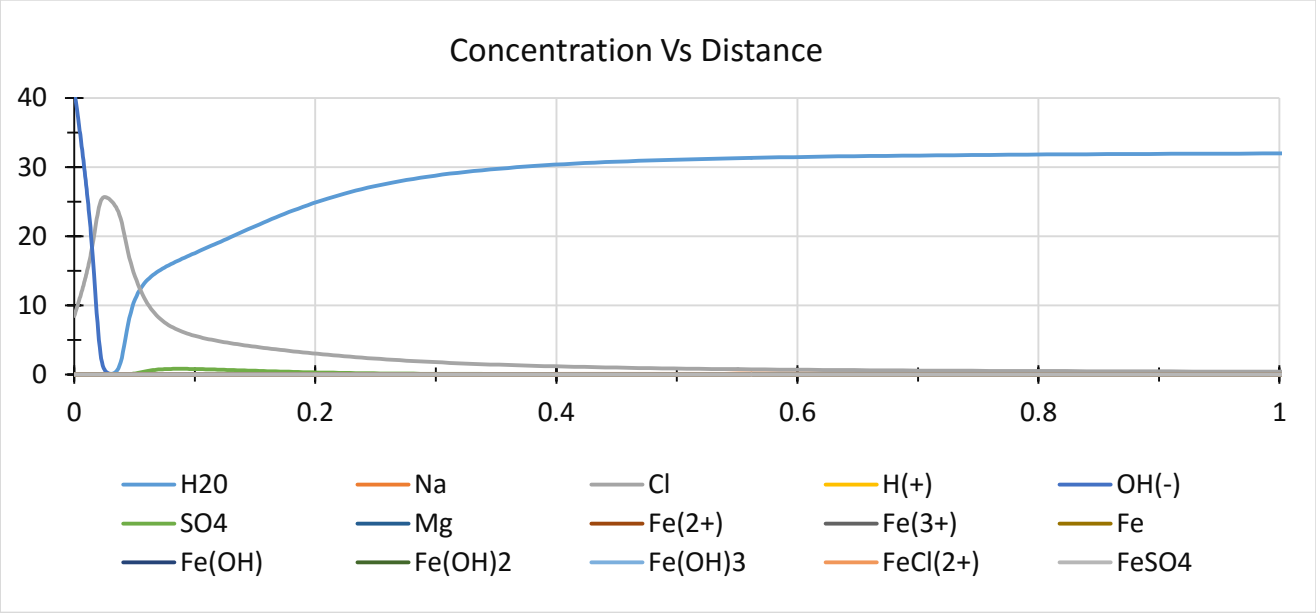

Figure 5.6. Concentration Vs Distance graph for 0.8V

It can be observed that the concentration of the Cl^- ions is 9 particle/nm^3 whereas the concentration of the OH^- ions is 40 e/nm^3. The SO_4^{2-} ions are pushed away further from the metal surface. Meanwhile, the water molecules at this voltage is further pushed away from the metal surface. It is clear from the figure that H_2O concentration at the metal surface is negligible at the metal surface, and it increases gradually away from the metal surface towards the bulk.

Packing factor at this voltage is identical to the 0.5V profile. The maximum density 0.65 at this voltage is at the metal surface and it remains constant over a short distance away from the metal

surface. The minimum density is at 0.2nm away from the metal surface, and increase gradually till 0.5nm. After 0.5 nm it remains constant towards the bulk.

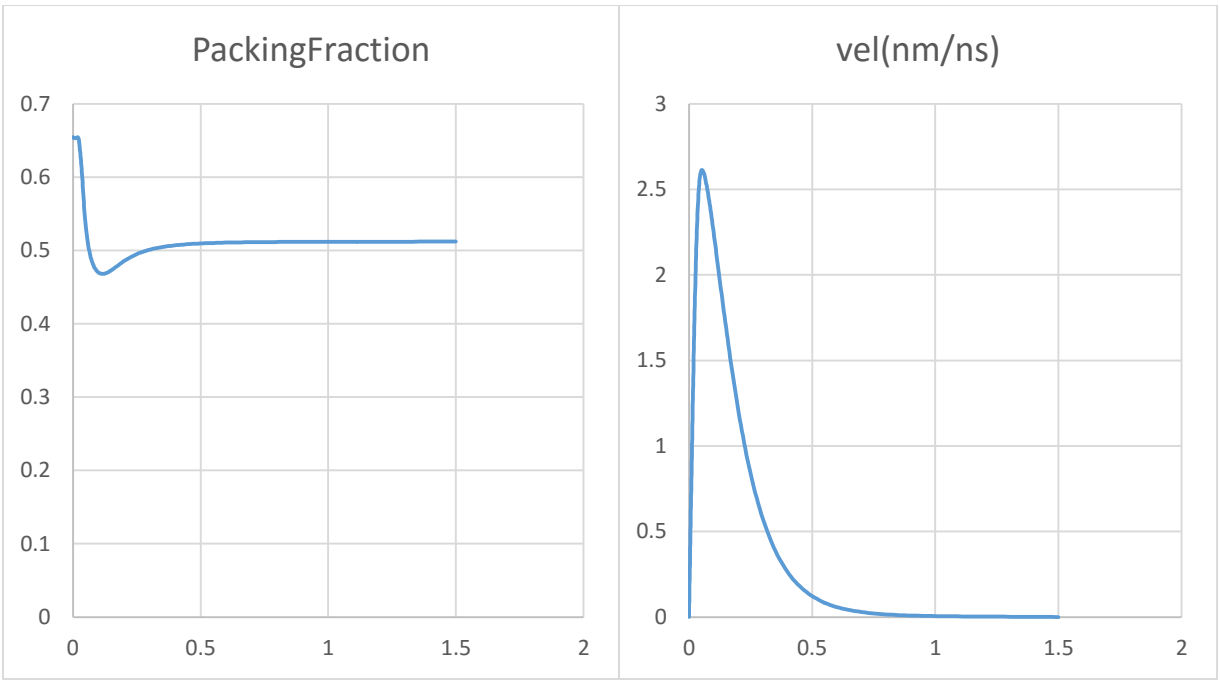

Figure 5.7.Packing factor and Velocity Vs Distance graph for 0.5V

The velocity of the ions at the metal surface is zero. It rises up exponentially over the short distance away from the metal surface. The maximum velocity at this voltage is 2.7nm/ns. In the earlier of 0.5V the velocity over the same distance is 1nm/ns, which is considerbaly less compare at this voltage. The velocity of ions decreases exponentially from 0.1 nm away from the metal surface.

5.1.5 Numerical observation applying 1.2V to the system

Increasing the voltage to 1.2V, it can be observed that dominating concentration near the metal surface is OH^- ions. The OH^- ions concentration at the metal surface is 65 particle/nm^3. The concentrations of the other cations such as, Cl^- and SO_4^{2}, pushed away from the metal surface at higher rate. At the same time the H_2O molecules at this voltage is further pushed away from the metal surface. The concentrations of the other cations such as, Cl^- and SO_4^{2-}, pushed away from

the metal surface at higher rate. This implies the rate of pitting corrosion decreases at this voltage.

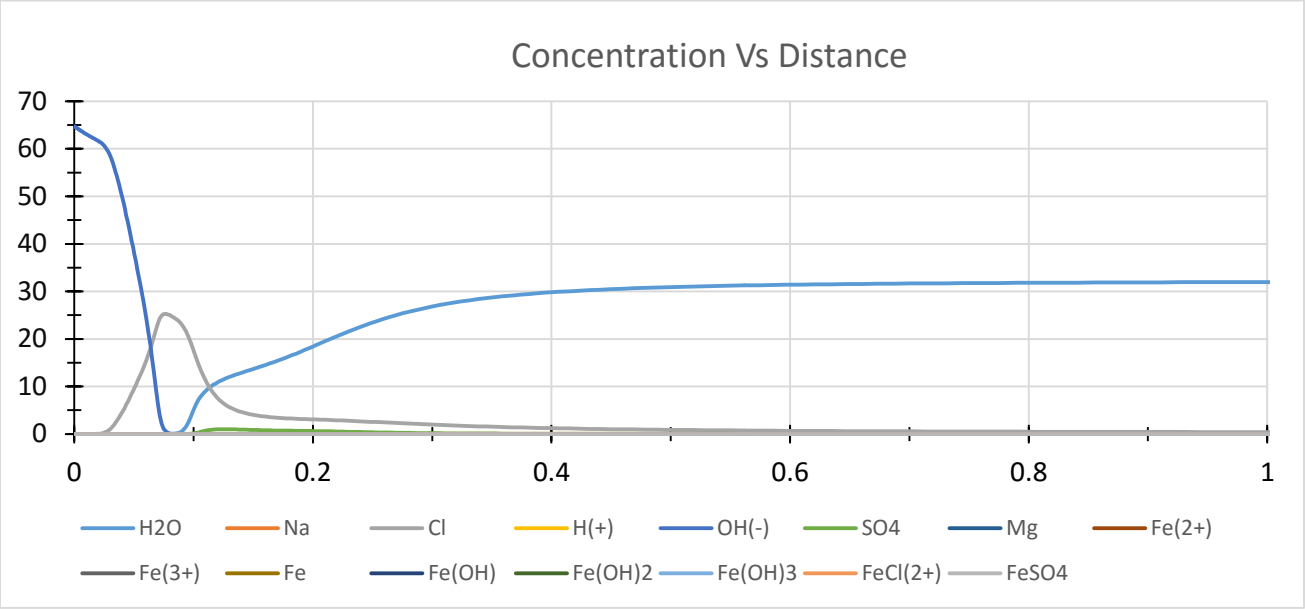

Figure 5.8. Concentration Vs Distance graph for 1.2V

It is clear from the above figure that H_2O concentration at the metal surface is negligible at the metal surface till 0.1nm, and it increases gradually away from the metal surface towards the bulk.

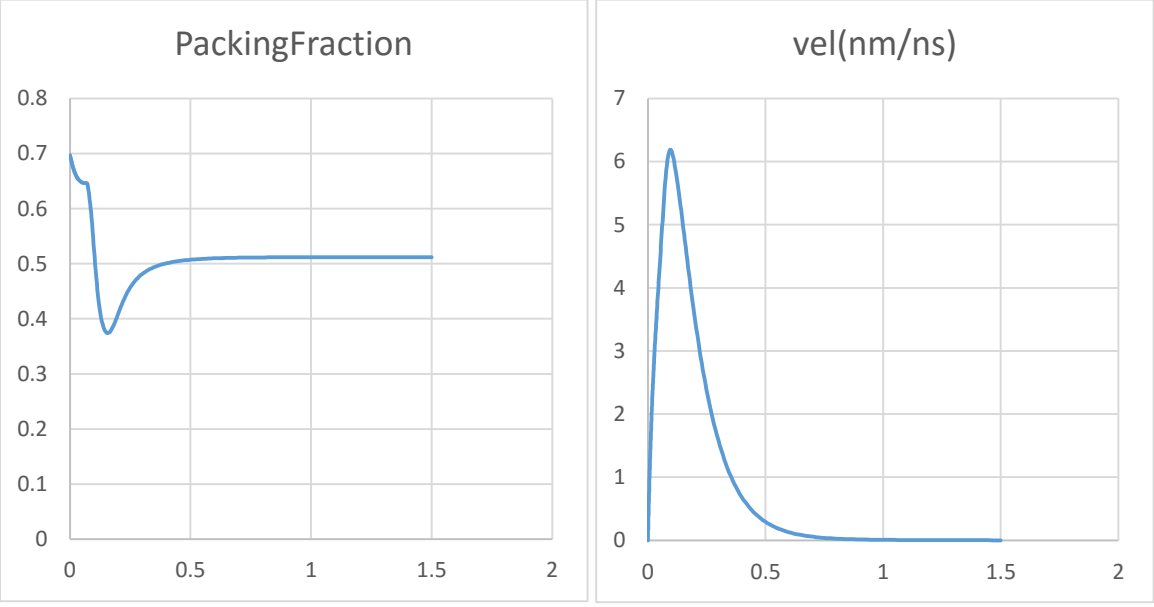

Figure 5.9. Packing factor and Velocity Vs Distance graph for 1.2V

The maximum density of the solution (0.7) is at the metal surface and it decreases gradually till 0.07 nm away from the metal surface. After 0.07nm the velocity of the corroding ions decreases gradually till 0.2 nm. The minimum density is at 0.2nm away from the metal surface 0.375. The minimum density is at 0.2nm away from the metal surface 0.375. It is noticed that this is the minimum velocity among all the earlier cases lower than 1.2V

The velocity of the solution is minimum at the metal surface and 1nm away from the metal surface towards the bulk. It rises up exponentially over the short distance away from the metal surface. The maximum velocity at this voltage is 6.2nm/ns. In the earlier at 0.8V the velocity over the same distance is 2.8nm/n. That implies at this volatge in the region of 0.01 to 0.2nm region the mobility of the ions are high. The velocity of ions decreases exponentially from 0.1 nm away from the metal surface towards the bulk.

5.1.6 Numerical observation applying 1.7V to the system

Further, increasing the voltage to 1.7V the OH^- concentration at the surface increses to 68 e/nm^3.

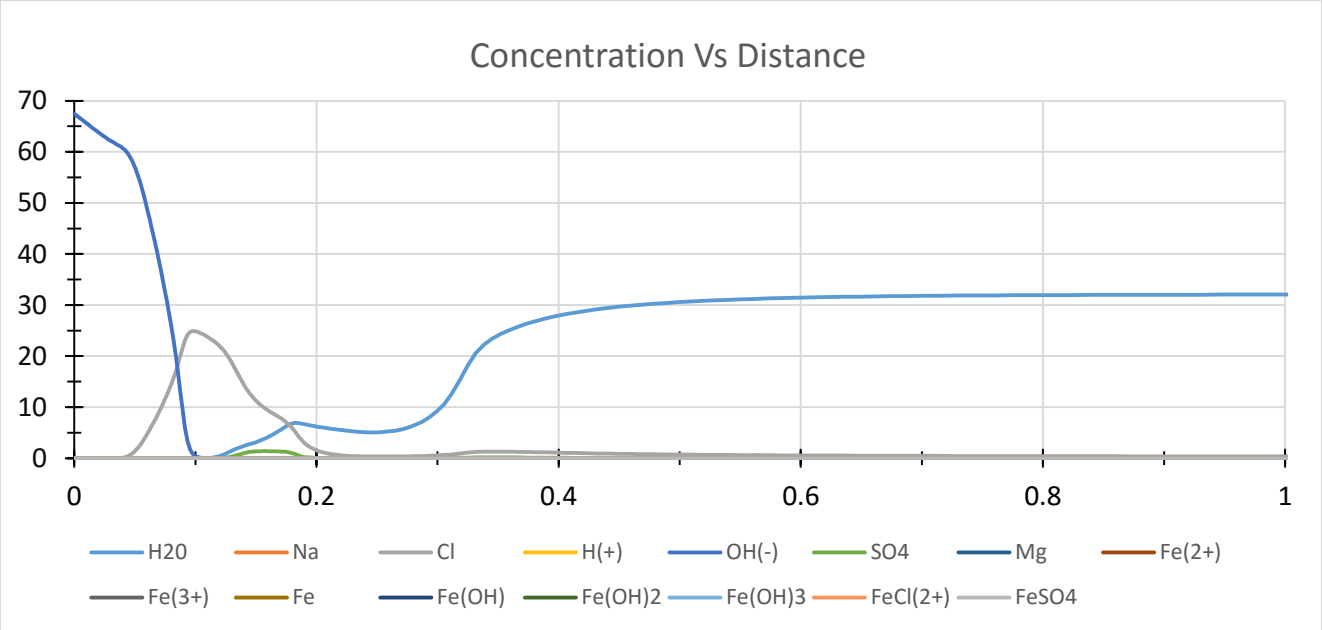

Figure 5.10. Concentration Vs Distance graph for 1.7V

The change in concentration of OH^- ions at the metal surface is not huge. But the concentration of the OH^- ions near the metal surfaces increases from 0.08nm at 1.2V to 0.1nm at this voltage. This indicates that OH^- is ions are the dominating concentration around the metal surface.The Cl^- and SO_4^{2-} ions are pushed further away from the metal surface. the concentration of Cl^- and SO_4^{2-} near the metal surface is less. Therefore, at this voltage the pitting corrosion rate is slow compare to all the low voltages. Meanwhile, the H_2O concentration at the metal surface is negligible at the metal surface till 0.13nm, and it increases gradually away from the metal surface towards the bulk.

The density of the ions are maximum at the metal surface 0.73. The minimum density is 0.08 at 0.2nm from the metal surface. The region of 0.2nm away from the metal surface is the most ions denser region.

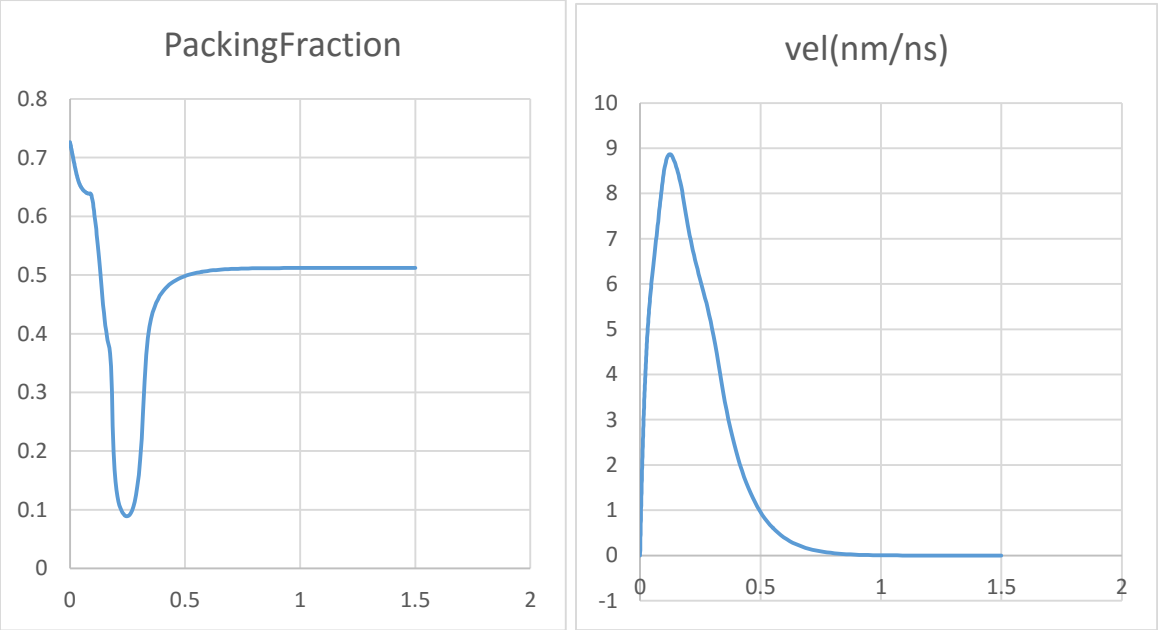

Figure 5.11. Packing factor and Velocity Vs Distance graph for 1.7V

The velocity of the ions is minimum at the metal surface. It rises up exponentially over the short distance away from the metal surface. The maximum velocity at this voltage is 8.9 nm/ns. That implies at this volatge in the region of 0.01 to 0.2nm region the mobility of the ions are high. The velocity of ions decreases exponentially from 0.1 nm away from the metal surface towards the bulk.

5.2 Numerical results and observation varying voltage with electric flux

Another important parameter in the double layer structure is the metal ion flux at the metal surface. The flux for any volatge is calculated by the polarization curve for the Fe metal as shown in the fig. The polarization curve is the basic kinetic law for any electrochemical reaction. Therefore it is important to study the metal flux at different voltages.

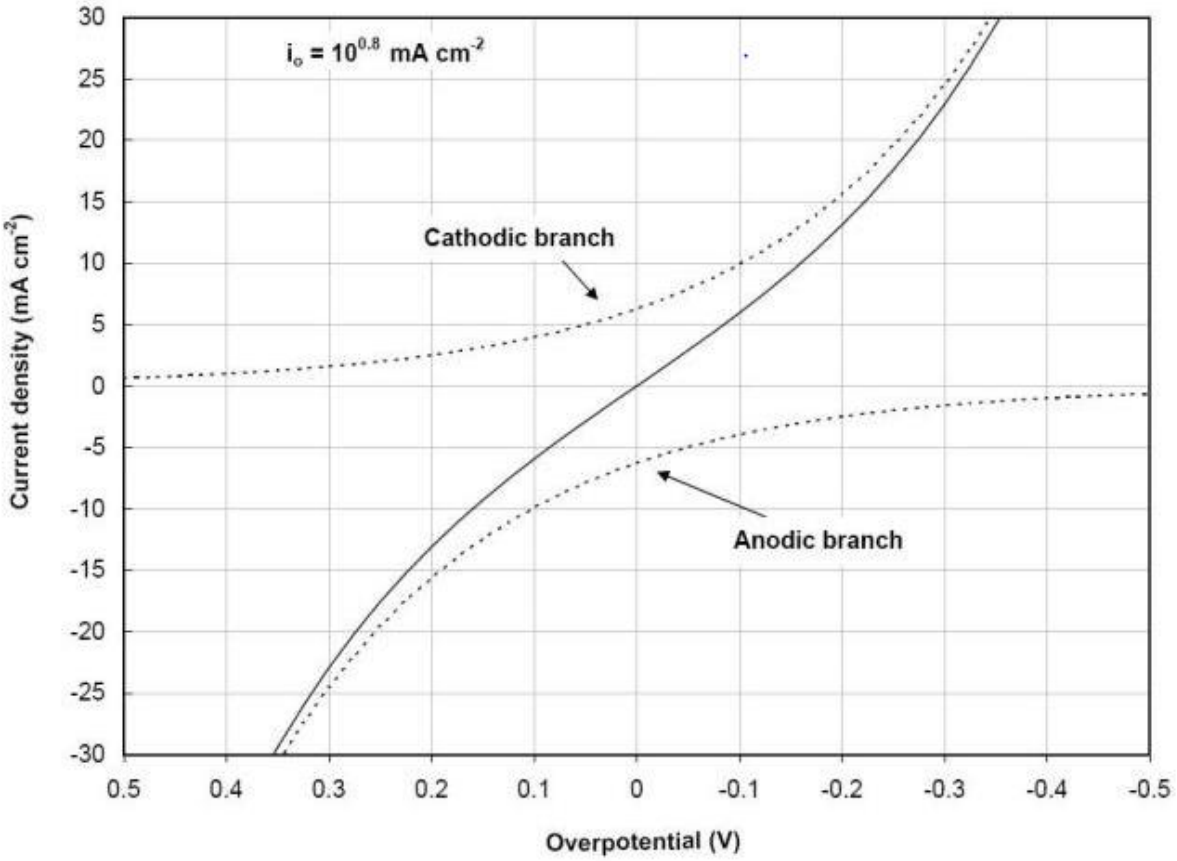

Figure. 5.12.Current density vs overpotential graph for steel[25]

To calculate, metal flux below equation is used

$$ia = io \exp\left(\frac{\beta\, n\, F\, \eta}{R\, T}\right)$$

Current density, $\eta = \text{ba. Log}\left(\frac{\text{i}}{\text{io}}\right)$

Anodic slope, $ba = 2.303\frac{R\, T}{\beta\, n\, F}$

ia = Anodic Current Density,

io = Exchange Current Density,

ß = Anodic Charge transfer Coefficient

F = Faraday Constant = 96500 C/mol

η = Over potential, V,

R = Gas Constant, 8.314 J mol-1 K-1

T = Temperature

5.2.1 Numerical observation applying 3.365d-10 e/nm^2 /ns to the system

At 0.5V the Fe flux is 3.365d-10 e/nm^2 /ns. The concentration in electrical double layer structuce is plotted in the figure.

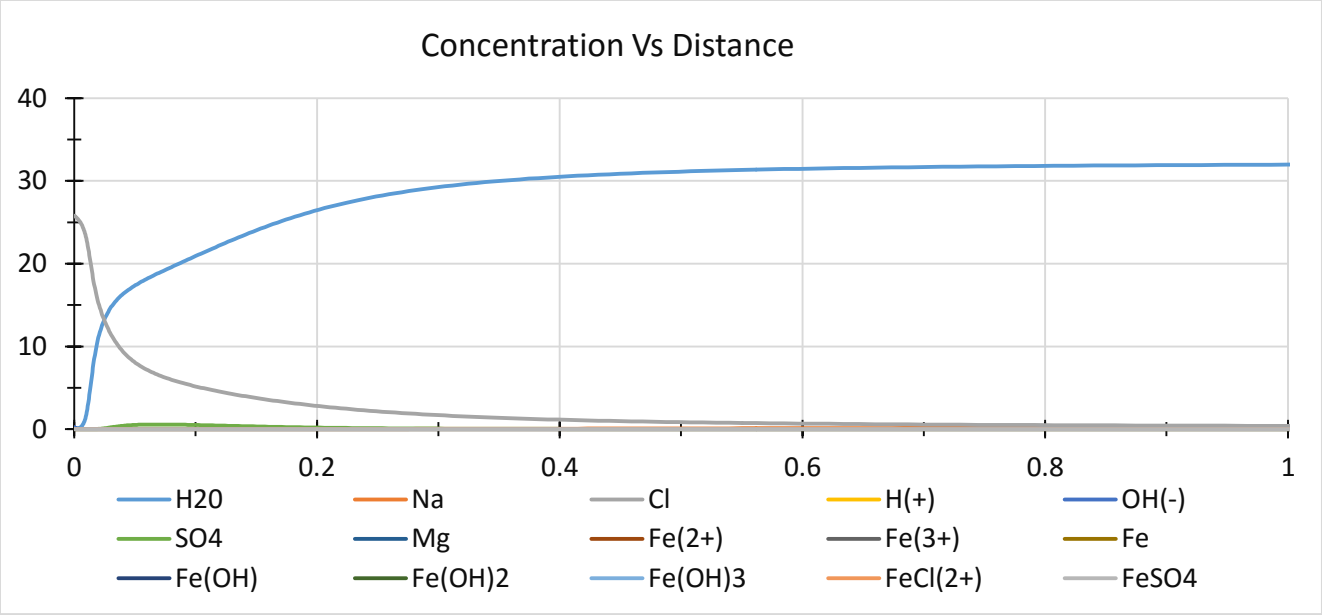

Figure 5.13. Concentration Vs Distance graph for 3.365d-10 e/nm2 /ns

It is observed that in the electrical double layer structure, Cl^- concentraion is the dominatind species at the metal surface. The concentration profiles of all the ions in the electrical double structure is same, as compare to the 0.5V without applying flux in the system.

The packing factor of the ions in seawater at the metal surface is maximum. The maximum packing factor of the ions at 0.5V for 3.365d-10 e/nm^2 /ns metal ion flux is 0.65. The important observation in this case is that, the profile of packing factor in this case is same as compare to the case without flux at the same voltage.

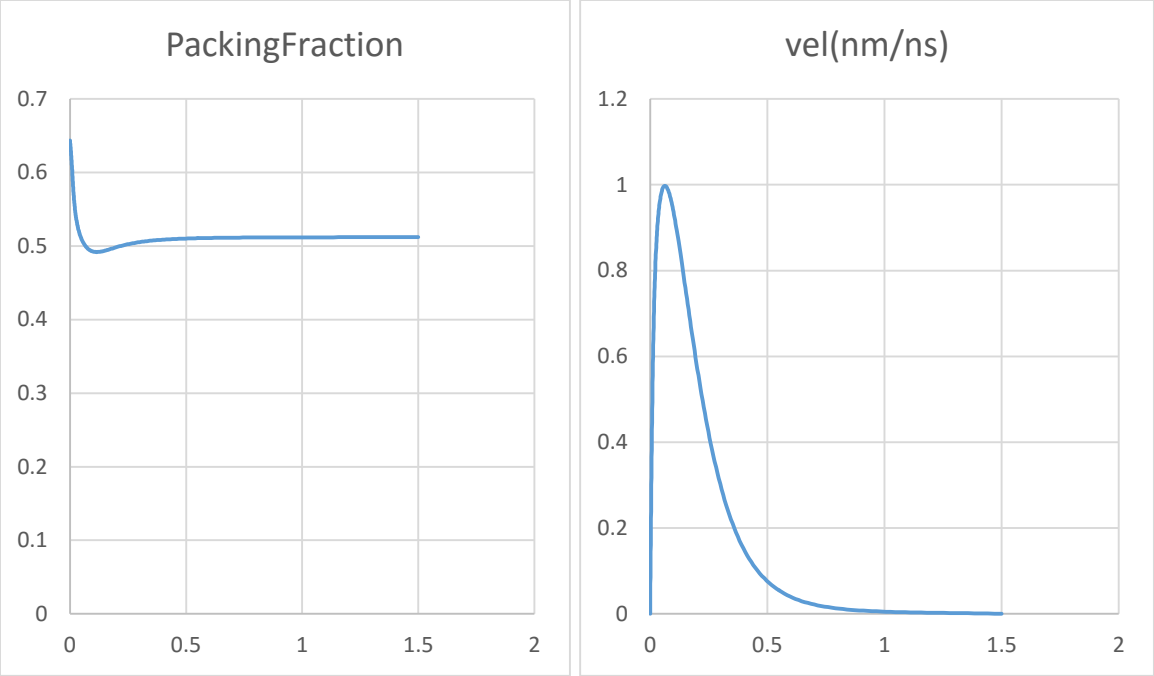

Figure 5.14. Packing factor and Velocity Vs Distance graph 3.365d-10 e/nm2 /ns

At the metal surface the ions velocity is zero. The maximum velocity in this case is 1nm/ns obtained at 0.1 nm. It is observed, the velocity profile in this case is same as compare to the case without flux at the same voltage.

5.2.2 Numerical observation applying 2.993d-9 e/nm^2 /ns to the system

Increasing the voltage to 1V and Fe flux 2.993d-9 e/nm^2 /ns changes the concentration of ions in the double layer structure.

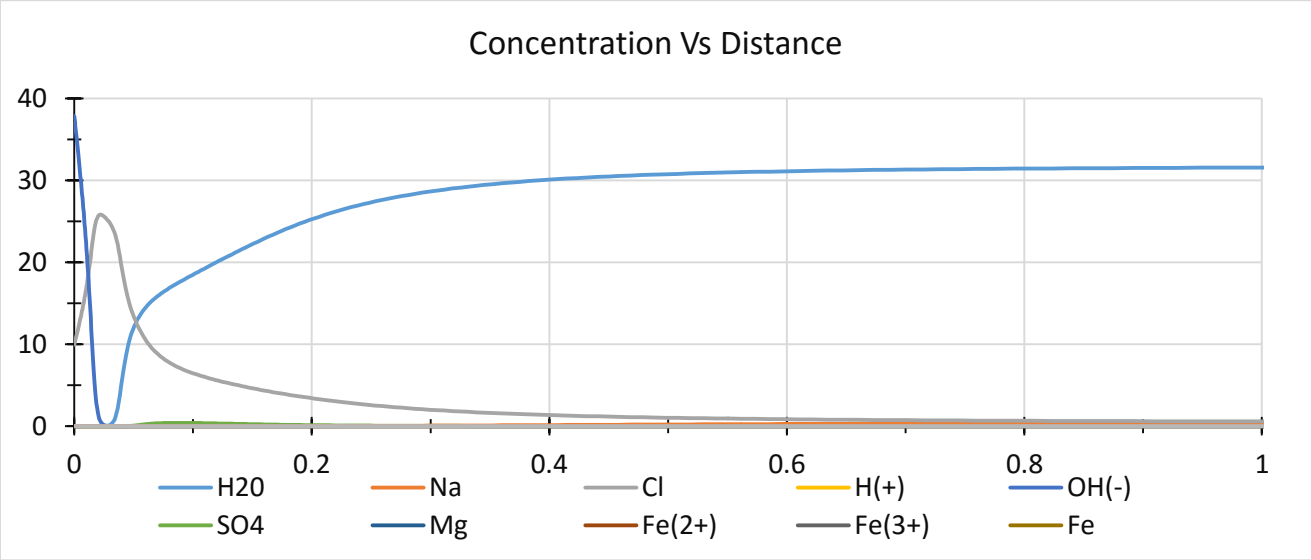

Figure 5.15. Concentration Vs Distance graph for 2.993d-9 e/nm2 /ns

It can be observed in the electrical double layer that, the concentration of the Cl^- ions is 9 e/nm^3 whereas the concentration of the OH^- ions is 40 particle/nm^3. The SO_4^{2-} ions are pushed away further from the metal surface. Therefore the OH^- concentration at the metal surface is dominating. High concentration of OH^- ions at the metal surface will reduce the pitting corrosion. It is observed that, concentration profiles of all the ions in the electrical double structure is same, as compare to the 1V without applying flux in the system..

Packing factor at this voltage is identical to the 0.5V profile. The maximum density at this voltage is at the metal surface and it remains constant over a short distance away from the metal surface. The minimum density is at 0.2nm away from the metal surface. The important observation in this case is that, the profile of packing factor in this case is same as compare to the case without flux at the same voltage.

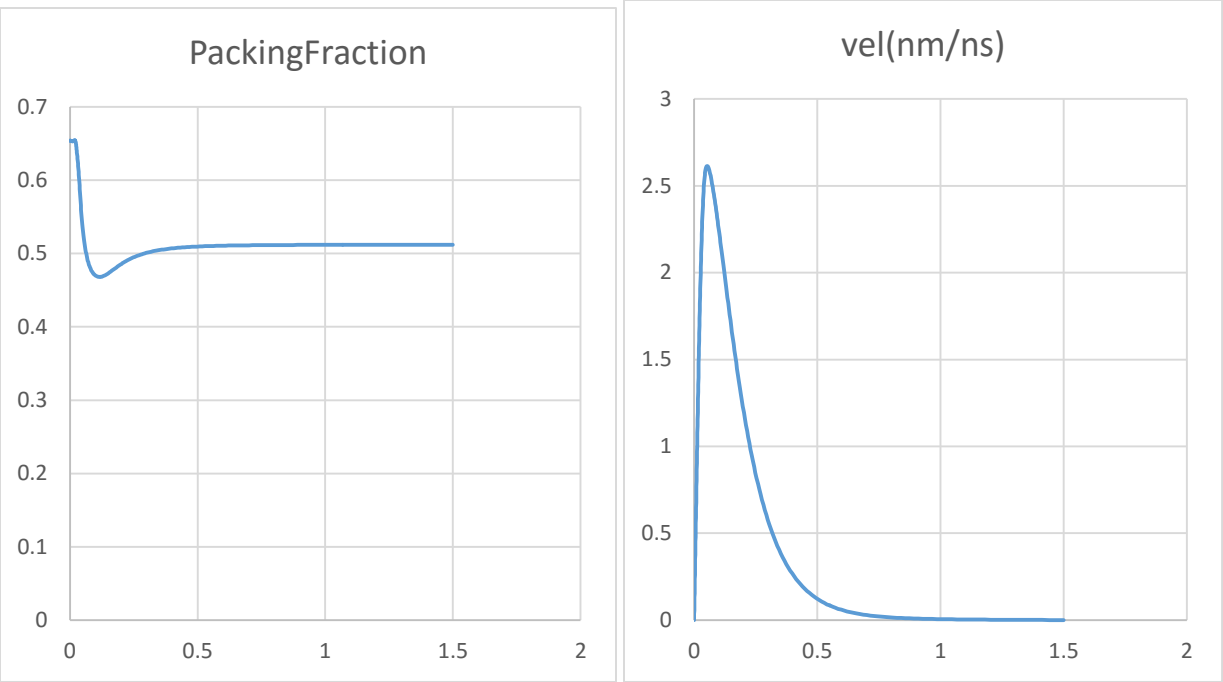

Figure 5.16. Packing factor and Velocity Vs Distance graph for 2.993d-9 e/nm2 /ns

The velocity of the ions at the metal surface is zero. It rises up exponentially over the short distance away from the metal surface. The maximum velocity at this voltage is 2.7nm/ns. The velocity profile in this case is same as compare to the case without the flux at the same voltage.

5.2.3 Numerical observation applying 1.153d-8 e/nm^2 /ns to the system

Further, increasing the voltage to 1.2V and meta ion flux to 1.153d-8 e/nm^2 /ns, there is noticable change in ions consentation in the double layer structure.

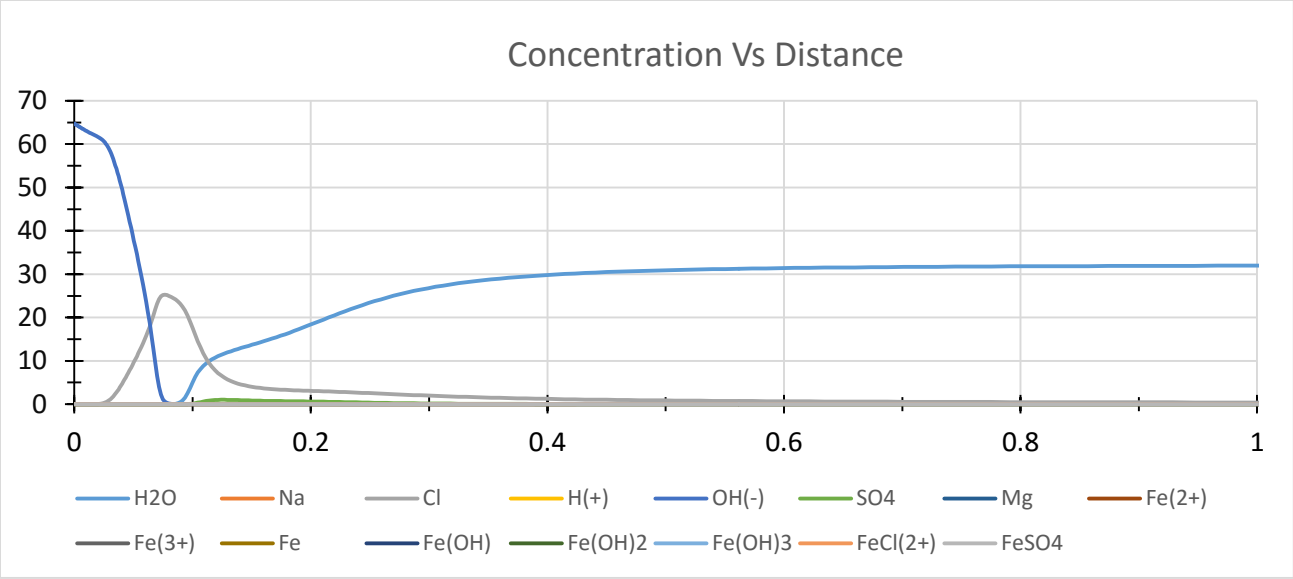

Figure 5.17. Concentration Vs Distance graph for 1.153d-8 e/nm2 /ns

The dominating concentration near the metal surface is OH^- ions. The OH^- ions concentration at the metal surface is 65 particle/nm^3. The concentrations of the other cations such as, Cl^- and SO_4^{2-}, pushed away from the metal surface at higher rate. Concentration profiles of all the ions in the electrical double structure is same, as with 1.2V without applying flux in the system.

The maximum density (0.7) is at the metal surface and it decreases gradually till 0.07 nm away from the metal surface. After 0.07nm the velocity of the corroding ions decreases gradually till 0.2 nm. The minimum density is at 0.2nm away from the metal surface 0.375. The minimum density is at 0.2nm away from the metal surface 0.375. It is noticed that this is the minimum velocity among all the earlier cases lower than 1.2V. The important observation in this case is that, the profile of packing factor in this case is same as compare to the case without flux at the same voltage.

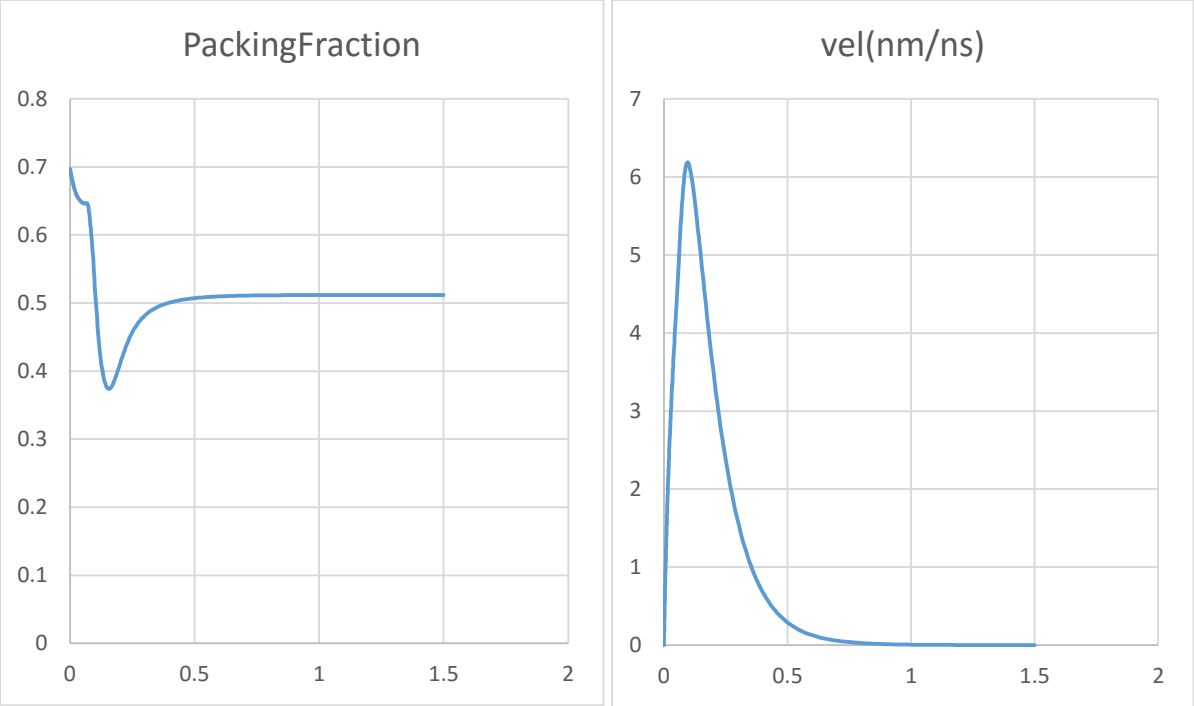

Figure 5.18. Packing factor and Velocity Vs Distance graph for 2.993d-9 e/nm2 /ns

The velocity of the corroding ions is minimum at the metal surface and 1nm away from the metal surface towards the bulk. It rises up exponentially over the short distance away from the metal surface. The maximum velocity at this voltage is 6.2nm/ns. In the earlier at 0.8V the velocity over the same distance is 2.8nm/n. That implies at this volatge in the region of 0.01 to 0.2nm region the mobility of the ions are high. The velocity of ions decreases exponentially from 0.1 nm away from the metal surface towards the bulkIt is observed, the velocity profile in this case is same as compare to the case without flux at the same voltage.

5.3 Numerical observations increasing Cl^- concentration

The initial concentrations of ions is the integral factor in the electric double layer. The concentration of anions contributes more towards the corrosion process. Therefore it is important to analyze and observe the change in initial concentration of the cations in the electric double layer. In all the earlier cases to observe the effect of voltage and metal ion flux, the initial

concentration of the ions kept constant. In the current case, the change in concentration of the cations are observed.

5.3.1 Numerical observations increasing Cl^- concentration to 0.501 e/nm^3 at 0.2V

Increasing the initial concentration of the C^{l-} ions from 0.310 to 0.501 e/nm^3 at 0.2V, the following figure is obtained for the concentration of ions in the double layer.

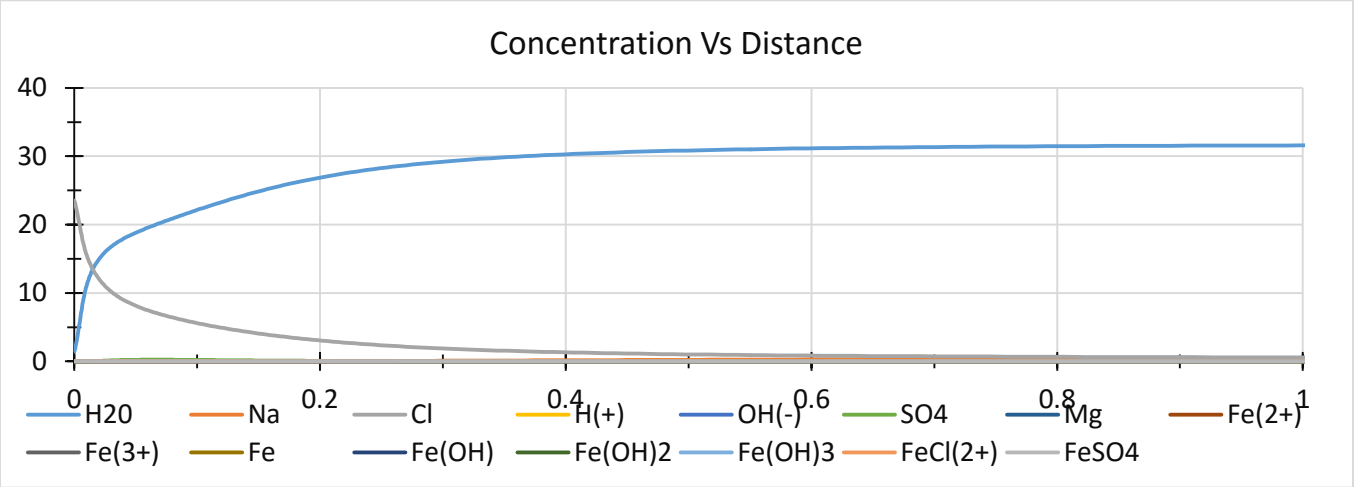

Figure 5.19. Concentration Vs Distance graph for increase in Cl- concentration to 0.501 e/nm3 at 0.2V

It is observed in the graph that Cl^- concentration on the metal surface is high, and it is decreasing away from the metal surface. The Cl^- ions are attracted toward the metal surface at higher concentration. The concentration of Cl^- ions at the metal surface is 24 e/nm^3. The concentration of Cl^- ions at the metal surface when the initial concentration is 0.301 e/nm^3 obtained as 15 e/nm^3. Compare to that at the Cl^- ions concentration in this case is 24 e/nm^3 at the metal surface for the same voltage. It is observed that with the increase in initial concentration of the Cl^- ions, the concentration of the Cl^- ions near the metal surface considerably increase. At the same time SO_4^{2-} concentration is very less at the metal surface and away from the metal surface. Meanwhile the water molecules are pushed away from the metal surface at this voltage. The water molecules concentration at this voltage is still on the higher side.

The packing factor in this case is observed to be change a lot compared to the initial concentration of the Cl^- ions 0.310 e/nm^3 at the same voltage

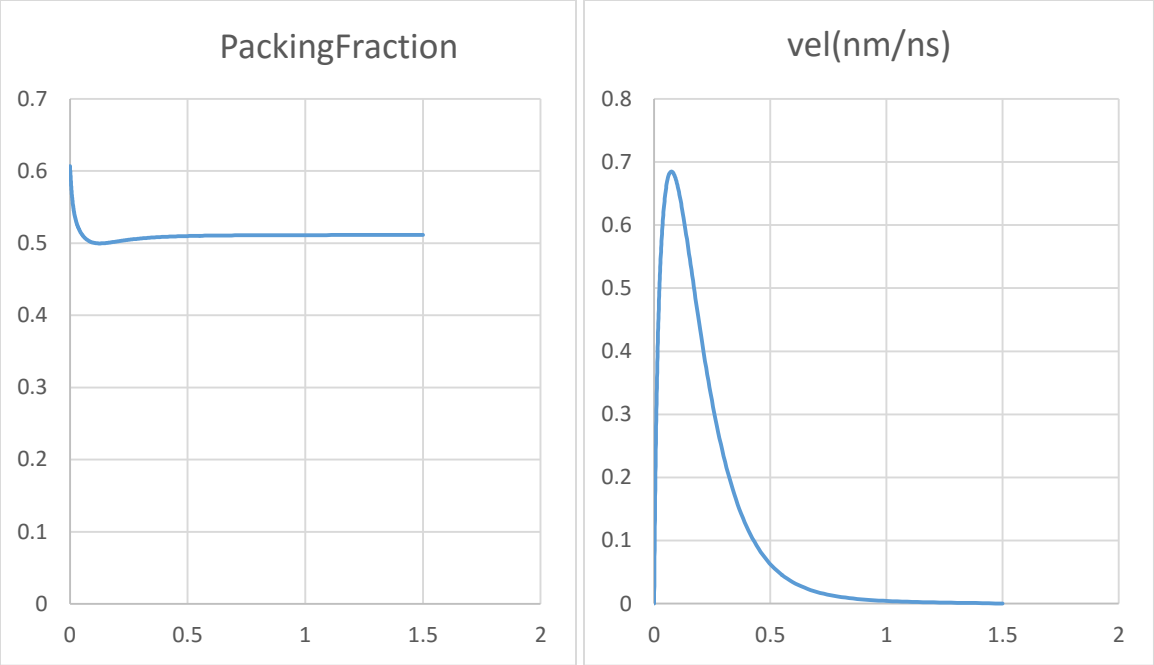

Figure 5.20. Packing factor and Velocity Vs Distance graph for increase in Cl- concentration to 0.501 e/nm3 at 0.2V

The maximum packing factor is at the metal surface 0.6 and minimum 0.5 at 0.15nm away from the metal surface. The nature of the curve is same as compare to the curve of initial concentration at 0.301 e/nm^3. However, the maximum and the minimum packing factor in this case is higher than the packing factor, at the low initial concentration at the same voltage. The density of the ions after a certain value away from the metal surface remains constant all over the bulk.

The velocity of the ions changes in the electric double layer because of the increase in initial concentration of the Cl^- ions in the system. The maximum velocity of the ions in this case is 0.68nm/ns at 0.07nm away from the metal surface. The nature of the velocity profile is same as compare to the nature of velocity profile for lower concentration Cl^- ions at the same voltage.

However the maximum velocity of the ions in this case is higher compare to the original Cl^- concentration.

5.3.2 Numerical observations increasing Cl^- concentration to 0.501 e/nm^3 at 0.8V

Increasing the initial concentration of the Cl^- ions to 0.501 e/nm^3 at 0.8V.

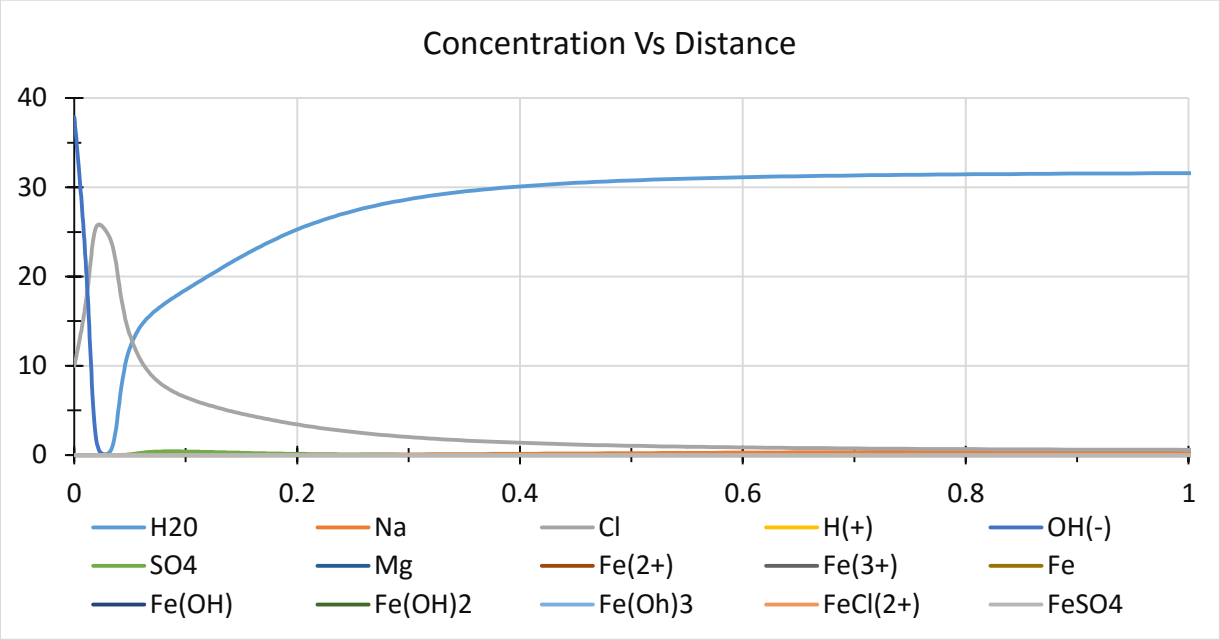

Figure 5.21. Concentration Vs Distance graph for increase in Cl- concentration to 0.501 e/nm3 at 0.8V

It can be observed that the concentration of the Cl^- ions is 9 particle/nm^3 whereas the concentration of the OH^- ions is 40 particle/nm^3. In this case the concentration of the Cl- ions at the metal surface at increased initial concentration is same as, in the initial concentration of Cl^- ions 0.301. The OH^- ions concentration is dominating at the metal surface. The SO_4^{2-} ions are pushed away further from the metal surface. Meanwhile, the water molecules at this voltage is further pushed away from the metal surface. It is clear from the figure that H_2O concentration at the metal surface is negligible at the metal surface, and it increases gradually away from the metal surface towards the bulk.

Packing factor curves and the velocity profiles of the ions at this increased initial concentration of Cl^- 0.501 e/nm^3 is same as compare to the lower concentration of 0.301 e/nm^3 at the same voltage.

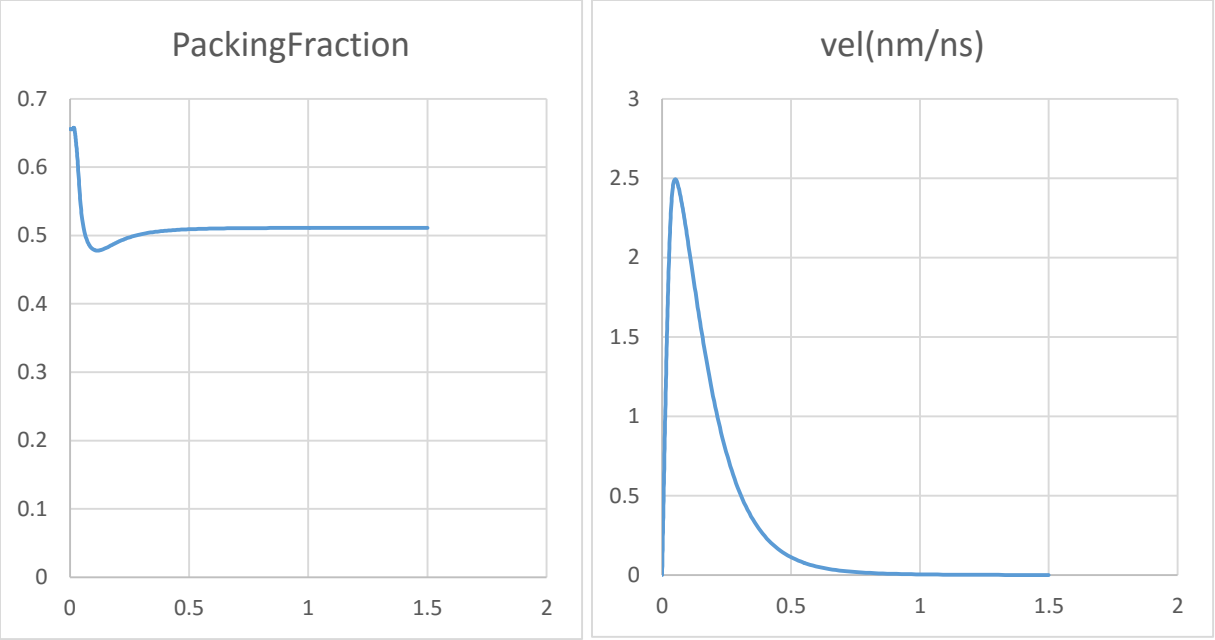

Figure 5.22. Packing factor and Velocity Vs Distance graph for increase in Cl- concentration to 0.501 e/nm3 at 0.8V

The maximum values of density at the metal surface is same in both the cases. However the maximum value of velocity in both the cases for initial concentration of Cl^- ions is different over the same distance. The maximum velocity in this case 2.5nm/ns, and in the lower concentration case it is 2.65nm/ns. The important observation here is, the velocity in lower concentration case is higher.

5.3.3 Numerical observations increasing Cl^- concentration to 0.501 e/nm^3 at 1.2V

Further increase in the initial concentration Cl^- ions to 0.501 e/nm^3 at higher voltage 1.2V. The concentration in electrical double layer structuce is plotted in the figure. . It is observed that dominating concentration near the metal surface is OH^- ions. The OH^- ions concentration at the metal surface is 65 particle/nm^3. The concentrations of the other cations such as, Cl^- and SO_4^{2-}, pushed away from the metal surface at higher rate. In this case the concentration of the Cl- ions

at the metal surface, with increased initial concentration of Cl^- ions is same as in the case of initial concentration of Cl^- ions 0.301 e/nm^3.

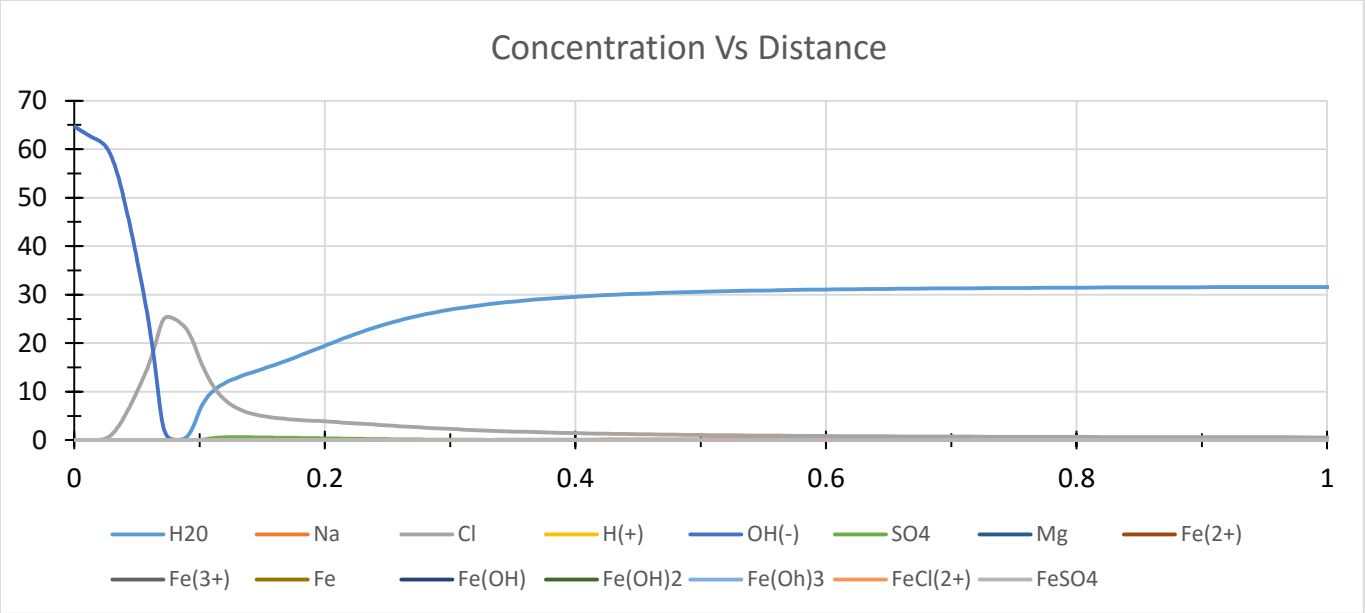

Figure 5.23. Concentration Vs Distance graph for increase in Cl- concentration to 0.501 e/nm3 at 1.2V

The important observation in this particular case obtained that the Cl- ions in both the case is pushed away from the metal surface at the same magnitude.

Packing factor curves and the velocity profiles of the ions at this increased initial concentration of Cl^- 0.501 e/nm^3 is same as compare to the lower concentration of 0.301 e/nm^3 at same voltage

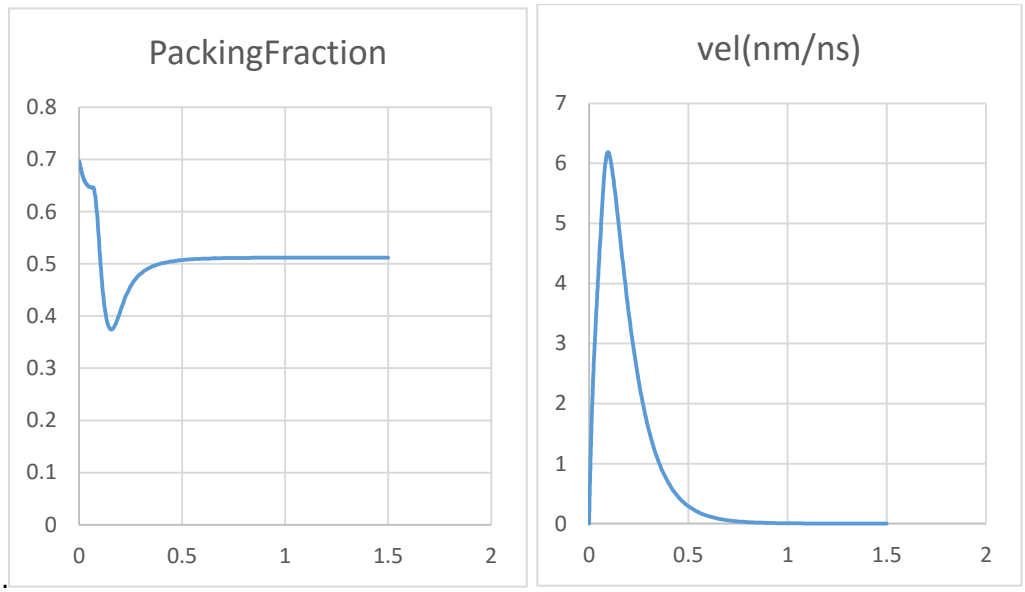

Figure 5.24. Packing factor and Velocity Vs Distance graph for increase in Cl- concentration to 0.501 e/nm3 at 0.8V

The maximum value of density at the metal surface is same in both the condition of initial concentration of Cl^- ions is 0.7. Similarly the maximum value of velocity in both the cases for initial concentration of Cl^- ions is same 6.25 nm/ns over the same distance.

5.4 Numerical observations increasing SO_4^{2-} concentration

Another important anion in sea water which mainly contributes towards the corrosion is SO_4^{2-}. Therefore in this case the effects on the electrical double layer observed, by increasing the initial concentration of SO_4^{2-} at different voltages.

5.4.1 Numerical observations increasing the SO_4^{2-} concentration to 0.138 at 0.2V

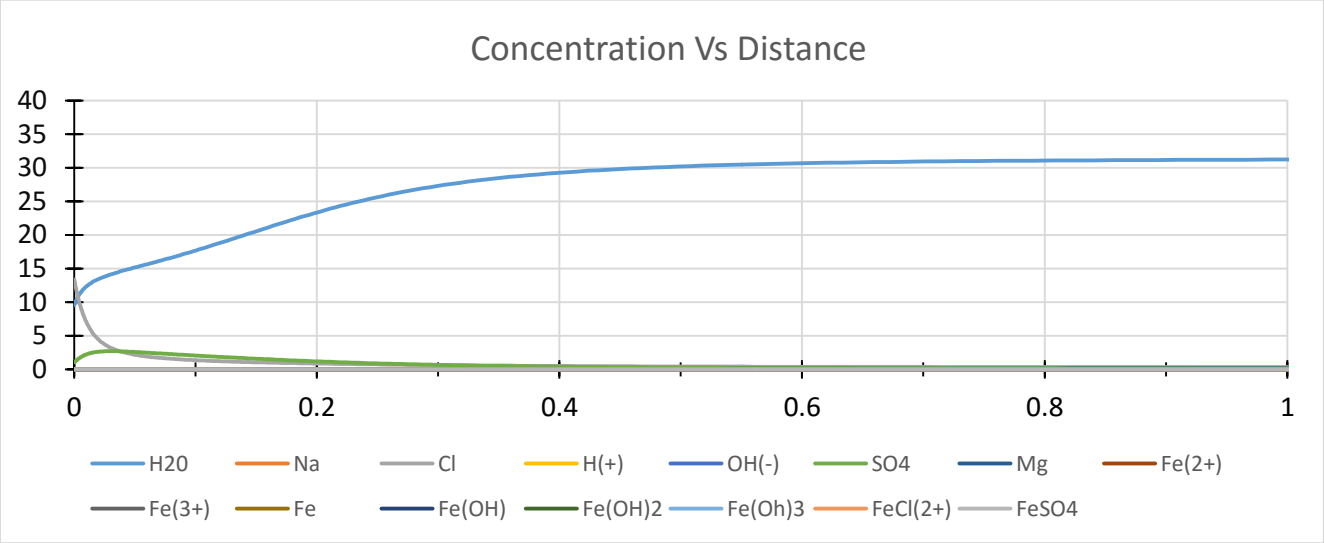

Figure 5.25. Concentration Vs Distance graph for increase in SO42- concentration to 0138 e/nm3 at 0.2V

It is observed that the SO_4^{2-} ions concentration at the metal surface increase to 2 e/nm3, when the initial concentration of the SO_4^{2-} increases at this voltage. The rise in the SO_4^{2-} concentration is 30% more, as compare to the original initial concentration of system 0.002 at the same voltage. The change is the SO_4^{2-} ions concentration is significant compare to all the other cases at the metal surface. Meanwhile, there is not any significant change in the concentration of the other ions at the metal surface.

The maximum packing fraction in this case is 0.58 which is higher at the metal surface. The minimum facing factor is 0.49 at 0.15nm away from the metal surface. However, the maximum

and the minimum packing factor in this case is higher than the packing factor, at the low initial concentration at the same voltage. The density of the ions after a certain value away from the metal surface remains constant all over the bulk.

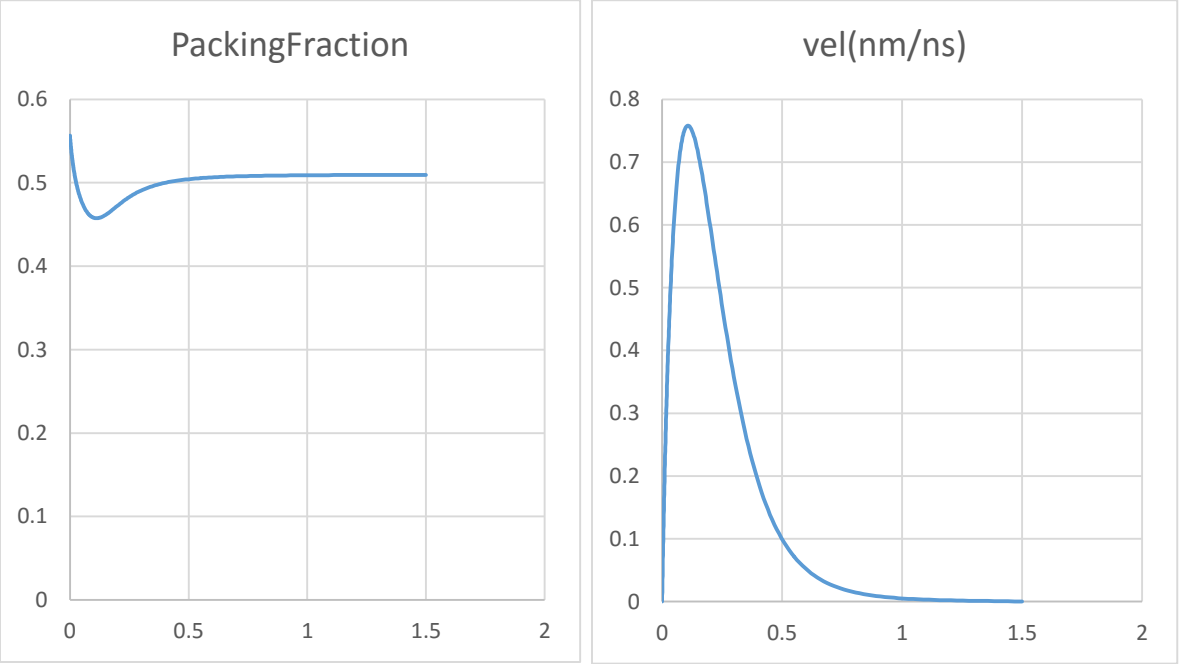

Figure 5.26. Packing factor and Velocity Vs Distance graph for increase in SO42- concentration to 0138 e/nm3 at 0.2V

The velocity of the ions changes in the electric double layer because. The maximum velocity of the ions in this case is 0.75 nm/ns at 0.07nm away from the metal surface. The nature of the velocity profile is same as compare to the nature of velocity profile for lower concentration SO_4^{2-} ions at the same voltage. However the maximum velocity of the ions in this case is higher comparatively.

5.4.2 Numerical observations increasing the SO_4^{2-} concentration to 0.138 at 0.8V

Increasing the initial concentration of SO_4^{2-} to 0.138 e/nm3 at 0.8V

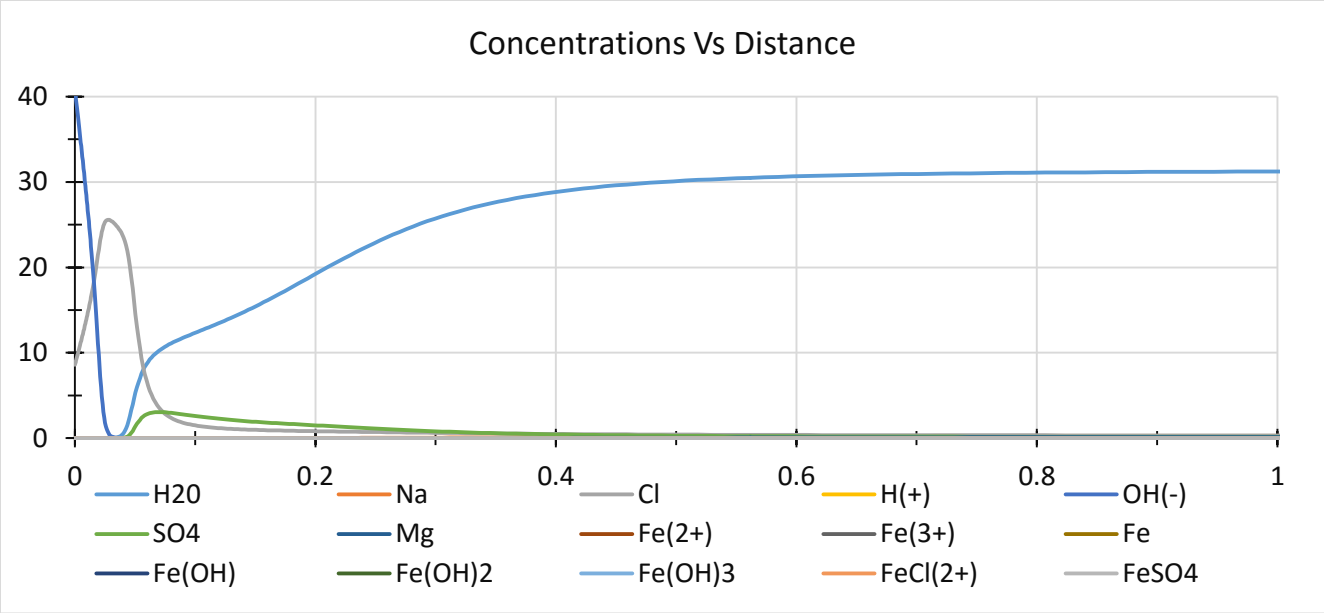

Figure 5.27. Concentration Vs Distance graph for increase in SO42- concentration to 0138 e/nm3 at 0.8V

It can be observed that the concentration of the Cl^- ions is 9 particle/nm^3 whereas the concentration of the OH^- ions is 40 particle/nm^3. In this case the concentration of the SO_4^2 ions at the metal surface for increased initial concentration, is same as in case of initial concentration of SO_4^2 ions 0.138. The OH- ions concentration is dominating at the metal surface. Meanwhile, the water molecules at this voltage is further pushed away from the metal surface. It is clear from the figure that H_2O concentration at the metal surface is negligible at the metal surface, and it increases gradually away from the metal surface towards the bulk.

The nature of the packing factor curve in this case is same as in case of SO_4^{2-} initial concentration is 0.002 e/nm^3. The maximum packing fraction in this case is same as the SO_4^{2-} original concentration. However the minimum packing factor in this case is 0.4, which is less compare to the original initial concentration case over the same distance.

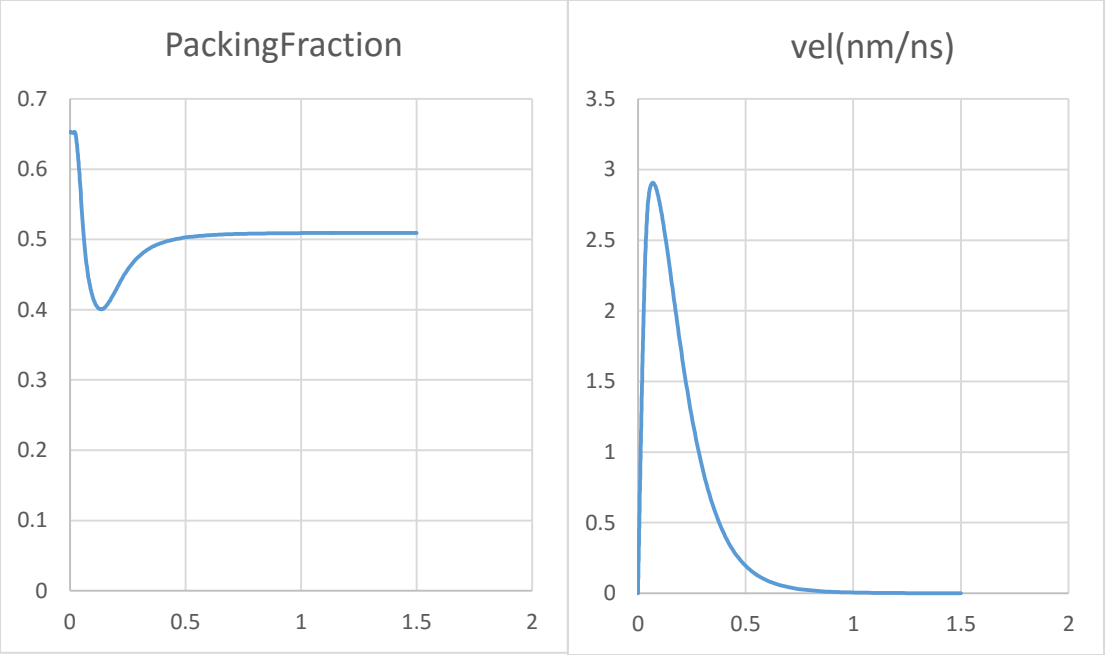

Figure 5.28. Packing factor and Velocity Vs Distance graph for increase in SO42- concentration to 0138 e/nm3 at 0.8

The velocity profile is same in this case compare to the SO_4^{2-} ions initial concentration at 0.002 e/nm^3. The maximum velocity is 2.8nm/ns at the metal surface. The maximum velocity in both the cases is different over the same difference. It is observed that the maximum velocity in this case is higher compare to SO_4^{2-} ions initial concentration at 0.002 e/nm^3.

5.4.3 Numerical observations increasing the SO_4^{2-} concentration to 0.138 at 1.2V

Further, increasing the initial concentration of SO_4^{2-} ions concentration to 0.138 e/nm3 at 1.2V. It is observed that, the dominating concentration near the metal surface is OH^- ions. The OH^- ions concentration at the metal surface is 65 particle/nm^3. The concentrations of the other cations such as, Cl^- and SO_4^{2-}, pushed away from the metal surface at higher rate. Although, the initial concentration of SO_4^{2-} at 1.2V is increases to 0.318e/nm, the SO_4^{2-} concentration at the metal surface is still same as earlier cases. At the same time the H_2O molecules at this voltage is further pushed away from the metal surface. The concentration of H_2O molecules increases gradually

0.2 nm away from the surface. It remains constant after 0.5 nm away from the metal surface, towards the bulk.

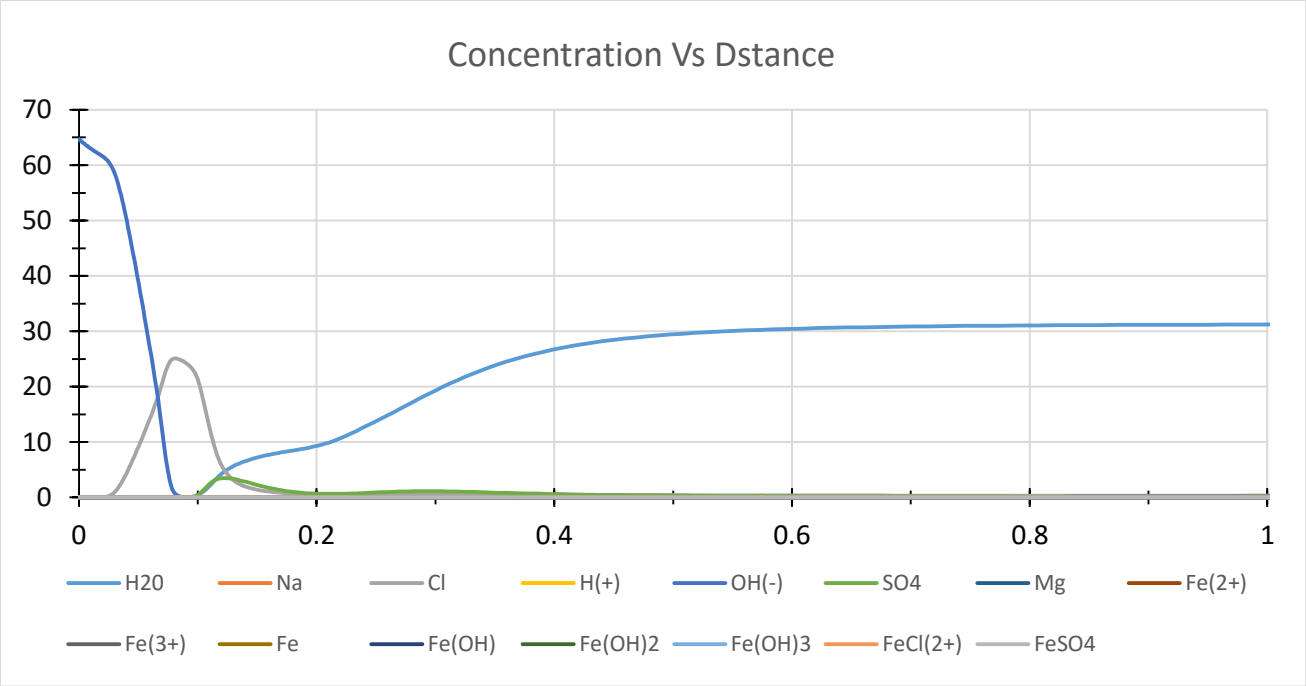

Figure 5.29. Concentration Vs Distance graph for increase in SO42- concentration to 0138 e/nm3 at 1.2V

Packing factor curves and the velocity profiles of the ions at this increased initial concentration of SO_4^{2-} ions 0.312 e/nm^3, is same as compare to the lower concentration of 0.002 e/nm^3 at same voltage.

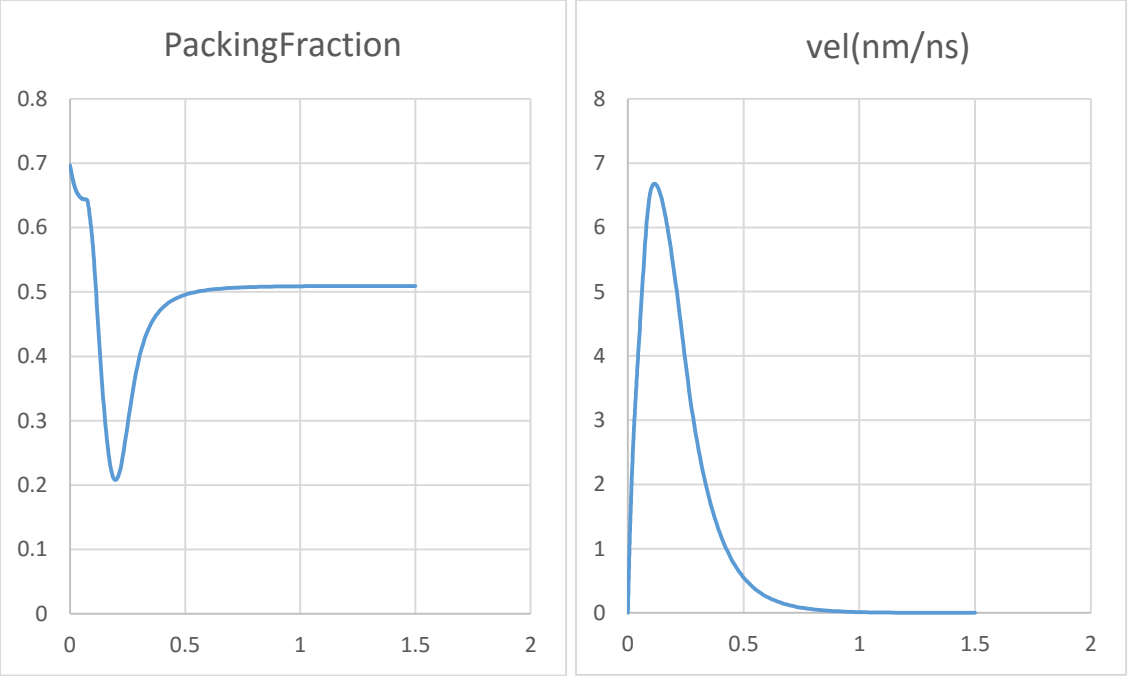

Figure 5.30. Packing factor and Velocity Vs Distance graph for increase in SO42- concentration to 0138 e/nm3 at1.2

The maximum packing fraction in this case is same as the SO_4^{2-} original concentration. However the minimum packing factor in this case is 0.2, which is less compare to the original initial concentration of SO_4^{2-}case over the same distance. The maximum velocity is 6.7nm/ns at the 0.175 away from the metal surface. The maximum velocity in both the cases is different over the same distance. It is observed that the maximum velocity in this case is higher compare to SO_4^{2-} ions initial concentration at 0.002 e/nm^3

CHAPTER 6

NUMERICAL RESULTS DISCUSSION

6.1 Significance of varying voltage

Voltage is the integral factor in the interfacial electric double layer structure. In the electric double layer structure, it is important to study the concentration of the ions contributing to the corrosion mechanism. The concentration of the anion in the electric double layer is responsible for the anodic corrosion.

The concentration of the ions changes in the electric double layer structure with the voltage. In the earlier chapter, it is observed that at 0.2V the Cl^- ions concentration is dominating at the metal surface. The metal in the system is Fe. The Fe reduces to Fe^{2+} and $2e^-$, and this $2e^-$ leaves the metal surface in the bulk. At the low voltage 0.2V, the Cl^- ions gets attracted towards the Fe^{2+}

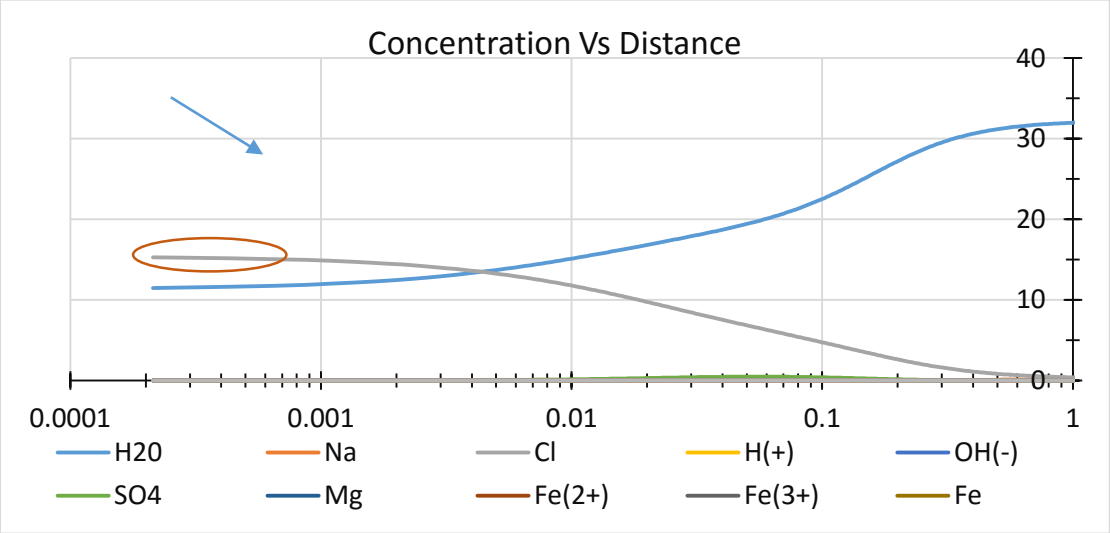

Figure 6.1. Concentration Vs Distance logarithmic graph for 0.2V

Although, SO_4^{2-} ions are also present in the double layer structure, but it not the dominating species at the metal surface. The SO_4^{2-} ions are not the dominating species at the metal surface, because the diffusivity of the SO_4^{2-} ions is less than Cl^- . Therefore stokes radius of Cl^-

ions is less than SO_4^{2-} ions. Hence, the concentration of Cl^- ions at the metal surface is dominating as shown in figure. The increase in Cl^- ions concentration at the metal surface promote the pitting corrosion. As the voltage increases in the system, the ions concentration keep changing in the electric double layer. As discussed in the earlier chapter at 0.5V, the concentration of Cl^- ions is high compare to all the other ions present in the sea water. The concentration of Cl^- is high because of its affinity toward the opposite pole and its concentration is higher in percentage.

It is observed that at 0.8V, the OH^- ions concentration is greater than all the other ions in the sea water. The concentration of OH- ions is dominating at the metal surface as shown in fig, because the OH- is dipole. The dipole of the OH- is strong. The Cl- ions which has the domination concentration till this voltage is saturated at this point. Therefore OH- ions concentration increases rapidly at this point.

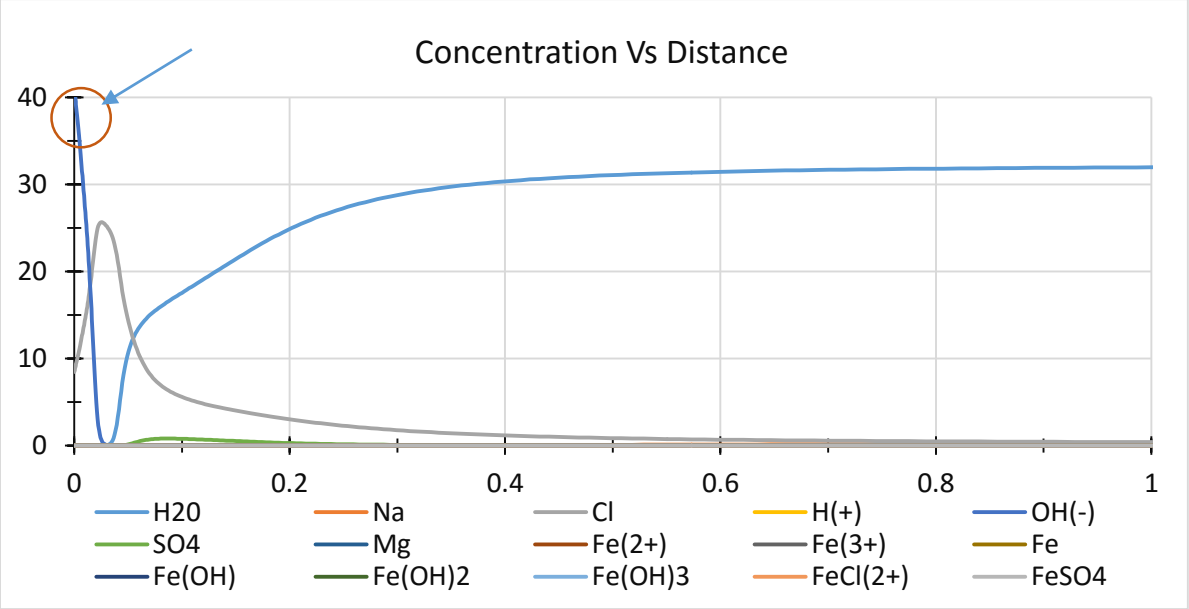

Figure 6.2. Concentration Vs Distance graph for 0.8V

Further, increasing the voltage in the system, it is observed and discussed in the earlier chapter that, concentration of OH^- ions is dominating at the metal surface. That implies, for the voltages

greater than 0.8V, OH^- ions are the dominating specie because of its high diffusivity as shown in figures.

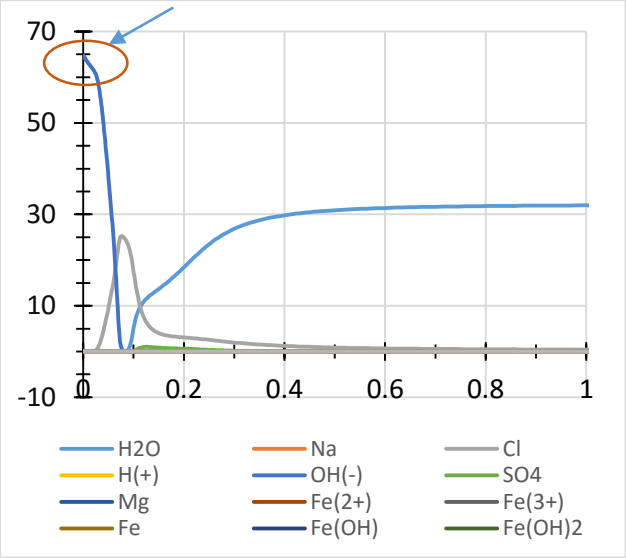

Figure 6.3. Concentration Vs Distance graph for 1.2V

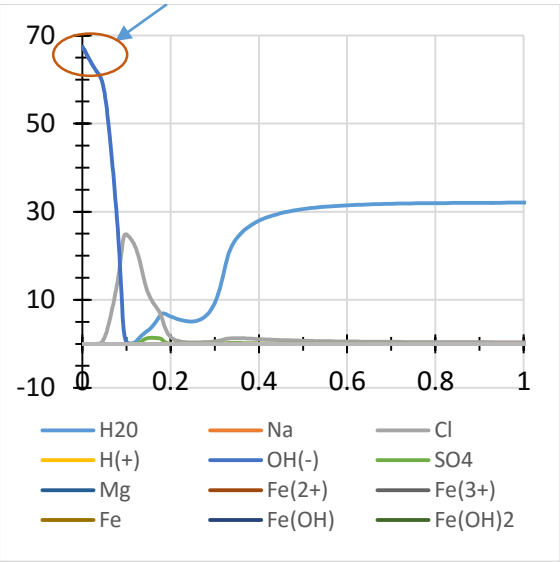

Figure 6.4. Concentration Vs Distance graph for 1.7V

As the voltage increases greater than 0.8V, the concentration of the OH^- ions increases at the metal surface. The Cl^- ions which has the domination concentration till this voltage is saturated at particular voltage point. Therefore OH^- ions concentration increases rapidly after that this point.

The other anions such as, Cl- ans SO_4^{2-} get pushed away from the metal surface with increases in voltage greater than 0.8V. These anions get pushed away from the metal surface because of the OH- ions. The layer of OH- ions form near the metal surface with the increases in voltage. With the increases in voltage, this layer of OH- ions increases and thus other anions get pushed away further from the metal surface.

There is significant effect on tha packing fraction, velocity, and pressure of the ions present in the sea water, with increase in the voltage to the system. The packing factor of the ions are maximum at the metal surface for all the voltages. At the metal surface the oxidation reaction of Fe takes place. The oxidation reactions produces Fe^{2+} ions at the meteal surface, and this oxidation reaction continues to take place in the metal. As a result of which Fe^{2+} ions deopsited at the metal surface. These Fe^{2+} ions attract the counter ions towards the metal surface. Therefore, maximum number of anions are attracted towards the metal surface. Hence the packing factor at the metal is maximum. The packing factor gradually decreases with the distance away from the metal surface for all the voltages.

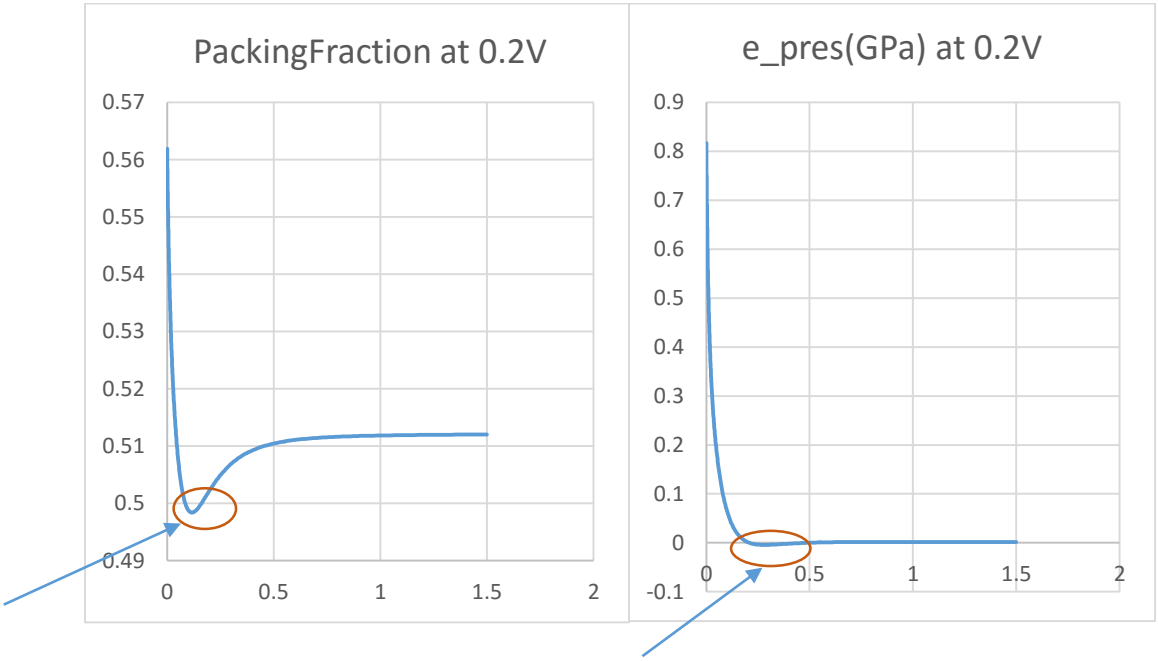

Figure 6.5. Packing factor Vs ePressure graph for 0.2V

As the voltages increases in the system, the density of the ions at the metal surface increases. The density of ions at the steel metal surface increases because more number of counter ions get attracted towards the metal surface.

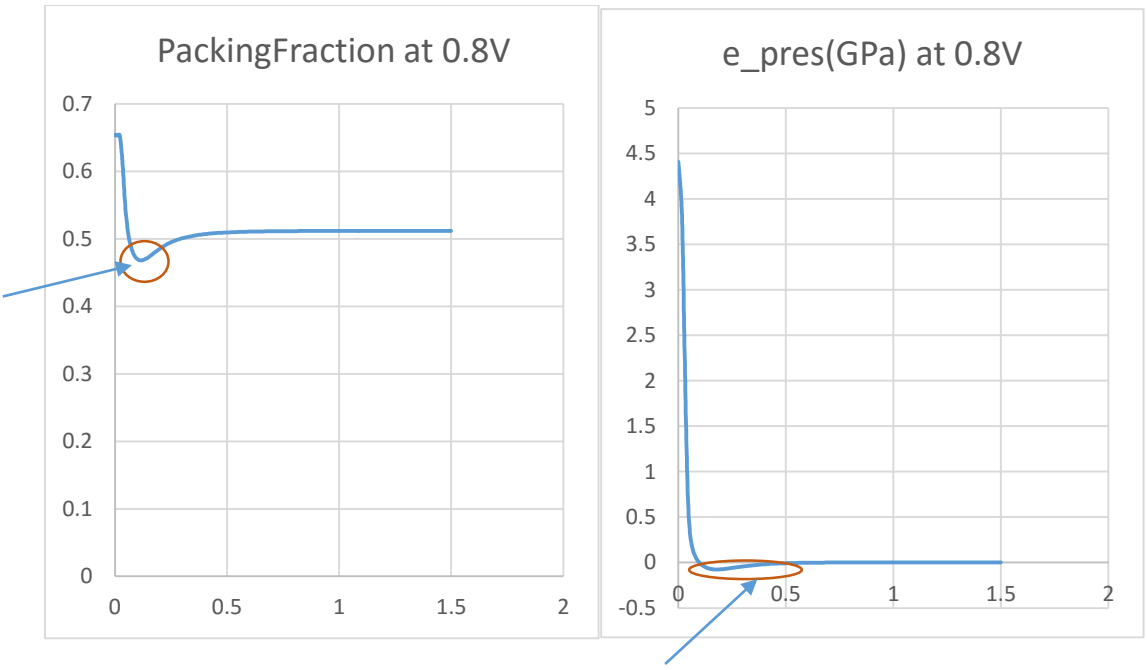

Figure 6.6. Packing factor and Vs ePressure graph for 0.8V

In the pressure profile it is clear that negative pressure zone is followed by the sudden rise in pressure at 0.1nm away from the metal surface. This sudden change in the pressure at 0.1nm gives rise to cavitation. Cavitation is the formation of vapor cavities in a liquid. Those small liquid- bubbles are the consequence of forces acting upon the liquid. It usually occurs when a liquid it is subjected to rapid changes of pressure that cause the formation of cavities where the pressure is relatively low. When subjected to higher pressure, the voids implode and can generate an intense shock wave. There is a negative pressure zone from 0.47 to 0.1nm in this system shown in the figure. The pressure suddenly increases towards the metal surface after 0.1nm. This leads to the cavitation in the system. At the same time the density of ions after 0.1nm, increases towards the metal surface.

6.2 Effect of change in initial concentration

In the earlier chapter 5.3 and 5.4 it is observed that the change in initial concentration of anions in the sea water changes the ion concentration in the electrical double layer system. The change in initial concentration and of Cl^- and SO_4^{2-} ions, the concentration curves profile remains the same, except the concentration of Cl^- and SO_4^{2-} ions.

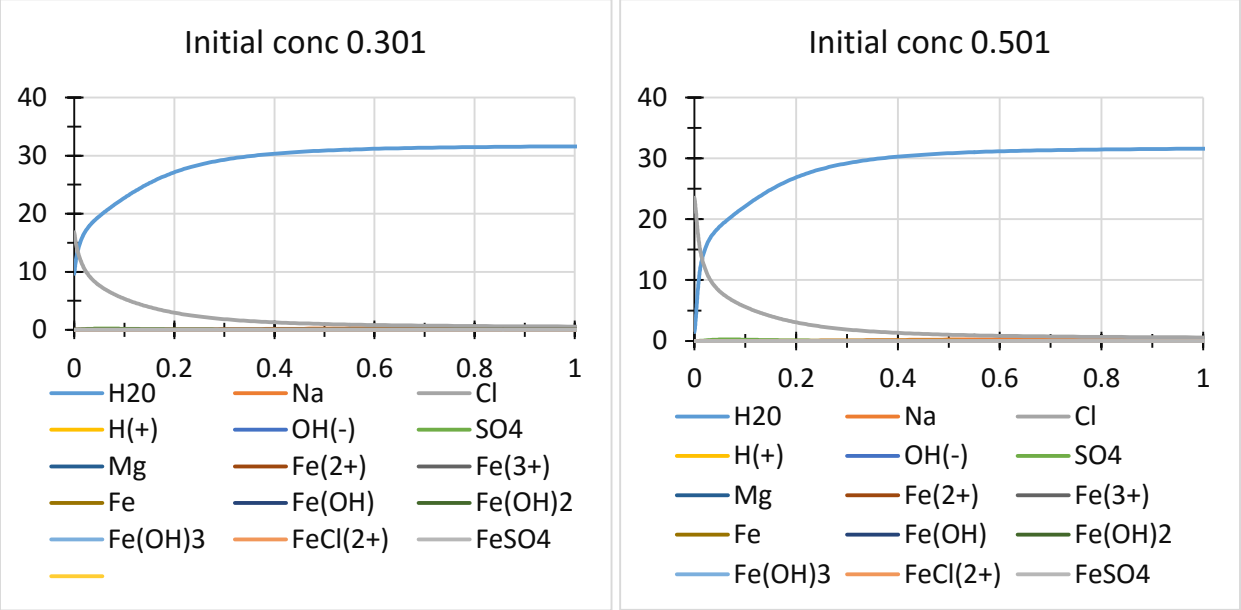

Figure 6.7. Comparison of concentration Vs distance graph for 0.301 and 0.501 e/nm3 at 0.2V

The Cl^- ions concentration increases as comapre to low initial concentration case at 0.2V because there are more number of Cl^- ions are present in the bulk. Furthermore, diffusivity of Cl^- ions are higher than all the other anions present currently in the sea water. Therefore the Cl^-ions concentration at higher initial concentration is higher as compare to low intitial concentration case.

However, with the increases in the voltage, it does not stick to the same priciple. At the higher voltage 0.8V,the Cl^- ions saturated and the OH^- concentration invreases. The OH^- ions concentration dominates at the metal surface despite increases in the initial concentration of Cl^-

ions because it has a strong dipole. At higher voltage the intial concnetration does not affect the electric double layer structure concentration's of ion as shown in the figure.

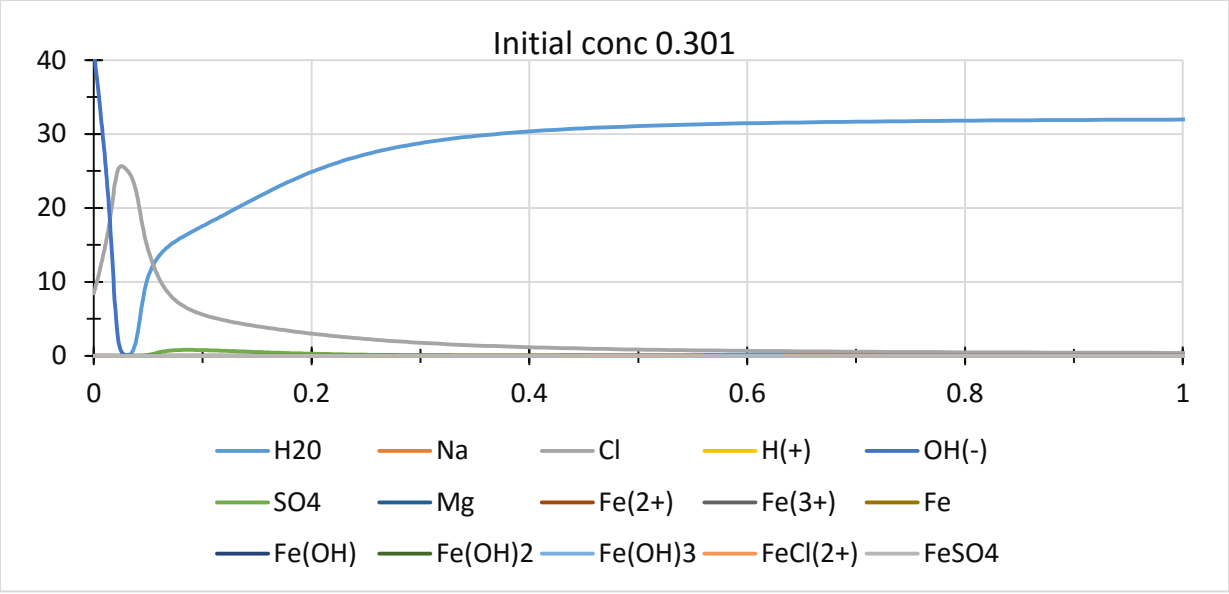

Figure 6.8.Concentration Vs Distance graph for increase in Cl- concentration to 0.301 e/nm3 at 0.8V

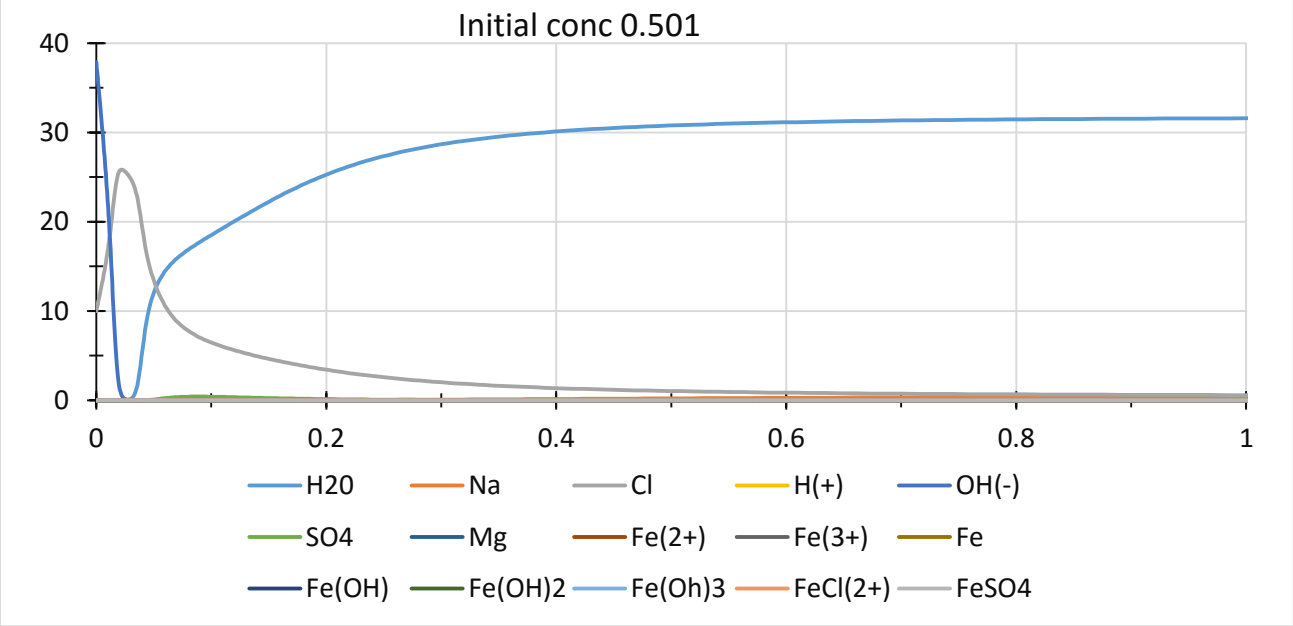

Figure 6.9.Concentration Vs Distance graph for increase in Cl- concentration to 0.501 e/nm3 at 0.8

The packing fraction and the pressure profiles at high initial concentration case, exibits the same nature as the low initial concentration case at all the voltages.

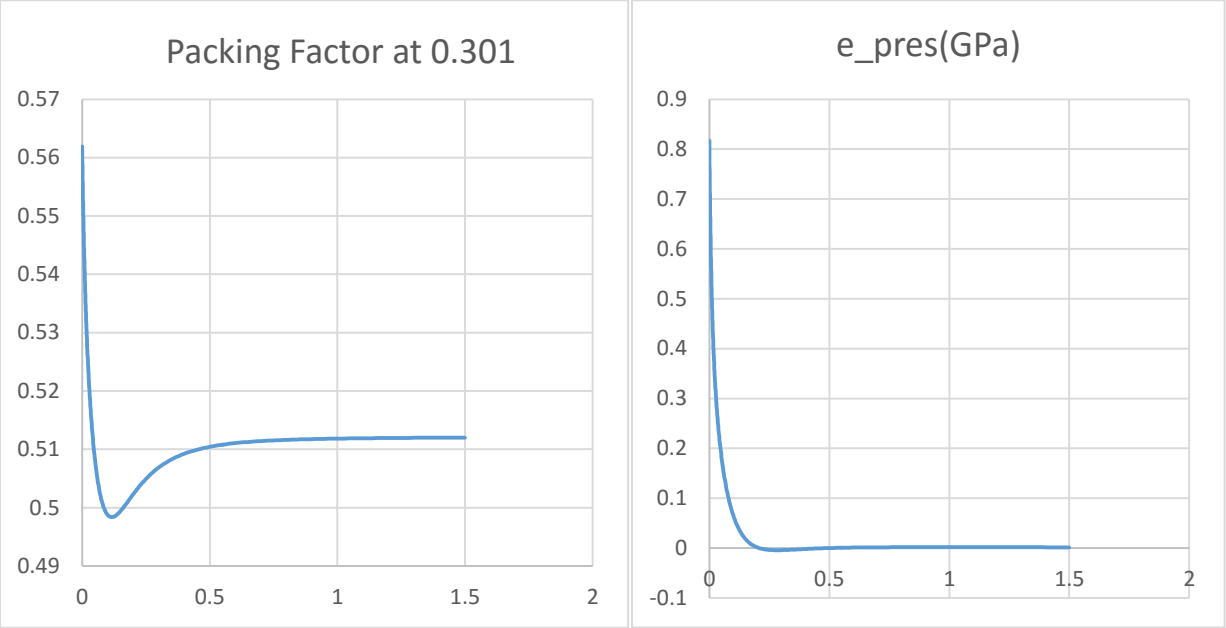

Figure6.10. Packing factor Vs ePressure graph for 0.2V for 0.301 e/nm3

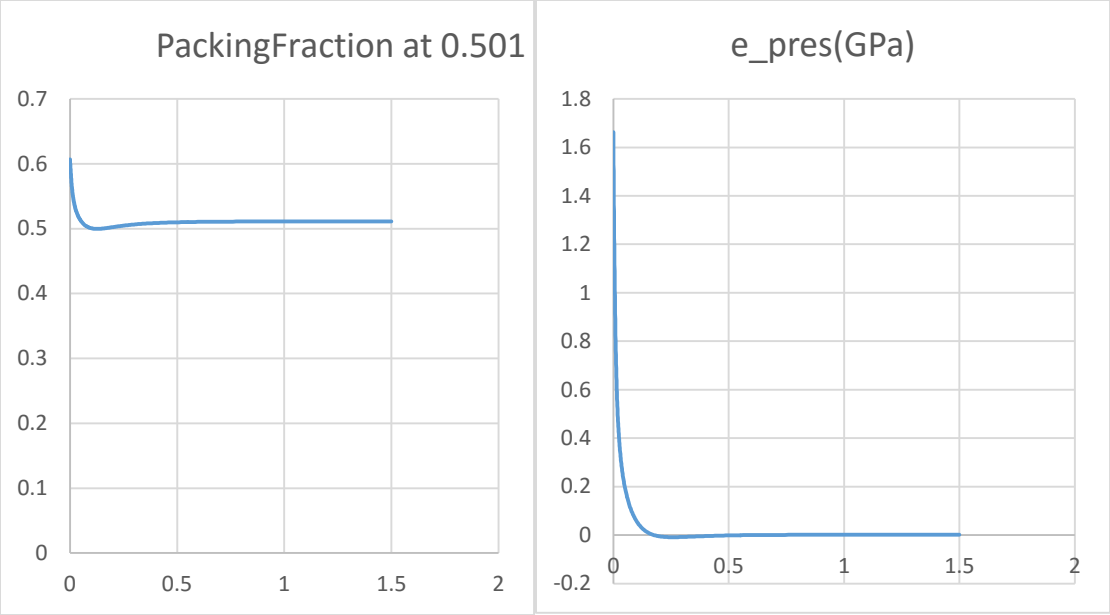

Figure 6.11. Packing factor Vs ePressure graph for 0.2V for 0.501 e/nm3

The maximum pressure at the metal surface is the higher initial concentration case is more than thelower initial concentration case because there are more number of the Cl- ions are depositing at the surface of Fe metal.

Similarly for the increases in the intial concentration of SO_4^{2-} ions at different voltages exibits the same nature. At the voltages lower than 0.8V, the concentration of SO_4^{2-} ions near the

metal srface increases.

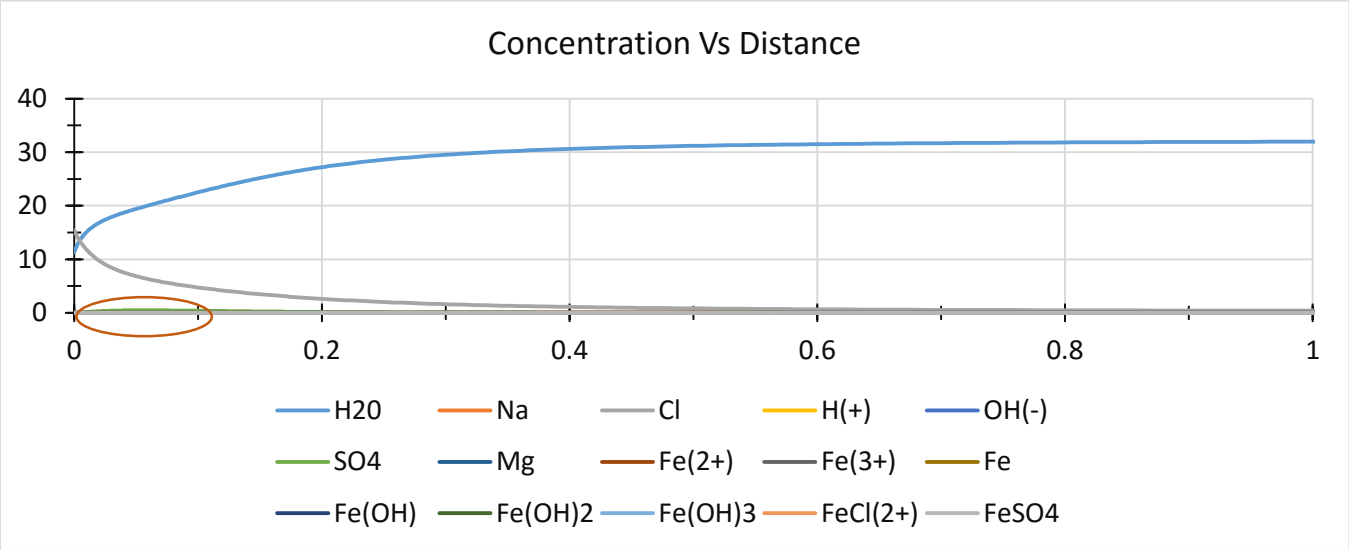

Figure 6.12.Concentration Vs Distance graph for increase in SO42- concentration to 0.002 e/nm3 at 0.2V

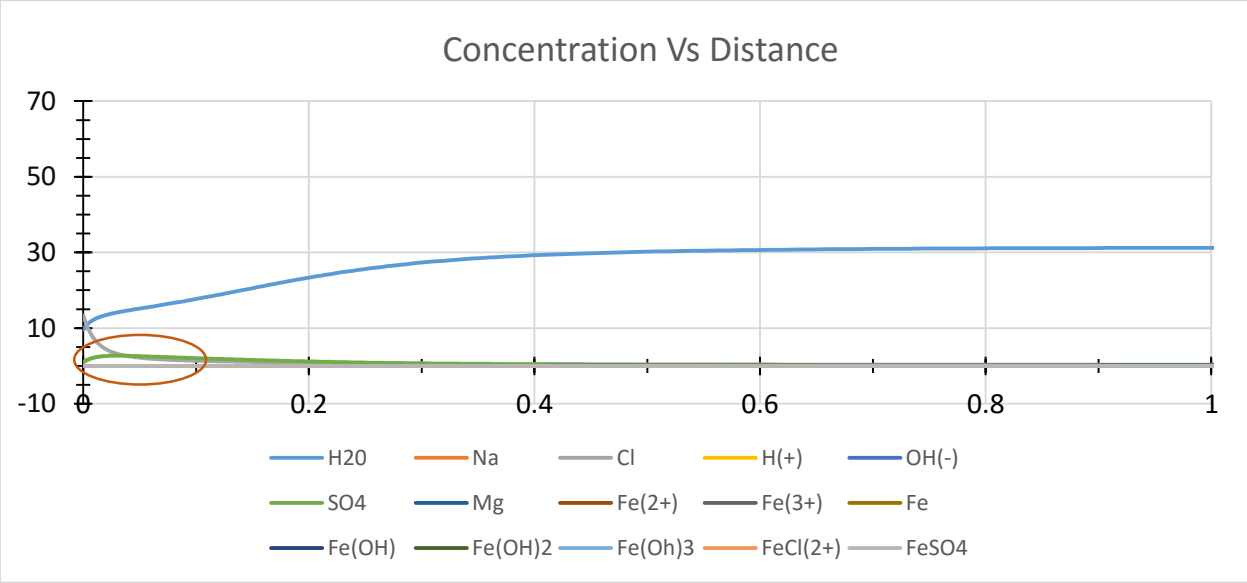

Figure 6.13.Concentration Vs Distance graph for increase in SO42- concentration to 0138 e/nm3 at 0.2V

At the same time the voltages greater than 0.8V the concentration of OH- ions increases at the metal surfacae and the SO_4^{2-} ions pushed away in the same magnitute as in the case of lower initial concentration

CHAPTER 7

CONCLUSION

The study of electric double layer structure in the sea water, throws light on some important parameter in marine engineering corrosion. From the above observations and results it can be concluded that

- The voltage is the important parameter in the electrical double layer structure.
- When the voltage is 0.1 to 0.8V in the system, then the concentration of Cl- ions is dominating at the metal surface. The SO4- ions pushed further away with the increases in voltage.
- When the voltage increases above the 0.8V, the OH- ions concentration is dominating near the metal surface. The diffused layer in this case is of OH- ions.
- The packing factor (density of the ions), is maximum at the metal surface for all the voltages.
- The concentration of the anions at the metal surface in electric double layer structure, dose not affected by the induced metal flux in the system.
- Increases in initial concentration of the Cl- and SO4- anions in the system behaves differently with change in voltage
- With increases in initial concentration of anions till 0.8V, the concentration of those anions increases at the metal surface.
- However above 0.8V, the same anions pushed further away from the metal surface and OH- ions concentration dominates at the metal surface.

Appendix

Input profiles

1. Input profile applying 0.2V at 373K

```
***********1D Problem******************
1              !=1 if planar; =2 if cylindrical; =3 if spherical
300            !Temperature(K)
***********Domain and Grid******************
0, 1.5, 250, 1.02       !XStt,XEnd(nm),Total # of divisions,Mesh-grading power
***********Involved Chemical Components*********
15      !Total#Of Involved Chemical Components
1, 2,3, 4, 5, 6,8, 9,10,12,13,14,15,17,19       !Above#X(ID_Glb Of Involved Chemical Component)
***********Involved Chemical Reactions*********
10      !Total#Of Involved Chemical Reactions
2,3,4,5,6,7,11,12,13,14 !Above#X(ID_Glb Of Involved Chemical Reaction)
*************Simulation Time & Steps*********************
23, 23  !NtotTimeSteps,NtotSnapShots
0              !ITimeStt(=0, first time run; >0, to restart based on ITimeStt-1 step)
*************Initial Uniform Concentrations**********************
32.125, 0.301 0.301, 0.602d-7, 0.602d-7, 0.02d-1,0.02d-1, 0, 0,0,0,0,0,0,0 !C(particle/nm^3)///MUST Follow the above order of involved chemical components
*************Boundary Condition*************
!---repeat below !NthC,Ramp1Jump2,2(Flux0_End,SpringCoef_End,C_Eqilibrium_End)
0, 1, 0, 1.d3, 0.2, 0, 1.d3, 0                  !electric (Displacement=Displacement0+Coef*(V-V0)) with displacement_unit:e/nm^2
1, 2, 0, 0, 0, 0, 1.d3, 32.125                  !chemical (flux=flux0+Coef*(C-C0)) with flux_unit:particle/nm^2/ns, and C_unit:particle/nm^3
2, 2, 0, 0, 0, 0, 1.d3, 0.301                   !chemical (flux=flux0+Coef*(C-C0)) with flux_unit:particle/nm^2/ns, and C_unit:particle/nm^3
3, 2, 0, 0, 0, 0, 1.d3, 0.301                   !chemical (flux=flux0+Coef*(C-C0)) with flux_unit:particle/nm^2/ns, and C_unit:particle/nm^3
4, 2, 0, 0, 0, 0, 1.d3, 0.602d-7                !chemical (flux=flux0+Coef*(C-C0)) with flux_unit:particle/nm^2/ns, and C_unit:particle/nm^3
5, 2, 0, 0, 0, 0, 1.d3, 0.602d-7                !chemical (flux=flux0+Coef*(C-C0)) with flux_unit:particle/nm^2/ns, and C_unit:particle/nm^3
6, 2, 0, 0, 0, 0, 1.d3, 0.02d-1
7, 2, 0, 0, 0, 0, 1.d3, 0.02d-1              !chemical (flux=flux0+Coef*(C-C0)) with flux_unit:particle/nm^2/ns, and C_unit:particle/nm^3
8, 2, 0, 0, 0, 0, 1.d3, 0                 !chemical (flux=flux0+Coef*(C-C0)) with flux_unit:particle/nm^2/ns, and C_unit:particle/nm^3
9, 2, 0, 0, 0, 0, 1.d3, 0                  !chemical (flux=flux0+Coef*(C-C0)) with flux_unit:particle/nm^2/ns, and C_unit:particle/nm^3
10, 2, 0, 0, 0, 0, 1.d3, 0                  !chemical (flux=flux0+Coef*(C-C0)) with flux_unit:particle/nm^2/ns, and C_unit:particle/nm^3
11, 2, 0, 0, 0, 0, 1.d3, 0                  !chemical (flux=flux0+Coef*(C-C0)) with flux_unit:particle/nm^2/ns, and C_unit:particle/nm^3
12, 2, 0, 0, 0, 0, 1.d3, 0                  !chemical (flux=flux0+Coef*(C-C0)) with flux_unit:particle/nm^2/ns, and C_unit:particle/nm^3
13, 2, 0, 0, 0, 0, 1.d3, 0                  !chemical (flux=flux0+Coef*(C-C0)) with flux_unit:particle/nm^2/ns, and C_unit:particle/nm^3
14, 2, 0, 0, 0, 0, 1.d3, 0                  !chemical (flux=flux0+Coef*(C-C0)) with flux_unit:particle/nm^2/ns, and C_unit:particle/nm^3
15, 2, 0, 0, 0, 0, 1.d3, 0                  !chemical (flux=flux0+Coef*(C-C0)) with flux_unit:particle/nm^2/ns, and C_unit:particle/nm^3
*************Numerical Parameters*********************
90000, 1.d-3, 1000, 0.002       !IteratMax,ErrAllow,IteratDisplay,ARelax
*****************************************************************

************All Chemical Components***********************
20      !Total # of chemical components
--repeat (above #) below--!ID;Valance;Relative_Permittivity@Linear;StokesRadius;PhysicalRadius;EtaOverEpsil0((V/nm)^2-nS);AvdW0
 1,  0,   79, 0.09687,   0.1552,  0.113d1, 2.03d-1                    !H2O(0)(10)
 2,  1,   10,  0.1704,    0.102,  0.113d1, 0.0195                      !Na(1+)(11)
 3, -1,   10,  0.1082,    0.181,  0.113d1, 0.241                       !Cl(1-)(17)
 4,  1,    0,  0.0244,   0.1552,  0.113d1, 9.06d-3                     !H(1+)(1):CInf_H+=0.602d-7(pH=7)
 5, -1, 64.4,  0.0431,   0.137,  0.113d1, 0.20294                      !OH(1-)(9):CInf_OH-=0.602d-7(pH=7)
 6, -2, 17.6,   0.232,   0.258 , 0.113d1, 1.36d-1                     !SO4(2-)(48)
 7, 0, 6.89,   0.109,   0.135 , 0.113d1, 5.02d-2                      !O2(16)
 8,  2,  7.6,   0.311,    0.072, 0.113d1, 0.20294                     !Mg(2+)
9,  2,   16,  0.3851,    0.06,  0.113d1, 0.20294                     !Fe(2+)(26)
10,  3, 15.8,  0.3861,   0.07,   0.113d1, 0.20294                     !Fe(3+)
 11,  0, 15.1,   0.213,    0.161, 0.113d1, 0                          !HCl
 12,  1,   16,  0.3851,    0.126,  0.113d1, 0                         !Fe
 13,  1, 14.2,   0.164,    0.216, 0.113d1, 0                          !FeOH(+1)
 14,  0, 14.2,   0.165,   0.369,  0.113d1, 0                          !Fe(OH)2
 15, 0, 14.2,   0.380,   0.382,  0.113d1, 0                           !Fe(OH)3
16,  1, 13.8,  0.4613,   0.2246, 0.113d1, 0                           !Fe(OH)Cl(1+)
 17,  2, 14.6,  0.4613,   0.2246, 0.113d1, 0                          !FeCl(2+)
18,  1, 14.6,  0.4613,   0.2246, 0.113d1, 0                          !FeCl2
 19,  1, 14.3,  0.3913,   0.1846, 0.113d1, 0                          !FeSO4
20,  1,  5.6,   0.311,   0.1847, 0.113d1, 0                          !MgCl(1+)
************All Chemical Reactions***********************
15      !Total # of Chemical Reactions
--repeat (above #) below--ID,KConst(MUST be consistent to generate rate by particle/nm^3/ns),4(NCLnr,KLnr),8(NC_Involved,Vnce#)
 1, 7.83d-3, 0, 0, 0, 0, 0, 0, 0, 0,  12, -1, 9, 1, 0, 0, 0, 0,  0, 0, 0, 0, 0, 0, 0, 0         !Fe>Fe(2+)+2e(-)
 2, 1.34d-17, 0, 0, 0, 0, 0, 0, 0, 0,   7, -1, 4, -1, 5, 1, 0, 0, 0, 0, 0, 0, 0, 0, 0, 0        !O2+4H(+)+4e(-)>4OH(-)
 3, 5.24d-7, 0, 0, 0, 0, 0, 0, 0, 0,   9, -1, 5, -2, 14, 1, 0, 0, 0, 0, 0, 0, 0, 0, 0, 0        !Fe(2+)+2OH(-)>Fe(OH)2
 4, 8.68d-8, 0, 0, 0, 0, 0, 0, 0, 0,   14, -4, 7, -1, 1, -2, 15, 4, 0, 0, 0, 0, 0, 0, 0, 0      !4Fe(OH)2+O2+2H2O>4Fe(OH)3
 5, 8.64d-2, 0, 0, 0, 0, 0, 0, 0, 0,   9, -4, 4, -4, 7, -1, 10, 4, 1, 2, 0, 0, 0, 0, 0, 0       !4Fe(2+)+4H(+)+O2>4Fe(3+)+2H20
 6, 1.59d-7, 0, 0, 0, 0, 0, 0, 0, 0,   10, -1, 5, -3, 15, 1, 0, 0, 0, 0, 0, 0, 0, 0, 0, 0       !Fe(3+)+3OH(-)>Fe(OH)3
 7, 3.57d-9, 0, 0, 0, 0, 0, 0, 0, 0,   10, -1, 3, -1, 17, 1, 0, 0, 0, 0, 0, 0, 0, 0, 0, 0       !Fe(3+)+Cl(-)>FeCl(2+)
 8, 2.13d-10, 0, 0, 0, 0, 0, 0, 0, 0,   18, -1, 1, -2, 14, 1, 4, 1, 3, 1, 0, 0, 0, 0, 0, 0     !FeCl2+2H20>Fe(OH)2+H(+)+Cl(-)
 9, 1.02d-10, 0, 0, 0, 0, 0, 0, 0, 0,   12, -1, 1, -1, 3, -1, 16, 1, 4, 1, 0, 0, 0, 0, 0, 0    !Fe+H2O+Cl(-)>FeCl(OH)(-)+H(+)+e(-)
10, 1.37d-13, 0, 0, 0, 0, 0, 0, 0, 0,  16, -1, 4, -1, 9, 1, 3, 1,  1, 1, 0, 0, 0, 0, 0, 0      !FeCl(OH)+H(+)>Fe(2+)+Cl(-)+H20
11, 4.12d-15, 0, 0, 0, 0, 0, 0, 0, 0,  9, -1, 6, -1, 19, 1, 0, 0,  0, 0, 0, 0, 0, 0, 0, 0      !Fe(2+)+SO4(-)>FeSO4
12, 2.6d-14, 0, 0, 0, 0, 0, 0, 0, 0,   1, -1, 4, 1, 5, -1, 0, 0, 0, 0, 0, 0, 0, 0, 0, 0        !H2O>H(+)+OH(-)
13, 2.16d2, 0, 0, 0, 0, 0, 0, 0, 0,   4, -1, 5, -1, 1, 1, 0, 0, 0, 0, 0, 0, 0, 0, 0, 0        !H(+)+OH(-)>H2O
14, 1.09d-3, 0, 0, 0, 0, 0, 0, 0, 0,   8, -1, 3, -1, 20, 1, 0, 0, 0, 0, 0, 0, 0, 0, 0, 0      !Mg(2+)+Cl(-)>MgCl(-)
15, 5.5d-4, 0, 0, 0, 0, 0, 0, 0, 0,   20, -1, 8, 1, 3, 1, 0, 0, 0, 0, 0, 0, 0, 0, 0, 0        !MgCl(-)>Mg(2+)+Cl(-)
```

2. Input profile applying 1V and Fe flux 2.993d-9 e/nm^2 /ns

```
************1D Problem*******************
1               !=1 if planar; =2 if cylindrical; =3 if spherical
300             !Temperature(K)
************Domain and Grid*******************
0, 1.5, 250, 1.02       !XStt,XEnd(nm),Total # of divisions,Mesh-grading power
************Involved Chemical Components*********
15      !Total#Of Involved Chemical Components
1, 2,3, 4, 5, 6,8, 9,10,12,13,14,15,17,19       !Above#X(ID_Glb Of Involved Chemical Component)
************Involved Chemical Reactions*********
10      !Total#Of Involved Chemical Reactions
2,3,4,5,6,7,11,12,13,14 !Above#X(ID_Glb Of Involved Chemical Reaction)
**************Simulation Time & Steps**********************
1, 1            !NtotTimeSteps,NtotSnapShots
0               !ITimeStt(=0, first time run; >0, to restart based on ITimeStt-1 step)
**************Initial Uniform Concentrations**********************
32.125, 0.301 0.301, 0.602d-7, 0.602d-7, 0.02d-1,0.02d-1, 0, 0,0,0,0,0,0,0 !C(particle/nm^3)///MUST Follow the above order of involved chemical components
**************Boundary Condition*************
!---repeat below !NthC,Ramp1Jump2,2(Flux0_End,SpringCoef_End,C_Eqilibrium_End)
0, 1, 0, 1.d3, 1, 0, 1.d3, 0                    !electric (Displacement=Displacement0+Coef*(V-V0)) with displacement_unit:e/nm^2
1, 2, 0, 0, 0, 0, 1.d3, 32.125                  !chemical (flux=flux0+Coef*(C-C0)) with flux_unit:particle/nm^2/ns, and C_unit:particle/nm^3
2, 2, 0, 0, 0, 0, 1.d3, 0.301                   !chemical (flux=flux0+Coef*(C-C0)) with flux_unit:particle/nm^2/ns, and C_unit:particle/nm^3
3, 2, 0, 0, 0, 0, 1.d3, 0.301                   !chemical (flux=flux0+Coef*(C-C0)) with flux_unit:particle/nm^2/ns, and C_unit:particle/nm^3
4, 2, 0, 0, 0, 0, 1.d3, 0.602d-7                !chemical (flux=flux0+Coef*(C-C0)) with flux_unit:particle/nm^2/ns, and C_unit:particle/nm^3
5, 2, 0, 0, 0, 0, 1.d3, 0.602d-7                !chemical (flux=flux0+Coef*(C-C0)) with flux_unit:particle/nm^2/ns, and C_unit:particle/nm^3
6, 2, 0, 0, 0, 0, 1.d3, 0.02d-1
7, 2, 0, 0, 0, 0, 1.d3, 0.02d-1                !chemical (flux=flux0+Coef*(C-C0)) with flux_unit:particle/nm^2/ns, and C_unit:particle/nm^3
8, 2, 2.993d-9, 0, 0, 0, 1.d3, 0                !chemical (flux=flux0+Coef*(C-C0)) with flux_unit:particle/nm^2/ns, and C_unit:particle/nm^3
9, 2, 0, 0, 0, 0, 1.d3, 0                   !chemical (flux=flux0+Coef*(C-C0)) with flux_unit:particle/nm^2/ns, and C_unit:particle/nm^3
10, 2, 0, 0, 0, 0, 1.d3, 0                   !chemical (flux=flux0+Coef*(C-C0)) with flux_unit:particle/nm^2/ns, and C_unit:particle/nm^3
11, 2, 0, 0, 0, 0, 1.d3, 0                   !chemical (flux=flux0+Coef*(C-C0)) with flux_unit:particle/nm^2/ns, and C_unit:particle/nm^3
12, 2, 0, 0, 0, 0, 1.d3, 0                   !chemical (flux=flux0+Coef*(C-C0)) with flux_unit:particle/nm^2/ns, and C_unit:particle/nm^3
13, 2, 0, 0, 0, 0, 1.d3, 0                   !chemical (flux=flux0+Coef*(C-C0)) with flux_unit:particle/nm^2/ns, and C_unit:particle/nm^3
14, 2, 0, 0, 0, 0, 1.d3, 0                   !chemical (flux=flux0+Coef*(C-C0)) with flux_unit:particle/nm^2/ns, and C_unit:particle/nm^3
15, 2, 0, 0, 0, 0, 1.d3, 0                   !chemical (flux=flux0+Coef*(C-C0)) with flux_unit:particle/nm^2/ns, and C_unit:particle/nm^3
**************Numerical Parameters**********************
90000, 1.d-3, 1000, 0.001       !IteratMax,ErrAllow,IteratDisplay,ARelax
*****************************************************************

************All Chemical Components**********************
20      !Total # of chemical components
--repeat (above #) below--!ID;Valance;Relative_Permittivity@Linear;StokesRadius;PhysicalRadius;EtaOverEpsil0((V/nm)^2-nS);AvdW0
 1,  0,   79, 0.09687,   0.1552,  0.113d1, 2.03d-1                    !H2O(0)(10)
 2,  1,   10,  0.1704,    0.102,  0.113d1, 0.0195                     !Na(1+)(11)
 3, -1,   10,  0.1082,    0.181,  0.113d1, 0.241                      !Cl(1-)(17)
 4,  1,    0,  0.0244,   0.1552,  0.113d1, 9.06d-3                    !H(1+)(1):CInf_H+=0.602d-7(pH=7)
 5, -1, 64.4,  0.0431,   0.137,  0.113d1, 0.20294                     !OH(1-)(9):CInf_OH-=0.602d-7(pH=7)
 6, -2, 17.6,   0.232,   0.258 , 0.113d1, 1.36d-1                     !SO4(2-)(48)
 7, 0, 6.89,   0.109,   0.135 , 0.113d1, 5.02d-2                      !O2(16)
 8,  2,  7.6,   0.311,    0.072, 0.113d1, 0.20294                     !Mg(2+)
9,  2,   16,  0.3851,    0.06,  0.113d1, 0.20294                     !Fe(2+)(26)
10,  3, 15.8,  0.3861,   0.07,   0.113d1, 0.20294                     !Fe(3+)
 11,  0, 15.1,   0.213,    0.161, 0.113d1, 0                          !HCl
 12,  1,   16,  0.3851,    0.126,  0.113d1, 0                         !Fe
 13,  1, 14.2,   0.164,    0.216, 0.113d1, 0                          !FeOH(+1)
 14,  0, 14.2,   0.165,   0.369,  0.113d1, 0                          !Fe(OH)2
 15, 0, 14.2,   0.380,   0.382,  0.113d1, 0                          !Fe(OH)3
16,  1, 13.8,  0.4613,   0.2246, 0.113d1, 0                          !Fe(OH)Cl(1+)
 17,  2, 14.6,  0.4613,   0.2246, 0.113d1, 0                         !FeCl(2+)
18,  1, 14.6,  0.4613,   0.2246, 0.113d1, 0                          !FeCl2
 19,  1, 14.3,  0.3913,   0.1846, 0.113d1, 0                         !FeSO4
20,  1,  5.6,   0.311,   0.1847, 0.113d1, 0                          !MgCl(1+)
************All Chemical Reactions**********************
15      !Total # of Chemical Reactions
--repeat (above #) below--ID,KConst(MUST be consistent to generate rate by particle/nm^3/ns),4(NCLnr,KLnr),8(NC_Involved,Vnce#)
 1, 7.83d-3, 0, 0, 0, 0, 0, 0, 0, 0,  12, -1, 9, 1, 0, 0, 0, 0,  0, 0, 0, 0, 0, 0, 0, 0         !Fe>Fe(2+)+2e(-)
 2, 1.34d-17, 0, 0, 0, 0, 0, 0, 0, 0,   7, -1, 4, -1, 5, 1, 0, 0, 0, 0, 0, 0, 0, 0, 0, 0       !O2+4H(+)+4e(-)>4OH(-)
 3, 5.24d-7, 0, 0, 0, 0, 0, 0, 0, 0,   9, -1, 5, -2, 14, 1, 0, 0, 0, 0, 0, 0, 0, 0, 0, 0       !Fe(2+)+2OH(-)>Fe(OH)2
 4, 8.68d-8, 0, 0, 0, 0, 0, 0, 0, 0,   14, -4, 7, -1, 1, -2, 15, 4, 0, 0, 0, 0, 0, 0, 0, 0     !4Fe(OH)2+O2+2H2O>4Fe(OH)3
 5, 8.64d-2, 0, 0, 0, 0, 0, 0, 0, 0,   9, -4, 4, -4, 7, -1, 10, 4, 1, 2, 0, 0, 0, 0, 0, 0      !4Fe(2+)+4H(+)+O2>4Fe(3+)+2H20
 6, 1.59d-7, 0, 0, 0, 0, 0, 0, 0, 0,   10, -1, 5, -3, 15, 1, 0, 0, 0, 0, 0, 0, 0, 0, 0, 0      !Fe(3+)+3OH(-)>Fe(OH)3
 7, 3.57d-9, 0, 0, 0, 0, 0, 0, 0, 0,   10, -1, 3, -1, 17, 1, 0, 0, 0, 0, 0, 0, 0, 0, 0, 0      !Fe(3+)+Cl(-)>FeCl(2+)
 8, 2.13d-10, 0, 0, 0, 0, 0, 0, 0, 0,   18, -1, 1, -2, 14, 1, 4, 1, 3, 1, 0, 0, 0, 0, 0, 0     !FeCl2+2H20>Fe(OH)2+H(+)+Cl(-)
 9, 1.02d-10, 0, 0, 0, 0, 0, 0, 0, 0,   12, -1, 1, -1, 3, -1, 16, 1, 4, 1, 0, 0, 0, 0, 0, 0    !Fe+H2O+Cl(-)>FeCl(OH)(-)+H(+)+e(-)
10, 1.37d-13, 0, 0, 0, 0, 0, 0, 0, 0,  16, -1, 4, -1, 9, 1, 3, 1,  1, 1, 0, 0, 0, 0, 0, 0      !FeCl(OH)+H(+)>Fe(2+)+Cl(-)+H20
11, 4.12d-15, 0, 0, 0, 0, 0, 0, 0, 0,  9, -1, 6, -1, 19, 1, 0, 0,  0, 0, 0, 0, 0, 0, 0, 0      !Fe(2+)+SO4(-)>FeSO4
12, 2.6d-14, 0, 0, 0, 0, 0, 0, 0, 0,   1, -1, 4, 1, 5, -1, 0, 0, 0, 0, 0, 0, 0, 0, 0, 0       !H2O>H(+)+OH(-)
13, 2.16d2, 0, 0, 0, 0, 0, 0, 0, 0,   4, -1, 5, -1, 1, 1, 0, 0, 0, 0, 0, 0, 0, 0, 0, 0        !H(+)+OH(-)>H2O
14, 1.09d-3, 0, 0, 0, 0, 0, 0, 0, 0,   8, -1, 3, -1, 20, 1, 0, 0, 0, 0, 0, 0, 0, 0, 0, 0      !Mg(2+)+Cl(-)>MgCl(-)
15, 5.5d-4, 0, 0, 0, 0, 0, 0, 0, 0,   20, -1, 8, 1, 3, 1, 0, 0, 0, 0, 0, 0, 0, 0, 0, 0        !MgCl(-)>Mg(2+)+Cl(-)
```

3. nput profile increasing the initial concentration of Cl^- to 0.501 e/nm3 at 0.2V

```
**********1D Problem******************
1              !=1 if planar; =2 if cylindrical; =3 if spherical
300            !Temperature(K)
**********Domain and Grid******************
0, 1.5, 250, 1.02       !XStt,XEnd(nm),Total # of divisions,Mesh-grading power
**********Involved Chemical Components*********
15      !Total#Of Involved Chemical Components
1, 2,3, 4, 5, 6,8, 9,10,12,13,14,15,17,19       !Above#X(ID_Glb Of Involved Chemical Component)
**********Involved Chemical Reactions*********
10      !Total#Of Involved Chemical Reactions
2,3,4,5,6,7,11,12,13,14 !Above#X(ID_Glb Of Involved Chemical Reaction)
**********Simulation Time & Steps**********************
12, 12  !NtotTimeSteps,NtotSnapShots
0              !ITimeStt(=0, first time run; >0, to restart based on ITimeStt-1 step)
**********Initial Uniform Concentrations**********************
31.703, 0.501, 0.501, 0.602d-7, 0.602d-7, 0.02d-1, 0.02d-1, 0, 0,0,0,0,0,0,0 !C(particle/nm^3)///MUST Follow the above order of involved chemical components
**********Boundary Condition************
!---repeat below !NthC,Ramp1Jump2,2(Flux0_End,SpringCoef_End,C_Eqilibrium_End)
0, 1, 0, 1.d3, 0.2, 0, 1.d3, 0                  !electric (Displacement=Displacement0+Coef*(V-V0)) with displacement_unit:e/nm^2
1, 2, 0, 0, 0, 0, 1.d3, 31.703                  !chemical (flux=flux0+Coef*(C-C0)) with flux_unit:particle/nm^2/ns, and C_unit:particle/nm^3
2, 2, 0, 0, 0, 0, 1.d3, 0.501                   !chemical (flux=flux0+Coef*(C-C0)) with flux_unit:particle/nm^2/ns, and C_unit:particle/nm^3
3, 2, 0, 0, 0, 0, 1.d3, 0.501                   !chemical (flux=flux0+Coef*(C-C0)) with flux_unit:particle/nm^2/ns, and C_unit:particle/nm^3
4, 2, 0, 0, 0, 0, 1.d3, 0.602d-7                !chemical (flux=flux0+Coef*(C-C0)) with flux_unit:particle/nm^2/ns, and C_unit:particle/nm^3
5, 2, 0, 0, 0, 0, 1.d3, 0.602d-7                !chemical (flux=flux0+Coef*(C-C0)) with flux_unit:particle/nm^2/ns, and C_unit:particle/nm^3
6, 2, 0, 0, 0, 0, 1.d3, 0.02-1
7, 2, 0, 0, 0, 0, 1.d3, 0.02d-1                !chemical (flux=flux0+Coef*(C-C0)) with flux_unit:particle/nm^2/ns, and C_unit:particle/nm^3
8, 2, 0, 0, 0, 0, 1.d3, 0                  !chemical (flux=flux0+Coef*(C-C0)) with flux_unit:particle/nm^2/ns, and C_unit:particle/nm^3
9, 2, 0, 0, 0, 0, 1.d3, 0                   !chemical (flux=flux0+Coef*(C-C0)) with flux_unit:particle/nm^2/ns, and C_unit:particle/nm^3
10, 2, 0, 0, 0, 0, 1.d3, 0                   !chemical (flux=flux0+Coef*(C-C0)) with flux_unit:particle/nm^2/ns, and C_unit:particle/nm^3
11, 2, 0, 0, 0, 0, 1.d3, 0                   !chemical (flux=flux0+Coef*(C-C0)) with flux_unit:particle/nm^2/ns, and C_unit:particle/nm^3
12, 2, 0, 0, 0, 0, 1.d3, 0                   !chemical (flux=flux0+Coef*(C-C0)) with flux_unit:particle/nm^2/ns, and C_unit:particle/nm^3
13, 2, 0, 0, 0, 0, 1.d3, 0                   !chemical (flux=flux0+Coef*(C-C0)) with flux_unit:particle/nm^2/ns, and C_unit:particle/nm^3
14, 2, 0, 0, 0, 0, 1.d3, 0                   !chemical (flux=flux0+Coef*(C-C0)) with flux_unit:particle/nm^2/ns, and C_unit:particle/nm^3
15, 2, 0, 0, 0, 0, 1.d3, 0                   !chemical (flux=flux0+Coef*(C-C0)) with flux_unit:particle/nm^2/ns, and C_unit:particle/nm^3
**********Numerical Parameters**********************
90000, 1.d-3, 1000, 0.002       !IteratMax,ErrAllow,IteratDisplay,ARelax
****************************************************************

**********All Chemical Components**********************
20      !Total # of chemical components
--repeat (above #) below--!ID;Valance;Relative_Permittivity@Linear;StokesRadius;PhysicalRadius;EtaOverEpsil0((V/nm)^2-nS);AvdW0
 1,  0,   79, 0.09687,   0.1552,  0.113d1, 2.03d-1                    !H2O(0)(10)
 2,  1,   10,  0.1704,    0.102,  0.113d1, 0.0195                     !Na(1+)(11)
 3, -1,   10,  0.1082,    0.181,  0.113d1, 0.241                      !Cl(1-)(17)
 4,  1,    0,  0.0244,   0.1552,  0.113d1, 9.06d-3                    !H(1+)(1):CInf_H+=0.602d-7(pH=7)
 5, -1, 64.4,  0.0431,   0.137,  0.113d1, 0.20294                     !OH(1-)(9):CInf_OH-=0.602d-7(pH=7)
 6, -2, 17.6,   0.232,   0.258 , 0.113d1, 1.36d-1                     !SO4(2-)(48)
 7, 0, 6.89,   0.109,   0.135 , 0.113d1, 5.02d-2                      !O2(16)
 8,  2,  7.6,   0.311,    0.072, 0.113d1, 0.20294                     !Mg(2+)
 9,  2,   16,  0.3851,    0.06,  0.113d1, 0.20294                     !Fe(2+)(26)
10,  3, 15.8,  0.3861,   0.07,   0.113d1, 0.20294                     !Fe(3+)
 11,  0, 15.1,   0.213,    0.161, 0.113d1, 0                          !HCl
 12,  1,   16,  0.3851,    0.126,  0.113d1, 0                         !Fe
 13,  1, 14.2,   0.164,    0.216, 0.113d1, 0                          !FeOH(+1)
 14,  0, 14.2,   0.165,   0.369,  0.113d1, 0                          !Fe(OH)2
 15, 0, 14.2,   0.380,   0.382,  0.113d1, 0                           !Fe(OH)3
16,  1, 13.8,  0.4613,   0.2246, 0.113d1, 0                          !Fe(OH)Cl(1+)
 17,  2, 14.6,  0.4613,   0.2246, 0.113d1, 0                         !FeCl(2+)
18,  1, 14.6,  0.4613,   0.2246, 0.113d1, 0                          !FeCl2
 19,  1, 14.3,  0.3913,   0.1846, 0.113d1, 0                         !FeSO4
20,  1,  5.6,   0.311,   0.1847, 0.113d1, 0                          !MgCl(1+)
**********All Chemical Reactions**********************
 --repeat (above #) below--ID,KConst(MUST be consistent to generate rate by particle/nm^3/ns),4(NCLnr,KLnr),8(NC_Involved,Vnce#)
  1, 7.83d-3, 0, 0, 0, 0, 0, 0, 0, 0,  12, -1, 9, 1, 0, 0, 0, 0,  0, 0, 0, 0, 0, 0, 0, 0         !Fe>Fe(2+)+2e(-)
  2, 1.34d-17, 0, 0, 0, 0, 0, 0, 0, 0,   7, -1, 4, -1, 5, 1, 0, 0, 0, 0, 0, 0, 0, 0, 0, 0        !O2+4H(+)+4e(-)>4OH(-)
  3, 5.24d-7, 0, 0, 0, 0, 0, 0, 0, 0,   9, -1, 5, -2, 14, 1, 0, 0, 0, 0, 0, 0, 0, 0, 0, 0        !Fe(2+)+2OH(-)>Fe(OH)2
  4, 8.68d-8, 0, 0, 0, 0, 0, 0, 0, 0,   14, -4, 7, -1, 1, -2, 15, 4, 0, 0, 0, 0, 0, 0, 0, 0      !4Fe(OH)2+O2+2H2O>4Fe(OH)3
  5, 8.64d-2, 0, 0, 0, 0, 0, 0, 0, 0,   9, -4, 4, -4, 7, -1, 10, 4, 1, 2, 0, 0, 0, 0, 0, 0       !4Fe(2+)+4H(+)+O2>4Fe(3+)+2H20
  6, 1.59d-7, 0, 0, 0, 0, 0, 0, 0, 0,   10, -1, 5, -3, 15, 1, 0, 0, 0, 0, 0, 0, 0, 0, 0, 0       !Fe(3+)+3OH(-)>Fe(OH)3
  7, 3.57d-9, 0, 0, 0, 0, 0, 0, 0, 0,   10, -1, 3, -1, 17, 1, 0, 0, 0, 0, 0, 0, 0, 0, 0, 0       !Fe(3+)+Cl(-)>FeCl(2+)
  8, 2.13d-10, 0, 0, 0, 0, 0, 0, 0, 0,   18, -1, 1, -2, 14, 1, 4, 1, 3, 1, 0, 0, 0, 0, 0, 0     !FeCl2+2H20>Fe(OH)2+H(+)+Cl(-)
  9, 1.02d-10, 0, 0, 0, 0, 0, 0, 0, 0,   12, -1, 1, -1, 3, -1, 16, 1, 4, 1, 0, 0, 0, 0, 0, 0    !Fe+H2O+Cl(-)>FeCl(OH)(-)+H(+)+e(-)
 10, 1.37d-13, 0, 0, 0, 0, 0, 0, 0, 0,  16, -1, 4, -1, 9, 1, 3, 1,  1, 1, 0, 0, 0, 0, 0, 0       !FeCl(OH)+H(+)>Fe(2+)+Cl(-)+H20
 11, 4.12d-15, 0, 0, 0, 0, 0, 0, 0, 0,  9, -1, 6, -1, 19, 1, 0, 0,  0, 0, 0, 0, 0, 0, 0, 0      !Fe(2+)+SO4(-)>FeSO4
 12, 2.6d-14, 0, 0, 0, 0, 0, 0, 0, 0,   1, -1, 4, 1, 5, -1, 0, 0, 0, 0, 0, 0, 0, 0, 0, 0        !H2O>H(+)+OH(-)
 13, 2.16d2, 0, 0, 0, 0, 0, 0, 0, 0,   4, -1, 5, -1, 1, 1, 0, 0, 0, 0, 0, 0, 0, 0, 0, 0         !H(+)+OH(-)>H2O
 14, 1.09d-3, 0, 0, 0, 0, 0, 0, 0, 0,   8, -1, 3, -1, 20, 1, 0, 0, 0, 0, 0, 0, 0, 0, 0, 0       !Mg(2+)+Cl(-)>MgCl(-)
 15, 5.5d-4, 0, 0, 0, 0, 0, 0, 0, 0,   20, -1, 8, 1, 3, 1, 0, 0, 0, 0, 0, 0, 0, 0, 0, 0         !MgCl(-)>Mg(2+)+Cl(-)
```

4. Input profile increasing the initial concentration of SO_4^{2-} concentration to 0.138 at 0.2V

```
************1D Problem******************
1               !=1 if planar; =2 if cylindrical; =3 if spherical
300             !Temperature(K)
************Domain and Grid******************
0, 1.5, 250, 1.02       !XStt,XEnd(nm),Total # of divisions,Mesh-grading power
************Involved Chemical Components*********
15      !Total#Of Involved Chemical Components
1, 2,3, 4, 5, 6,8, 9,10,12,13,14,15,17,19       !Above#X(ID_Glb Of Involved Chemical Component)
************Involved Chemical Reactions*********
10      !Total#Of Involved Chemical Reactions
2,3,4,5,6,7,11,12,13,14 !Above#X(ID_Glb Of Involved Chemical Reaction)
**************Simulation Time & Steps**********************
12, 12  !NtotTimeSteps,NtotSnapShots
0               !ITimeStt(=0, first time run; >0, to restart based on ITimeStt-1 step)
**************Initial Uniform Concentrations**********************
31.320, 0.301, 0.301, 0.602d-7, 0.602d-7, 0.138, 0.138, 0, 0,0,0,0,0,0,0 !C(particle/nm^3)///MUST Follow the above order of involved chemical components
**************Boundary Condition*************
!---repeat below !NthC,Ramp1Jump2,2(Flux0_End,SpringCoef_End,C_Eqilibrium_End)
0, 1, 0, 1.d3, 0.2, 0, 1.d3, 0                  !electric (Displacement=Displacement0+Coef*(V-V0)) with displacement_unit:e/nm^2
1, 2, 0, 0, 0, 0, 1.d3, 31.320                  !chemical (flux=flux0+Coef*(C-C0)) with flux_unit:particle/nm^2/ns, and C_unit:particle/nm^3
2, 2, 0, 0, 0, 0, 1.d3, 0.301                   !chemical (flux=flux0+Coef*(C-C0)) with flux_unit:particle/nm^2/ns, and C_unit:particle/nm^3
3, 2, 0, 0, 0, 0, 1.d3, 0.301                   !chemical (flux=flux0+Coef*(C-C0)) with flux_unit:particle/nm^2/ns, and C_unit:particle/nm^3
4, 2, 0, 0, 0, 0, 1.d3, 0.602d-7                !chemical (flux=flux0+Coef*(C-C0)) with flux_unit:particle/nm^2/ns, and C_unit:particle/nm^3
5, 2, 0, 0, 0, 0, 1.d3, 0.602d-7                !chemical (flux=flux0+Coef*(C-C0)) with flux_unit:particle/nm^2/ns, and C_unit:particle/nm^3
6, 2, 0, 0, 0, 0, 1.d3, 0.138
7, 2, 0, 0, 0, 0, 1.d3, 0.138                 !chemical (flux=flux0+Coef*(C-C0)) with flux_unit:particle/nm^2/ns, and C_unit:particle/nm^3
8, 2, 0, 0, 0, 0, 1.d3, 0                   !chemical (flux=flux0+Coef*(C-C0)) with flux_unit:particle/nm^2/ns, and C_unit:particle/nm^3
9, 2, 0, 0, 0, 0, 1.d3, 0                    !chemical (flux=flux0+Coef*(C-C0)) with flux_unit:particle/nm^2/ns, and C_unit:particle/nm^3
10, 2, 0, 0, 0, 0, 1.d3, 0                    !chemical (flux=flux0+Coef*(C-C0)) with flux_unit:particle/nm^2/ns, and C_unit:particle/nm^3
11, 2, 0, 0, 0, 0, 1.d3, 0                    !chemical (flux=flux0+Coef*(C-C0)) with flux_unit:particle/nm^2/ns, and C_unit:particle/nm^3
12, 2, 0, 0, 0, 0, 1.d3, 0                    !chemical (flux=flux0+Coef*(C-C0)) with flux_unit:particle/nm^2/ns, and C_unit:particle/nm^3
13, 2, 0, 0, 0, 0, 1.d3, 0                    !chemical (flux=flux0+Coef*(C-C0)) with flux_unit:particle/nm^2/ns, and C_unit:particle/nm^3
14, 2, 0, 0, 0, 0, 1.d3, 0                    !chemical (flux=flux0+Coef*(C-C0)) with flux_unit:particle/nm^2/ns, and C_unit:particle/nm^3
15, 2, 0, 0, 0, 0, 1.d3, 0                    !chemical (flux=flux0+Coef*(C-C0)) with flux_unit:particle/nm^2/ns, and C_unit:particle/nm^3
**************Numerical Parameters**********************
90000, 1.d-3, 1000, 0.002       !IteratMax,ErrAllow,IteratDisplay,ARelax
*****************************************************************

************All Chemical Components**********************
20      !Total # of chemical components
--repeat (above #) below--!ID;Valance;Relative_Permittivity@Linear;StokesRadius;PhysicalRadius;EtaOverEpsil0((V/nm)^2-nS);AvdW0
 1,  0,   79, 0.09687,   0.1552,  0.113d1, 2.03d-1                    !H2O(0)(10)
 2,  1,   10,  0.1704,    0.102,  0.113d1, 0.0195                     !Na(1+)(11)
 3, -1,   10,  0.1082,    0.181,  0.113d1, 0.241                      !Cl(1-)(17)
 4,  1,    0,  0.0244,   0.1552,  0.113d1, 9.06d-3                    !H(1+)(1):CInf_H+=0.602d-7(pH=7)
 5, -1, 64.4,  0.0431,    0.137,  0.113d1, 0.20294                    !OH(1-)(9):CInf_OH-=0.602d-7(pH=7)
 6, -2, 17.6,   0.232,   0.258 , 0.113d1, 1.36d-1                    !SO4(2-)(48)
 7, 0, 6.89,   0.109,   0.135 , 0.113d1, 5.02d-2                     !O2(16)
 8,  2,  7.6,   0.311,    0.072, 0.113d1, 0.20294                    !Mg(2+)
9,  2,   16,  0.3851,    0.06,  0.113d1, 0.20294                     !Fe(2+)(26)
10,  3, 15.8,  0.3861,   0.07,   0.113d1, 0.20294                    !Fe(3+)
 11,  0, 15.1,   0.213,    0.161, 0.113d1, 0                          !HCl
 12,  1,   16,  0.3851,    0.126,  0.113d1, 0                         !Fe
 13,  1, 14.2,   0.164,    0.216, 0.113d1, 0                          !FeOH(+1)
 14,  0, 14.2,   0.165,   0.369,  0.113d1, 0                          !Fe(OH)2
 15, 0, 14.2,   0.380,   0.382,  0.113d1, 0                          !Fe(OH)3
16,  1, 13.8,  0.4613,   0.2246, 0.113d1, 0                          !Fe(OH)Cl(1+)
 17,  2, 14.6,  0.4613,   0.2246, 0.113d1, 0                         !FeCl(2+)
18,  1, 14.6,  0.4613,   0.2246, 0.113d1, 0                          !FeCl2
 19,  1, 14.3,  0.3913,   0.1846, 0.113d1, 0                         !FeSO4
20,  1,  5.6,   0.311,   0.1847, 0.113d1, 0                          !MgCl(1+)
************All Chemical Reactions**********************
--repeat (above #) below--ID,KConst(MUST be consistent to generate rate by particle/nm^3/ns),4(NCLnr,KLnr),8(NC_Involved,Vnce#)
 1, 7.83d-3, 0, 0, 0, 0, 0, 0, 0, 0,  12, -1, 9, 1, 0, 0, 0, 0,  0, 0, 0, 0, 0, 0, 0, 0         !Fe>Fe(2+)+2e(-)
 2, 1.34d-17, 0, 0, 0, 0, 0, 0, 0, 0,   7, -1, 4, -1, 5, 1, 0, 0, 0, 0, 0, 0, 0, 0, 0, 0        !O2+4H(+)+4e(-)>4OH(-)
 3, 5.24d-7, 0, 0, 0, 0, 0, 0, 0, 0,   9, -1, 5, -2, 14, 1, 0, 0, 0, 0, 0, 0, 0, 0, 0, 0        !Fe(2+)+2OH(-)>Fe(OH)2
 4, 8.68d-8, 0, 0, 0, 0, 0, 0, 0, 0,   14, -4, 7, -1, 1, -2, 15, 4, 0, 0, 0, 0, 0, 0, 0, 0      !4Fe(OH)2+O2+2H2O>4Fe(OH)3
 5, 8.64d-2, 0, 0, 0, 0, 0, 0, 0, 0,   9, -4, 4, -4, 7, -1, 10, 4, 1, 2, 0, 0, 0, 0, 0, 0       !4Fe(2+)+4H(+)+O2>4Fe(3+)+2H20
 6, 1.59d-7, 0, 0, 0, 0, 0, 0, 0, 0,   10, -1, 5, -3, 15, 1, 0, 0, 0, 0, 0, 0, 0, 0, 0, 0       !Fe(3+)+3OH(-)>Fe(OH)3
 7, 3.57d-9, 0, 0, 0, 0, 0, 0, 0, 0,   10, -1, 3, -1, 17, 1, 0, 0, 0, 0, 0, 0, 0, 0, 0, 0       !Fe(3+)+Cl(-)>FeCl(2+)
 8, 2.13d-10, 0, 0, 0, 0, 0, 0, 0, 0,   18, -1, 1, -2, 14, 1, 4, 1, 3, 1, 0, 0, 0, 0, 0, 0     !FeCl2+2H20>Fe(OH)2+H(+)+Cl(-)
 9, 1.02d-10, 0, 0, 0, 0, 0, 0, 0, 0,   12, -1, 1, -1, 3, -1, 16, 1, 4, 1, 0, 0, 0, 0, 0, 0    !Fe+H2O+Cl(-)>FeCl(OH)(-)+H(+)+e(-)
10, 1.37d-13, 0, 0, 0, 0, 0, 0, 0, 0,  16, -1, 4, -1, 9, 1, 3, 1,  1, 1, 0, 0, 0, 0, 0, 0      !FeCl(OH)+H(+)>Fe(2+)+Cl(-)+H20
11, 4.12d-15, 0, 0, 0, 0, 0, 0, 0, 0,  9, -1, 6, -1, 19, 1, 0, 0,  0, 0, 0, 0, 0, 0, 0, 0      !Fe(2+)+SO4(-)>FeSO4
12, 2.6d-14, 0, 0, 0, 0, 0, 0, 0, 0,   1, -1, 4, 1, 5, -1, 0, 0, 0, 0, 0, 0, 0, 0, 0, 0        !H2O>H(+)+OH(-)
13, 2.16d2, 0, 0, 0, 0, 0, 0, 0, 0,   4, -1, 5, -1, 1, 1, 0, 0, 0, 0, 0, 0, 0, 0, 0, 0        !H(+)+OH(-)>H2O
14, 1.09d-3, 0, 0, 0, 0, 0, 0, 0, 0,   8, -1, 3, -1, 20, 1, 0, 0, 0, 0, 0, 0, 0, 0, 0, 0      !Mg(2+)+Cl(-)>MgCl(-)
15, 5.5d-4, 0, 0, 0, 0, 0, 0, 0, 0,   20, -1, 8, 1, 3, 1, 0, 0, 0, 0, 0, 0, 0, 0, 0, 0        !MgCl(-)>Mg(2+)+Cl(-)
```

REFERENCE

1. Al-Fozan, S. A., & Malik, A. U. (2008). Effect of seawater level on corrosion behavior of different alloys. *Desalination, 228*(1-3), 61-67. doi:10.1016/j.desal.2007.08.007
2. Corrosion in marine Environments. (n.d.). Retrieved May 02, 2016, from http://corrosion-doctors.org/Seawater/Introduction.htm
3. Johnsirani, V., Sathiyabama, J., Rajendran, S., & Prabha, A. S. (2012). Inhibitory Mechanism of Carbon Steel Corrosion in Sea Water by an Aqueous Extract of Henna Leaves. *ISRN Corrosion, 2012*, 1-9. doi:10.5402/2012/574321
4. Seawater Composition. (n.d.). Retrieved May 02, 2016, from http://www.marinebio.net/marinescience/02ocean/swcomposition.htm
5. Pawlowicz, R. (2015). The Absolute Salinity of seawater diluted by riverwater. *Deep Sea Research Part I: Oceanographic Research Papers, 101*, 71-79. doi:10.1016/j.dsr.2015.03.006
6. BRITISH STAINLESS STEEL ASSOCIATION Making the Most of Stainless Steel. (2013, April 03). From http://www.bssa.org.uk/topics.php?article=100
7. 5 Types of Ship Corrosion & Strategies for Prevention. (2015, January 11). From http://www.americanplatingcompany.com/5-types-of-ship-corrosion-strategies-for-prevention/
8. Atrens, A. (2004). Environmental Conditions Leading to Pitting/Crevice Corrosion of a Typical 12% Chromium Stainless Steel at 80 C. *Corrosion, 39*(12), 483-487. doi:10.5006/1.3577371
9. Caines, S., Khan, F., & Shirokoff, J. (2013). Analysis of pitting corrosion on steel under insulation in marine environments. *Journal of Loss Prevention in the Process Industries, 26*(6), 1466-1483. doi:10.1016/j.jlp.2013.09.010

10. MCF - Marine Corrosion Explained. (2014, April 05). From http://www.marinecorrosionforum.org/explain.htm

11. Cai, B., Liu, Y., Tian, X., Wang, F., Li, H., & Ji, R. (2010). An experimental study of crevice corrosion behaviour of 316L stainless steel in artificial seawater. *Corrosion Science, 52*(10), 3235-3242. doi:10.1016/j.corsci.2010.05.040

12. Crevice corrosion. (n.d.). From https://en.wikipedia.org/wiki/Crevice_corrosion

13. H.H. Uhlig, R.W. Revie, Corrosion and Corrosion Control, third ed., John Wiley & Sons, New York, 1985, p. 1.

14. A. Islami. (2013). Effect of Anions In Seawater To Corrosion Attack On Passive Alloys. *International Journal of Research in Engineering and Technology IJRET, 02*(12), 733-737. doi:10.15623/ijret.2013.0212124

15. Stojek, Z. (2005). The Electrical Double Layer and Its Structure. *Electroanalytical Methods,* 3-8. doi:10.1007/978-3-662-04757-6_1

16. Lashkari, M., & Arshadi, M. (2004). DFT studies of pyridine corrosion inhibitors in electrical double layer: Solvent, substrate, and electric field effects. *Chemical Physics, 299*(1), 131-137. doi:10.1016/j.chemphys.2003.12.019

17. Kirby, B.J. (2010). Micro- and Nano scale Fluid Mechanics: Transport in Microfluidic Devices. Cambridge University Press. ISBN 978-0-521-11903-0.

18. X. Luo & J. j. Davis (2013). Electrical biosensors and the label free detection of protein disease biomarkers. *Chemical Society Review,* issue13, 2013,42, 5944-5962. doi: 10.1039/C3CS60077G

19. Melcher, J. R. *Continuum electromechanics*. Vol. 2 (MIT press Cambridge, 1981).

20. Carnahan, N. F. & Starling, K. E. Equation of state for nonattracting rigid spheres. *The Journal of chemical physics* 51, 635-636 (1969).

21. Carnahan, N. F. & Starling, K. E. Intermolecular repulsions and the equation of state for fluids. *AIChE Journal* 18, 1184-1189 (1972).

22. Heinz, H., Vaia, R., Farmer, B. & Naik, R. Accurate simulation of surfaces and interfaces of face-centered cubic metals using 12− 6 and 9− 6 Lennard-Jones potentials. *The Journal of Physical Chemistry C* **112**, 17281-17290 (2008).

23. Wei, Y. S. & Sadus, R. J. Equations of state for the calculation of fluid-phase equilibria. *AIChE Journal* 46, 169-196 (2000).

24. Surface charge - Wikipedia Republished // WIKI 2. (n.d.). From https://en.wiki2.org/wiki/Surface_charge

25. Activation Polarization. (2011, March 15). From http://corrosion-doctors.org/Corrosion-Kinetics/Overpotential-activation.htm

Biographical Information

Pratik Kale was born June 26, 1990 in Wardha, India. He received the Bachelors of Engineering in Mechanical Engineering from Mumbai University in 2012. In May 2016, he graduated with Master of Science of Industrial Engineering.

It was during his Bachelors, Pratik participated in mechanical engineering internship with M/S. Hardev Construction Pvt Ltd, Deoghar. He worked as Assistant professor in OM college of engineering and, Agnihotri Polytechnic Technique, Department of mechanical from 2013 to 2014.